UNIVERSITÉ DU LUXEMBOURG

PhD-FSTC-2011-14
The Faculty of Sciences, Technology and Communication

DISSERTATION

Defense held on 29th September 2011 in Belvaux
to obtain the degree of

DOCTEUR DE L'UNIVERSITÉ DU LUXEMBOURG EN PHYSIQUE

by

Nora BECKER

Born on 16th July 1984 in Luxembourg (Luxembourg)

APPLICATION OF THE STORING MATTER TECHNIQUE TO ORGANIC SAMPLES: FUNDAMENTALS, APPLICATIONS, AND EVALUATION OF THE ANALYTICAL POTENTIAL

Dissertation defense committee:

Dr. Tom WIRTZ, dissertation supervisor
Head of the Scientific Instrumentation Unit (UIS), CRP – Gabriel Lippmann

Prof. Dr. Susanne SIEBENTRITT, co-supervisor
Head of the Laboratory for Photovoltaics (LPV), Université du Luxembourg

Prof. Dr. Patrick BERTRAND, Chairman
Head of the Unité de Physico-chimie et de Physique des Matériaux, Université catholique de Louvain

Dr. Serge DELLA-NEGRA
Institut de Physique Nucléaire d'Orsay

Prof. Dr. Hans Jörg MATHIEU, Vice Chairman
Emerited professor, Materials Science Institute (IMX), Ecole Polytechnique Fédérale de Lausanne

Prof. Dr. Henri-Noël MIGEON
Director of the Science and Analysis of Materials (SAM) department, CRP – Gabriel Lippmann

Centre de Recherche Public Gabriel Lippmann

aides à la formation recherche

Fonds National de la Recherche Luxembourg

The present project is supported by the National Research Fund, Luxembourg.

Acknowledgements

I would like to express my gratitude towards all those who, directly or indirectly, actively or passively, consciously or unknowingly, contributed to this thesis and/or my general well-being throughout the last three years.

I am very grateful to my supervisor, Dr. Tom Wirtz, for his guidance and availability, and for ensuring that the time I have spent in his research team has been a truly enriching experience on both the scientific and human level.

I kindly thank Prof. Susanne Siebentritt for being my co-supervisor and for her constructive comments during the review meetings.

I thank Prof. Henri-Noël Migeon, director of the SAM department, for giving me the opportunity to work in such a well-equipped laboratory and for being a member of the jury of my thesis.

I would like to thank Prof. Patrick Bertrand, Dr. Serge Della-Negra, and Prof. Hans Jörg Mathieu for being part of the thesis jury.

I thankfully acknowledge the support of Dr. Catalina Mansilla and Dr. Gilles Frache, who introduced me into the instrumental aspects of the Storing Matter and TOF-SIMS techniques and provided helpful advice throughout the years.

Very special thanks to Rachid Barrahma, Mathieu Gérard, Samir Menaouli, Arnaud Moschetta, and Alain Robert for their efficient engineering support and valuable technical assistance.

I am grateful to Dr. Jérôme Guillot, Joffrey Didierjean and Sébastien François for the XPS experiments and discussion of the results, as well as to Dr. Yves Fleming for the AFM measurements.

Many thanks to Antoine, Arindam, Beatrix, Ben, Canan, Catalina, Christophe, David, Hung, Lex, Ludovic, Mathieu, Nico, Oleksiy, Patrick, Peter, Quyen, Rachid, Sudharsan and Yves for their refreshing humor, some very inspiring discussions, and the pleasant international atmosphere in the UIS team.

My gratitude is also addressed to all those whose names are not mentioned here but who provided support of scientific, technical, or administrative nature.

I gratefully acknowledge financial support from the Fonds National de la Recherche, Luxembourg (FNR) by means of an AFR grant (grant number: TR-PHD BFR08-076).

Finally, I would like to thank my family and friends for animating the non-working part of the three years that I dedicated to this thesis.

Table of contents

Chapter I. Introduction 11

I.1 General context and scope of this thesis 11

I.2 Secondary Ion Mass Spectrometry (SIMS) 13

I.2. (a) Presentation of the technique 13

I.2. (b) Static and dynamic SIMS 13

I.2. (c) Mass-separation and detection of secondary ions 14

I.2. (d) Applications of SIMS 15

I.2. (e) Analytical performances and limitations of SIMS 15

I.3 The Storing Matter technique 18

I.3. (a) Principles of the technique 18

I.3. (b) The Storing Matter prototype instrument 19

I.3. (b) i) General description 19

I.3. (b) ii) The Argon etching chamber 20

I.3. (b) iii) The collector coating chamber 20

I.3. (b) iv) The sputter-deposition chamber 22

a. Sample stages 22

b. The floating low-energy ion gun 24

c. Raster controller and secondary electron detector 25

d. Electron gun 25

e. Secondary ion detector 25

I.3. (b) v) Collector transfer inside the Storing Matter prototype and to analytical instruments 26

Chapter II. SIMS analysis of organic materials.....29

II.1 Principles of TOF-SIMS.....29

II.1. (a) Primary ion beam.....29

II.1. (b) Mass separation of the secondary ions.....30

II.1. (c) Mass resolution.....31

II.2 TOF-SIMS instruments used for this work.....31

II.2. (a) The TOFIII instrument by ION-TOF.....31

II.2. (b) The TOF5 instrument by ION-TOF.....33

II.3 Fundamental aspects of molecular secondary ion emission.....34

II.3. (a) Sputtering by ion bombardment.....34

II.3. (a) i) Cascade regimes.....34

II.3. (a) ii) Sputter yields.....36

II.3. (a) iii) Characteristics of the emitted particles.....37

II.3. (b) Ionization and fragmentation mechanisms.....41

II.4 Matrix effects.....43

II.5 Organic secondary ion yield enhancement by ME-SIMS and MetA-SIMS.....44

II.6 Effect of the primary ion type on organic secondary ion emission.....46

II.7 Conclusions.....51

Chapter III. Sample preparation and characterization.....53

III.1 Silicon wafers.....53

III.2 Polymer samples.....53

III.3 Alq_3 samples.....55

III.4 Metallic collectors.....55

Chapter IV. Study of the key parameters of the Storing Matter technique in the case of organic samples.....63

IV.1 Introduction 63

IV.2 Experimental conditions.....65

IV.3 Identification of Storing Matter deposits on Ag collectors.....66

IV.3. (a) PVC sample 66

IV.3. (a) i) Positive secondary ions.....66

IV.3. (a) ii) Negative secondary ions.....69

IV.3. (b) PS samples.....70

IV.3. (b) i) Positive secondary ions.....70

IV.3. (b) ii) Negative secondary ions.....72

IV.3. (c) PMMA samples 73

IV.3. (c) i) Positive secondary ions 73

IV.3. (c) ii) Negative secondary ions.....74

IV.3. (d) Alq_3 sample.....75

IV.3. (e) Conclusions.....77

IV.4 Biasing of the sample-holder during sputter-deposition.....78

IV.5 Study of the key parameters of the Storing Matter technique for organic samples 81

IV.5. (a) The collector surface 81

IV.5. (a) i) Sample preparation and experimental conditions 83

IV.5. (a) ii) Ag vs. Si collector for Alq_3 deposits 83

IV.5. (a) iii) Comparison of Au, Ag and Cu collectors for a PVC deposit 86

IV.5. (a) iv) Cs collectors 91

IV.5. (a) v) Importance of UHV transfer of the deposits.....93

IV.5. (b) Sample preparation methods to enhance Ag-cationization for Storing Matter deposits of PS 95

IV.5. (b) i) Introduction 95

IV.5. (b) ii) Sample preparation 96

IV.5. (b) iii) Results and discussion 97

IV.5. (c) The amount of matter deposited on the collector 103

IV.5. (c) i) Introduction 103

IV.5. (c) ii) Experimental conditions 103

IV.5. (c) iii) Results and discussion 104

IV.5. (c) iv) Conclusions 107

IV.5. (d) The primary ion fluence used for sputter-deposition .. 108

IV.5. (d) i) Introduction 108

IV.5. (d) ii) Experimental conditions 108

IV.5. (d) iii) Results and discussion 109

IV.5. (d) iv) Conclusions 110

IV.5. (e) The primary ion energy used for sputter-deposition .. 111

IV.5. (e) i) Introduction 111

IV.5. (e) ii) Experimental conditions 112

IV.5. (e) iii) Results and discussion 112

IV.5. (f) Primary ion type used for the analysis step 114

IV.5. (f) i) Introduction 114

IV.5. (f) ii) Experimental conditions 114

IV.5. (f) iii) Results and discussion: Alq_3 sample 115

a. Reference sample 115

b. Storing Matter deposit 118

IV.5. (f) iv) Results and discussion: PS2000 sample 120

a. Reference sample 120

b. Storing Matter deposit 121

IV.5. (g) Conclusions about the experimental parameters of the Storing Matter technique applied to organic samples 124

Chapter V. Application of the Storing Matter technique to PS/PMMA blends 127

V.1 Introduction 127

V.1. (a) Context 127

V.1. (b) Sample preparation 128

V.1. (c) Determination of the surface composition by XPS 128

V.2 Characterization of PS/PMMA blends by TOF-SIMS 130

V.2. (a) Analysis with monoatomic primary ions 130

V.2. (b) Analysis with polyatomic primary ions 134

V.3 Storing Matter deposits of PS/PMMA blends on Ag collectors 135

V.4 MetA-SIMS: a simple way to reduce matrix effects in PS/PMMA blends 138

V.4. (a) Experimental conditions 139

V.4. (b) Results and discussion 139

V.5 Conclusions 141

Chapter VI. Conclusions and outlook 143

VI.1 General conclusions 143

VI.2 Outlook 147

Reference List 149

Chapter I. Introduction

I.1 General context and scope of this thesis

Although the domain of materials science has generated numerous and very diverse sub-domains during the last decades, its ultimate goal can still be resumed in one sentence: the development of "smart" materials with novel properties and the potential to revolutionize at least one scientific or technological area and, in parallel, the gain of deeper insights into the fundamental physical and chemical mechanisms that determine these specific properties. The two aspects require the sub-domain of materials analysis to rapidly adapt its techniques to the new trends, such as for example the characterization of ultra-shallow junctions for photovoltaic applications, the determination of doping profiles over a large concentration range in the domain of semi-conductors, or the study of interfacial reactions in nanomaterials. Due to the increasing complexity of the analytical requirements, time-consuming multi-technique characterization is often the only way to yield the desired information about a sample.

Secondary Ion Mass Spectrometry (SIMS) is among the techniques that are commonly used for surface or interface characterization. It is based on sputtering of solid (or liquid) surfaces by an ion beam and determination of the mass-to-charge ratio of the ionized fraction of the emitted particles. SIMS is characterized by its extreme surface sensitivity and very low detection limits that are in the ppb range for some applications. Elemental and molecular detection, surface imaging, depth profiling, and 3D-reconstruction of small sample volumes are possible for a large variety of materials. However the main limitation of SIMS is its inherent incapability of providing quantitative information about the sample composition. This is due to the so-called matrix effect: the ionization efficiency of an ejected particle (and thus its probability of being detected) strongly depends on its chemical environment in the sample.

Several approaches have been developed in order to reduce the matrix effect in SIMS. One of them is the Storing Matter technique developed at CRP – Gabriel Lippmann, which consists in decoupling the sputtering of the sample surface from the analysis step: first, the sample is sputtered by an ion beam, and the emitted particles (ions, neutrals, radicals, atoms and molecules) are deposited at sub-monolayer level onto a dedicated collector. The collector with the deposit is then transferred under ultra-high vacuum conditions to an analytical instrument (mainly static and dynamic SIMS). Since the deposit coverage on the collector is inferior to a monolayer, the deposited particles are surrounded by the same matrix, i.e. the collector material. The Storing Matter technique therefore reduces the matrix effect encountered in SIMS analyses while the sensitivity can be kept high by choosing a collector material that will optimize the subsequent SIMS analysis of the deposit. Since the assembly of the prototype instrument at SAM a few years ago, very promising results have been published about the application of the Storing Matter technique to inorganic materials[1,2], especially for samples typically used in the semiconductor industry.

The objective of this thesis was to study the different mechanisms involved in the Storing Matter technique in the case of organic materials and to establish a specific experimental protocol for the application of the technique to such organic materials, the main challenge being the retention of molecular information by a reduction of fragmentation. In this first chapter, a general introduction about SIMS and Storing Matter, as well as a detailed technical description of the Storing Matter prototype instrument will be provided. The second chapter deals with the fundamental and instrumental aspects of TOF-SIMS analysis of organic materials. The preparation of the collectors and of the organic samples is described in chapter 3. Chapter 4 presents the results of the detailed study of the different experimental parameters involved in the Storing Matter technique: the nature of the collector surface, the ion beam parameters for both the sputter-deposition and the analytical step, the amount of matter deposited onto the collector, as well as different preparation methods for the organic samples. Once the optimal experimental parameters are defined and the fundamental processes involved in the preparation and analysis of the organic Storing Matter deposits are better understood, the

technique is applied to polymer blends with varying compositions in order to evaluate its efficiency in circumventing matrix effects.

I.2 Secondary Ion Mass Spectrometry (SIMS)

I.2. (a) Presentation of the technique

In a SIMS instrument, the sample surface is bombarded by a primary ion beam. The impacting ions interact with the atoms and molecules close to the surface, and secondary particles (atoms, molecules, ions, electrons) are emitted. Only the ionized fraction, which represents less than 1% of the emitted matter, is detectable by SIMS. Identification of the secondary ion is possible by means of their mass-to-charge ratio (*m/z*).

I.2. (b) Static and dynamic SIMS

Depending on the primary ion conditions, two different analysis modes can be distinguished: static and dynamic SIMS.

Static SIMS (S-SIMS) was first introduced by Benninghoven[3,4]. This technique is mainly applied to organic samples, where it is necessary to preserve a certain amount of molecular information in order to identify the structure of the analyzed material. If the primary ion fluence is kept low (< 10^{13} ions/cm^2), less than 1% of the surface atoms are bombarded (for a surface atomic density of ~10^{15} atoms/cm^2) and chemical damage is limited. In these conditions it is possible to obtain "fingerprint" mass spectra that may even contain (quasi-) molecular ions for a large variety of organic materials[5]. S-SIMS provides chemical information only from the uppermost few monolayers of the sample.

In dynamic SIMS (D-SIMS), higher primary ion doses are used (up to 10^{19} ions/cm^2), and a considerable amount of sample material is eroded during the analysis. The intensities of selected secondary ions are recorded as a function of time. By converting the time-scale into a depth scale, one obtains

depth information with resolutions down to 1 nm in the case of low energy bombardment[6]. In general, little or no molecular information is preserved in dynamic SIMS, but only elemental ions and small clusters can be observed. However molecular depth profiling has become possible to some extent with the development of cluster ion sources (section II.6).

I.2. (c) Mass-separation and detection of secondary ions

An extraction potential accelerates the ejected secondary ions into the secondary column where they are mass-separated. Finally, detectors measure the ion currents for each *m/z*.

3 types of mass analyzers are used in SIMS[7]. Time-of-flight analyzers (TOF-SIMS) are used in static SIMS. The secondary ions are guided through a flight tube towards the detector. The time that a given ion needs to reach the detector (its "time-of-flight") is a function of its *m/z* ratio. Mass resolutions ($m/\Delta m$) higher than 10 000 can be reached. With this type of mass analyzer all masses can be detected in parallel, which is not possible for the quadrupole and the magnetic sector. The transmission is high and the *m/z* range is virtually unlimited. Further details about TOF-SIMS are given in the next chapter.

In a quadrupole analyzer, the secondary ions travel between 4 parallel hyperbolically shaped rods. Depending on the voltages that are applied to the different rods, only ions with a certain *m/z* ratio have a stable trajectory and reach the detector. Quadrupole analyzers are characterized by their small size, reasonable prizes, but poor mass resolutions.

Magnetic sector analyzers are the most commonly used for dynamic SIMS since they provide good mass resolution and high transmission. Their principle is based on the fact that ions with different *m/z* ratios follow different trajectories in a magnetic field that is perpendicular to their direction of motion.

I.2. (d) Applications of SIMS

SIMS analyses provide valuable information about the chemical composition of a large variety of materials emerging from different scientific and technological domains: semi-conductors, microelectronics, nanotechnology, life sciences, geology, polymers, metals, ceramics, etc. Depending on the sample type and the desired information, different analysis modes are used:

- mass spectra give information about the local composition of the outmost sample surface;
- depth profiles provide insight into vertical composition changes (e.g. multilayer samples, doping profiles etc);
- secondary ion imaging reveals the two-dimensional distribution of different elements on the sample surface.

In order to get a maximum of information about a sample, different analysis modes can be combined. For example, by acquiring secondary ion images at different depths, a three-dimensional reconstruction of a sample is possible.

I.2. (e) Analytical performances and limitations of SIMS

The analytical potential of SIMS is based on a unique combination of performances that distinguishes it from other surface analysis techniques:

- its high sensitivity (down to the ppb-range for some elements) allows for the detection of trace elements,
- all elements and isotopes (from H to U) are detectable,
- the high mass resolution (especially for TOF-SIMS) makes isotopic analysis possible,
- excellent lateral resolution for imaging applications (down to 50 nm),
- depth resolutions in the nm-range,

- high dynamic range for D-SIMS.

Nevertheless, SIMS is not a universal solution for all surface analysis problems. The major weak point of this technique is the so-called "matrix effect" that makes it very difficult to quantify the results. The ionization efficiency of an element can vary over several orders of magnitude depending on the sample composition (i.e. the matrix). An example of a strong matrix effect is illustrated in Fig. I-1: the useful yields of Si (obtained by dividing the number of the detected Si^+ ions by the number of sputtered Si atoms) for different Si-containing samples were measured for different primary ions[8]. This example shows that the chemical environment of the investigated element can dramatically influence its useful yield, which may easily lead to erroneous conclusions about the sample composition.

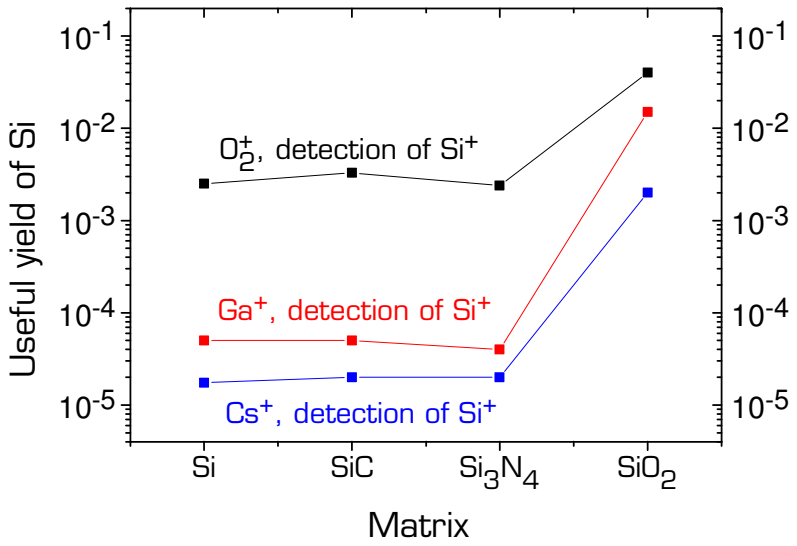

Fig. I-1: Useful yield of Si as a function of primary ion and sample composition. Adapted from [8].

The matrix effect can be used in a positive way in order to improve the sensitivity of the analysis. A common approach is the use of reactive primary ions that, after implantation into the sample surface, enhance the positive or negative secondary ion yields. An example is the use of Cs^+ primary ions: as the fluence increases, Cs atoms are implanted into the sample and lower the surface work function. According to the electron tunnelling model, the

formation of negatively charged species is then favoured[9,10]. If one is rather interested in positive secondary ions, the use of an O_2^+ beam may be useful. Here the positive ionization efficiencies are enhanced according to the bond-breaking model[11,12].

Similarly, the ionization efficiencies may be increased by flooding the vacuum chamber with reactive gases such as O_2 [13] or neutral Cs [14,15] during analysis.

Since it is difficult to directly quantify the measurements, SIMS is often used in combination with complementary surface analysis methods, for example X-ray Photoelectron Spectroscopy (XPS), which is a quantitative technique but has a detection limit in the percent-range.

Indirect quantification of SIMS results is possible with the help of calibration curves[7,16,17]. This requires several samples with well-known compositions that are very close to the "unknown" sample's composition. The ratio between the signal intensity of an element and its real concentration in the sample is established by SIMS measurements. If the unknown sample is then analyzed under the same experimental conditions, its composition can be determined with the help of this calibration curve. This method is quite time-consuming and is only possible if the sample composition is approximately known and homogenous.

A few experimental methods have been derived from SIMS in order to reduce the matrix effect. Secondary Neutral Mass Spectrometry (SNMS) consists in post-ionizing sputtered neutrals (which represent around 99% of the emitted particles) by an electron beam or a laser[18]. In this case the detection probability of an element only depends on its concentration and not on the sample composition. The major drawback of SNMS is that, due to geometrical constraints, only a small fraction of the sputtered neutrals can be ionized. Indeed, the sensitivity of SNMS is around 3 orders of magnitude lower than for SIMS.

Another experimental approach that reduces the matrix effect in SIMS is the detection of MCs_n^+ clusters in the case of Cs^+ primary ions and/or neutral Cs deposition[8,19-22]. It is assumed that these clusters are formed by

recombination of one or more Cs^+ ions with a neutral atom (or a molecular fragment[23]) M above the sample surface. The signal of these cluster ions is thus almost independent of the sample's composition.

The Storing Matter technique has been developed in order to obtain quantitative results for a large variety of samples without losing the high sensitivity of SIMS. Its principle and the dedicated prototype instrument are described in the next section.

I.3 The Storing Matter technique

I.3. (a) Principles of the technique

The Storing Matter technique is based on an idea by Prof. G. Slodzian[24]. Initially the project was an international collaboration between Luxembourg (CRP Gabriel Lippmann), Belgium (Université de Namur) and France (Meca2000).

Storing Matter consists in decoupling the sputtering of the specimen from the analysis step. First, the sample surface is sputtered by an ion beam, and the emitted particles (ions, neutrals, radicals, atoms and molecules) are deposited onto a dedicated collector. The collector with the deposit is then transferred under ultra-high vacuum conditions to an analytical instrument (mainly static and dynamic SIMS).

If the deposit coverage on the collector is less than a monolayer, most of the deposited particles are surrounded by the same matrix, i.e. the collector material. Thus the Storing Matter technique reduces the matrix effect frequently encountered in SIMS analyses. At the same time, the sensitivity can be kept high by choosing a collector material that will optimize the subsequent SIMS analysis of the deposit. For example, a material with a high (or low) work function enhances the positive (or negative) secondary ion yields. In the case of organic samples, noble metal substrates are chosen to promote cationization.

I.3. (b) The Storing Matter prototype instrument

I.3. (b) i) General description

The Storing Matter prototype instrument developed at SAM[25] consists of 3 main sections (Fig. I-2):

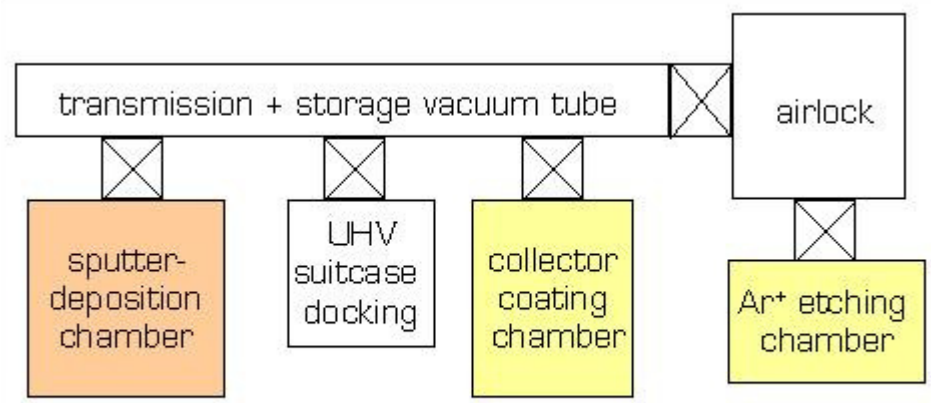

Fig. I-2: The different sections of the Storing Matter instrument.

- Collector preparation (sections in yellow in Fig. I-2): the collectors (e.g. Si wafers) can be etched by an Ar^+ ion beam in order to remove surface contaminants. In the collector coating chamber, thin metallic films are deposited by thermal evaporation under well-controlled conditions.
- The sputter-deposition chamber (section in orange in Fig. I-2) is equipped with a floating low-energy ion gun. The collector is positioned a few mm above the sputtered sample surface.
- Transfer and storage of the collectors (sections in white in Fig. I-2): the collectors can be transferred between the different parts of the instrument and to the analytical instruments without breaking the UHV conditions.

The following pages provide a more detailed description of each section of the prototype instrument.

I.3. (b) ii) The Argon etching chamber

The collector surface can be etched by a large uniform Ar^+ beam (diameter = 10 cm) in order to remove surface contaminations. The ion source (Kurt J. Lesker Company) delivers beam currents up to 2 mA at 25 eV and 67 mA at 1200 eV.

I.3. (b) iii) The collector coating chamber

In the collector coating chamber (Fig. I-3), metallic thin films can be deposited under well-defined conditions. Metal pellets of high purity (> 99.9%) are evaporated under UHV conditions (base pressure 10^{-9} mbar) and the evaporated material is deposited onto a substrate (generally cleaned silicon wafers).

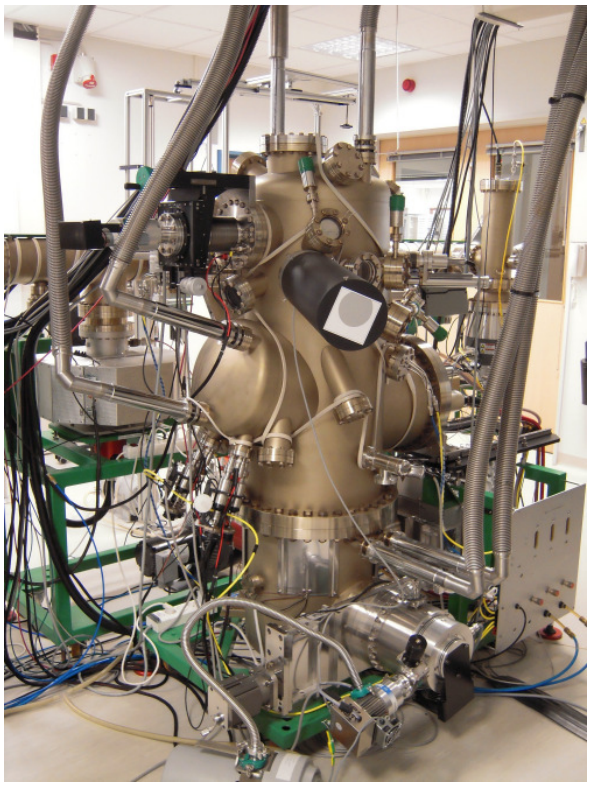

Fig. I-3: Global view of the collector coating chamber.

The collector coating chamber is equipped with several systems dedicated to the deposition of metallic layers:

- Metal pellets are brought to evaporation by an electron beam in a UHV Multi-Pocket Electron Beam Source (Model 568, Telemark). This method is called Electron Beam Physical Vapour Deposition (EB-PVD). An electron beam is generated by a filament and deflected towards one of 6 crucibles containing high purity metal pellets.
- Evaporation of the pellets can also be done in one of the 4 effusion cells (SEJ 25/40, Meca2000). Maximal temperatures are 1400 °C or 1700 °C (one high temperature effusion cell).
- 2 quartz microbalances (MAXTEK) are used for monitoring layer thickness and deposition rate.
- Reflection High-Energy Electron Diffraction (RHEED) gives real-time information about changes in the surface coverage by adsorbed particles and about crystallographic orientation and morphology. The source (RHEED 35 R, STAIB INSTRUMENTS) delivers a focussed electron beam (< 100 µm) that strikes the sample surface at a grazing angle. The incident electrons are diffracted by the surface atoms, and the diffraction pattern is detected by a CCD-camera and a phosphor screen (kSA 400, k-Space).
- Residual Gas Analyzer (RGA200, Stanford Research Systems): a small mass spectrometer (200 amu) monitors the concentrations of the component gases present inside the vacuum chamber.
- During the deposition, the sample stage can be rotated and heated (flash heating up to 1250 °C, heating during rotation up to 850 °C) in order to influence the growth mechanisms of the thin metallic films.

The evaporation sources (crucibles and effusion cells) are situated around 1m below the sample position, which makes it possible to obtain very

uniform deposits. Furthermore, the chamber is surrounded by a double wall that can be cooled by liquid nitrogen in order to improve the UHV conditions.

I.3. (b) iv) The sputter-deposition chamber

a. Sample stages

The sputter-deposition chamber contains two motorized high-precision sample stages (Fig. I-4). The lower stage holds the sample to be sputtered. It can be moved horizontally by a motor in X and Y directions. Furthermore, the sample position can be manually adjusted on the vertical axis and it can be rotated or slightly tilted. The position of the sample stage on the X- and Y-axes can be read from a sample stage controller with a precision of 1 µm (SPRITE HR2 stagecontroller joystick, Deben). It is possible to program linear movements of the sample stage at well-defined speeds.

The upper sample stage holds the collector. It can be translated by a high-precision motor along X, Y, Z axes and rotated around its own axis (SPRITE XYZR Meca2000 stagecontroller joystick, Deben). Rotation movements with a defined angular speed can be programmed.

During sputter-deposition experiments, the collector is placed 3-4 mm above the sample (Fig. I-4).

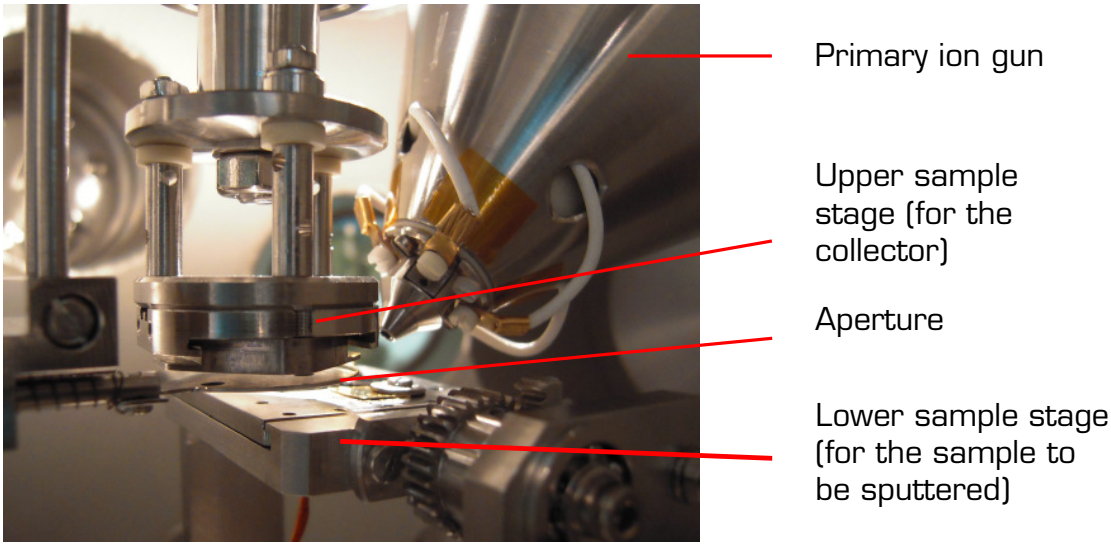

Fig. I-4: Position of the sample stages during sputter-deposition experiments.

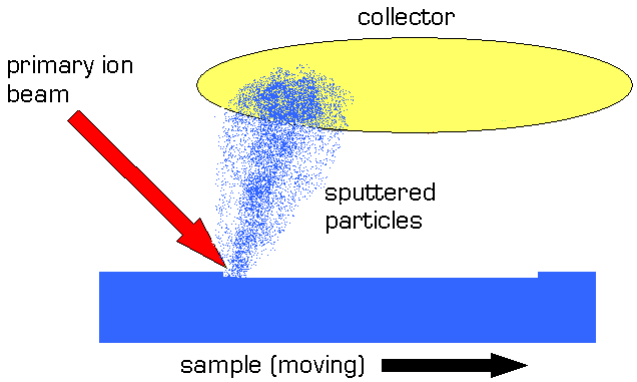

Fig. I-5: Experimental setup used for sputter-deposition of polymer samples under static bombardment conditions.

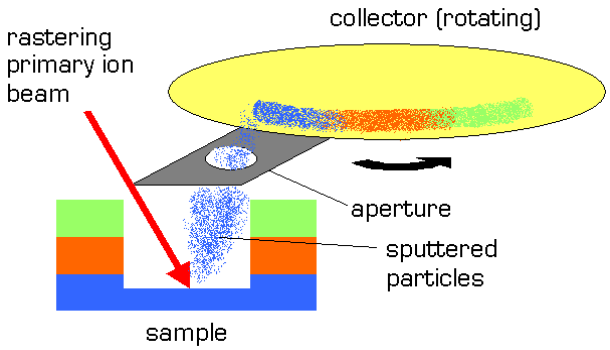

Fig. I-6: Experimental setup for making a depth profile of a multi-layered sample with the Storing Matter technique.

Two different experimental setups are used for sputter-deposition, depending on the sample type and the goal of the experiment:

- Moving the sample stage during sputter-deposition is useful if the primary ion fluence should be kept low (Fig. I-5). Particles emitted from different areas of the sample are deposited on the same spot on the collector. This setup is mainly used for homogenous organic samples for which the primary ion fluence needs to be below the static limit ($<10^{13}$ ions/cm^2) in order to preserve molecular information.
- For depth profiling with the Storing Matter technique, the sample stage is not moved but the collector is rotated during sputter-deposition. This makes it possible to transform depth information

from the sample into lateral information on the collector (Fig. I-6). In this case, an aperture of 0.5 mm in diameter is placed 1 mm below the collector (Fig. I-4). The exact position of this aperture with respect to the impact point of the primary ion beam on the sample needs to be carefully adjusted so that the maximum of secondary particles will pass through it.

b. The floating low-energy ion gun

The floating low-energy ion gun was designed to operate at impact energies ranging from 100 eV to 10 keV with beam currents up to several hundred nA and spot diameters in the µm range[26]. The impact angle of the beam on the sample is 45°. The primary ions (Ar^+, Xe^+ or O_2^+) are generated inside a cold-cathode duoplasmatron (Cameca) and accelerated by an extraction electrode. The ions enter into a flight tube, which is equipped with different optical components (lenses, deflectors, Wien filter). The flight tube is at high-voltage when the gun is operated in the floating mode. For positive ions of 200 eV (source at 200 V, target at ground) for example, the flight tube is floated to –7300 V.

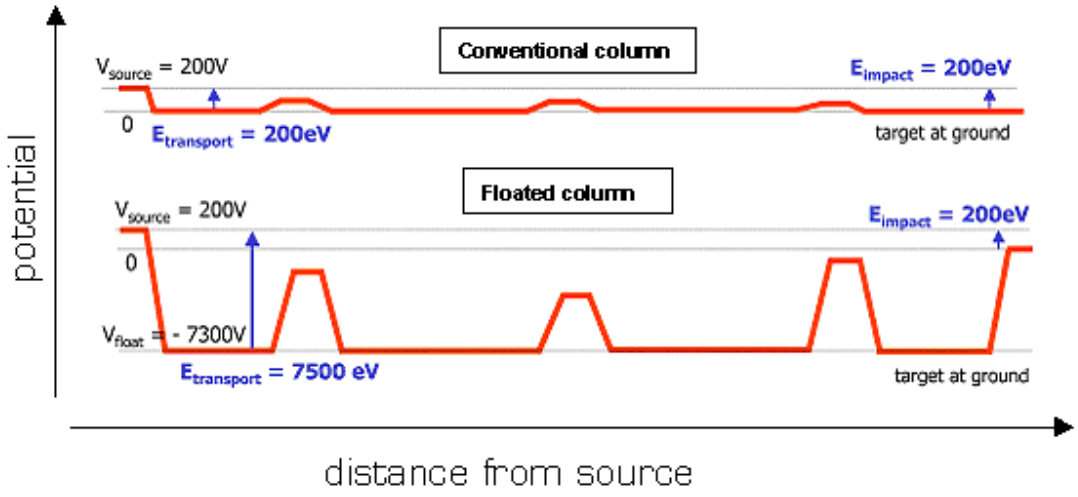

Fig. I-7: Potential drawings of a traditional column and a floating column. Adapted from [26].

The advantage of using the floating mode for low impact energies is that the transport energy stays high (7.5 keV in the case of the example in Fig. I-7). A

low transport energy *E* would lead to a high relative energy spread *(ΔE/E)*, *ΔE* being the energy spread of the ions at the exit of the source. The chromatic aberrations induced by the different elements of the column would increase drastically:

$$d_c = C_c \cdot \alpha \cdot \frac{\Delta E}{E} \quad \text{(Equation 1)}$$

where d_c is the diameter of the disk of least confusion induced by chromatic aberrations, C_c is the chromatic aberration constant depending on the ion optical system, α is the half-angle of the beam.

Furthermore, space charge repulsion during low energy beam transportation causes the beam to diverge, and the brightness of the ion source (and hence the ion current density) is proportional to the extraction voltage.

c. Raster controller and secondary electron detector

The ion beam is rastered over the sample surface by a set of 4 deflector plates (raster voltages up to 440 V, corresponding to a raster area of 1.5 · 1.5 mm^2 at 10 keV impact energy). The rastering of the ion beam is synchronized with a secondary electron/ion detection system (IGM 300, Ionoptika). Secondary electron imaging of calibration grids gives information about the spot size, which is in the µm-range for an impact energy of 10 keV.

d. Electron gun

The sputter-deposition chamber is also equipped with a Kimball Physics EMG-4212 electron gun, which may be used for charge compensation during sputtering of insulating samples or for SEM imaging in combination with the secondary electron detector installed on the same chamber. It can be operated at energies up to 30 keV.

e. Secondary ion detector

A secondary ion detector can be mounted to the sputter-deposition chamber for angular distribution measurements of the emitted secondary ions. Since the secondary ions have energies of only some tens of eV, they need to

be accelerated for an efficient detection. However, an electrostatic field would strongly distort the angular distribution of the secondary ions. Thus the housing and the entrance slit of the developed detector are grounded, and it is only inside the detector that the ions are successively post-accelerated by a series of three electrodes (Fig. I-8).

For angular distribution measurements, the detector is translated on an axis parallel to the sample surface. The ions detected for a given detector position correspond to a certain emission angle.

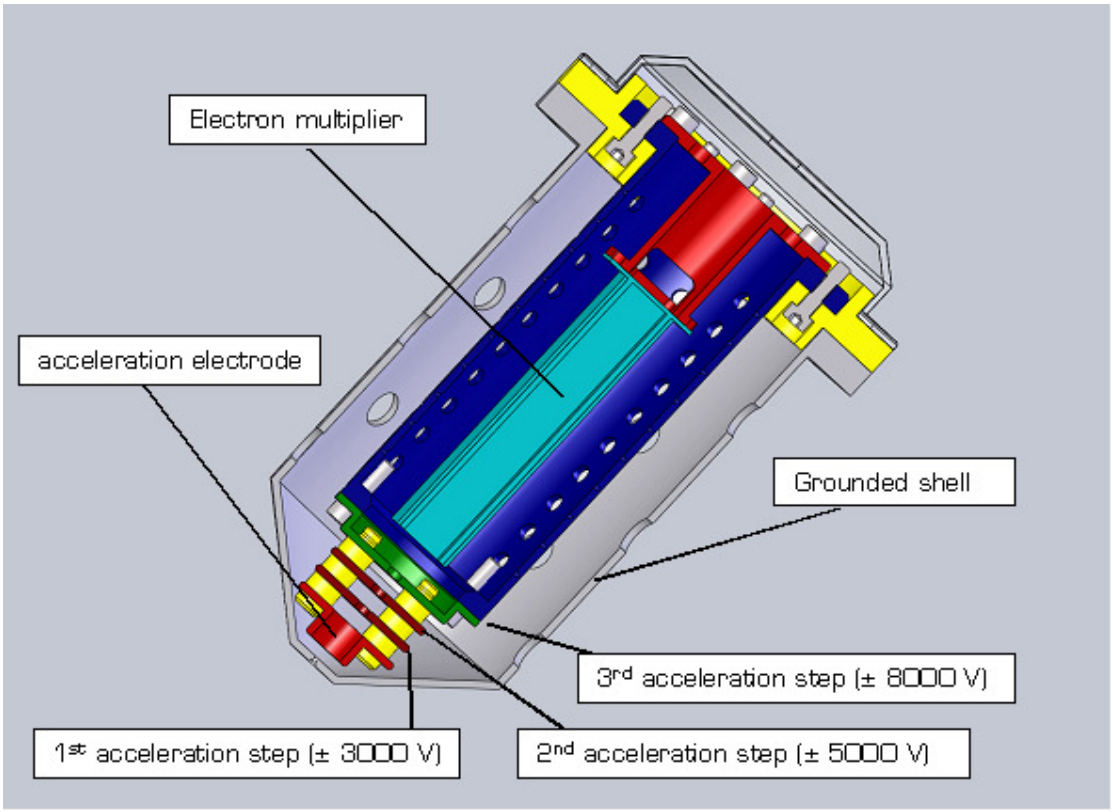

Fig. I-8: Schematic drawing of the secondary ion detector.

I.3. (b) v) Collector transfer inside the Storing Matter prototype and to analytical instruments

One of the most important criteria for the design of the prototype instrument was the cleanliness of the collectors. The entire Storing Matter process and the analysis step take place at pressures between 10^{-10} and 10^{-8} mbar, which greatly reduces the adsorption of air contaminants.

A specially designed cart with 10 sample positions (Fig. I-9) can be moved by a magnet through the 5 m long UHV transfer tube of the Storing Matter instrument. The collectors are introduced into the Ar^+ etching chamber, the collector coating chamber, the sputter-deposition chamber or the UHV suitcase by transfer rods.

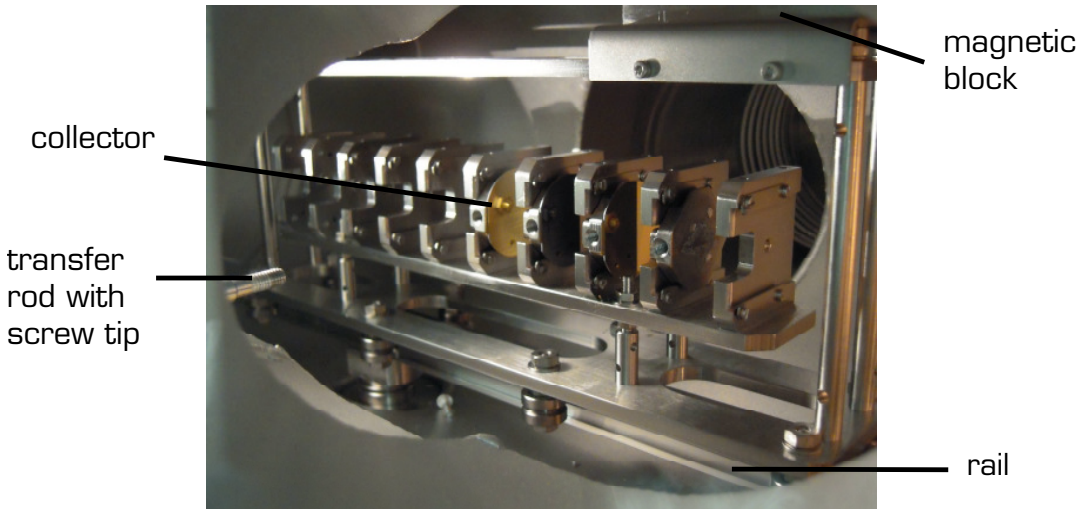

Fig. I-9: Cart for collector transfer between the different parts of the Storing Matter instrument.

For the transfer of the collectors to analytical instruments (static or dynamic SIMS, XPS, etc), three specially developed UHV suitcases (pressure: 10^{-9} mbar) with 5 sample positions are available at SAM (Fig. I-10)[27]. All analytical instruments at SAM (except TEM and SEM) are equipped with dedicated docking stations and universal sample-holders.

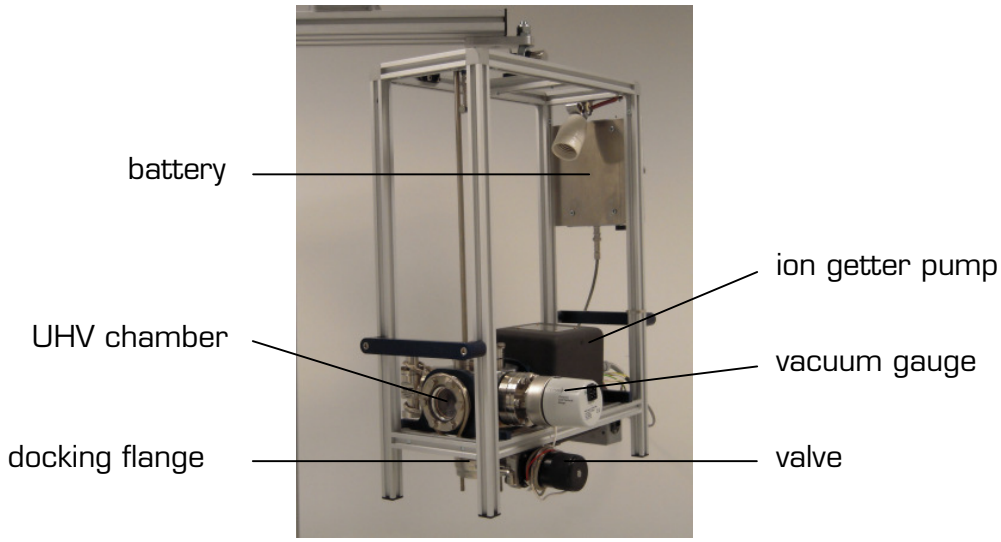

Fig. I-10: UHV suitcase for collector transfer between different instruments.

Chapter II. SIMS analysis of organic materials

SIMS is a very surface sensitive technique that provides fast and detailed molecular information about a large variety of materials. For organic samples, mainly Time of Flight SIMS (TOF-SIMS) instruments are used. This chapter deals with instrumental and fundamental aspects of TOF-SIMS and describes the ionization/fragmentation mechanisms leading to the emission of molecular secondary ions. In order to reduce the accumulation of chemical damage in organic materials, the mass spectra are generally acquired with a low primary ion fluence. This approach is called static SIMS (S-SIMS).

The two last sections of this chapter present experimental strategies dedicated to improving different aspects of a TOF-SIMS analysis: for example, metal-assisted SIMS (MetA-SIMS) enhances the cationization of organic fragments and parent-like molecules, and the development of cluster primary ion sources has made molecular depth profiling of many organic materials possible.

II.1 Principles of TOF-SIMS

II.1. (a) Primary ion beam

One of the main challenges in SIMS analyses of organic samples is the retention of molecular information that is necessary for an unambiguous identification of the analyzed substance(s). Thus the primary ion conditions need to be particularly soft in order to reduce the fragmentation mechanisms that occur during and after bombardment. In a TOF-SIMS instrument, this is mainly achieved by using a pulsed primary ion beam with a current of typically a few pA. Since the pulses are very short (~ 1 ns), the sample surface is exposed to the primary ion beam only during a small fraction of the acquisition time of a mass spectrum, and the probability of hitting the same atomic site twice during

the analysis is very low. The primary ion fluence (also called dose density) is defined as the number of impinging projectiles per surface area[28]:

$$d = \frac{It}{eA} \qquad \text{(Equation II-1)}$$

where I is the primary ion current, t the bombardment time, e the elementary charge (e = 1.6 · 10^{-19} C), and A is the area of the bombarded surface. Considering that typical surface atomic densities are of the order of 10^{15} atoms/cm^2, a fluence of 5 · 10^{12} ions/cm^2 means that only 0.5% of the surface atoms are hit by a projectile.

Commonly used primary ions include Ar^+, Ga^+, SF_5^+, C_{60}^+, Bi_n^+, Au_n^+ etc. The impact energy is typically around 5 - 25 keV. If insulating samples are analysed, a pulsed low energy electron flood gun can be used for charge compensation[29].

II.1. (b) Mass separation of the secondary ions

The secondary ions (either positive or negative) are accelerated to the same kinetic energy over a short distance by an extraction voltage of typically 2 kV. Their kinetic energy is given by the following equation:

$$E_{kin} = \frac{mv^2}{2} = zeV \qquad \text{(Equation II-2)}$$

where m is the mass of the considered ion, v its velocity, z the charge, e the elementary charge, and V the potential difference in the acceleration zone.

After being accelerated, the secondary ions fly through a long field-free drift region. The velocity of a charged particle is given by:

$$v = \sqrt{\frac{2zeV}{m}} \qquad \text{(Equation II-3)}$$

Mass separation is possible at this stage since a heavier ion needs more time to travel through the drift region:

$$t = L \cdot \sqrt{\frac{m/z}{2eV}} \qquad \text{(Equation II-4)}$$

t is the flight time of an ion and *L* is the length of the drift tube (typically 2 m). At the end of the drift region, the ions are post-accelerated (5 - 10 kV) towards a detection system composed by a channelplate, a scintillator and a photomultiplier. The secondary ion intensities are measured as a function of the flight time, and a mass spectrum is obtained by converting this time scale to a mass/charge *(m/z)* scale.

II.1. (c) Mass resolution

The mass resolution is defined by $m/\Delta m$, where Δm is the full width at half maximum (FWHM) of the considered peak. The width of a peak corresponding to a given *m/z* ratio is mainly determined by the pulse length of the primary ions and by the kinetic energy distribution (KED) of the secondary ions. A narrowing of the KED can be obtained by using a reflector to compensate for energy differences of the secondary ions. The reflector (also called "ion mirror") consists of circular electrodes that generate a repulsive electric field in which ions with identical *m/z* ratio but slightly different kinetic energies follow different trajectories, so that they will finally reach the detector at the same time. This principle is called achromatic filtering. Mass resolutions higher than 10000 can be achieved with the currently available instruments.

II.2 TOF-SIMS instruments used for this work

II.2. (a) The TOFIII instrument by ION-TOF

The TOFIII instrument (ION-TOF GmbH, Münster, Germany) (Fig. II-1) is equipped with an electron impact ion gun producing Ar^+ primary ions, a Ga^+ liquid metal ion gun (LMIG), a Cs^+ sputter gun, and a pulsed low-energy electron beam for charge compensation.

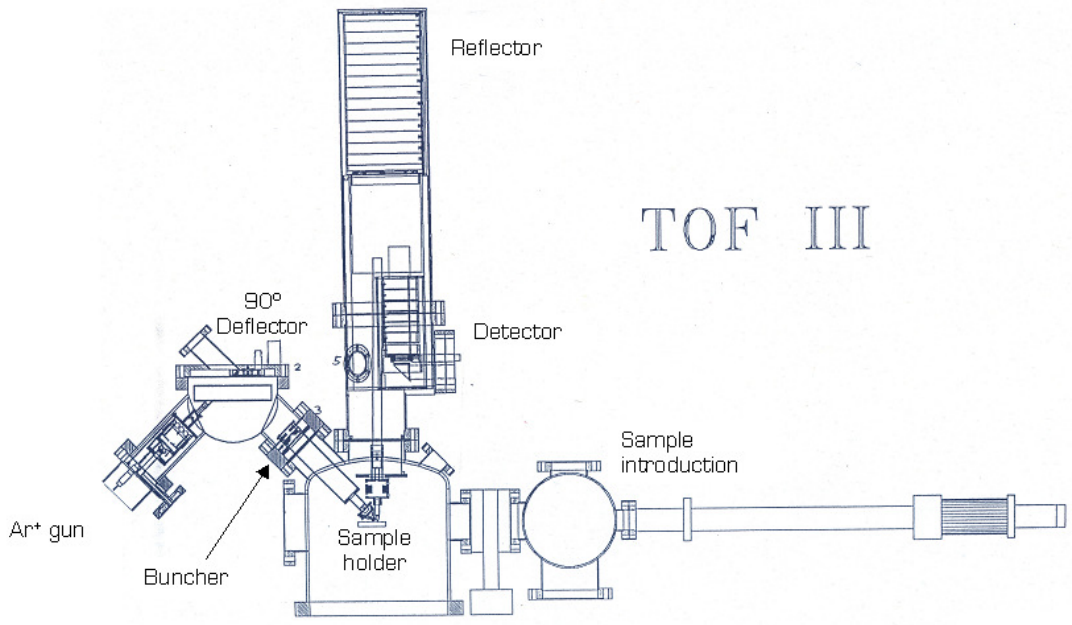

Fig. II-1: Schematic view of the TOFIII instrument by Ion-TOF. Only the Ar^+ gun is displayed. Figure adapted from Ion-TOF GmbH.

The majority of mass spectra acquired in the frame of this work were obtained with Ar^+ primary ions. A continuous Ar^+ beam is accelerated and focussed onto a deflection unit. Here, discrete packages of primary ions are formed and deflected by 90°. These pulses are bunched down to 2 - 3 ns by an electro-dynamic field. The pulsed beam is then focussed and rastered over a small area of the sample surface (100 · 100 μm^2). For this work, the Ar^+ gun was used with 10 keV impact energy and a 45° impact angle with respect to the sample normal. The pulsed ion current was ~0.5 pA and the cycle time was set to 150 µs. The secondary ions were extracted at 90° from the sample surface with a 2 keV extraction potential and then post-accelerated to 5 - 10 keV in front of the detector. Mass resolutions up to 10000 are achievable with this instrument.

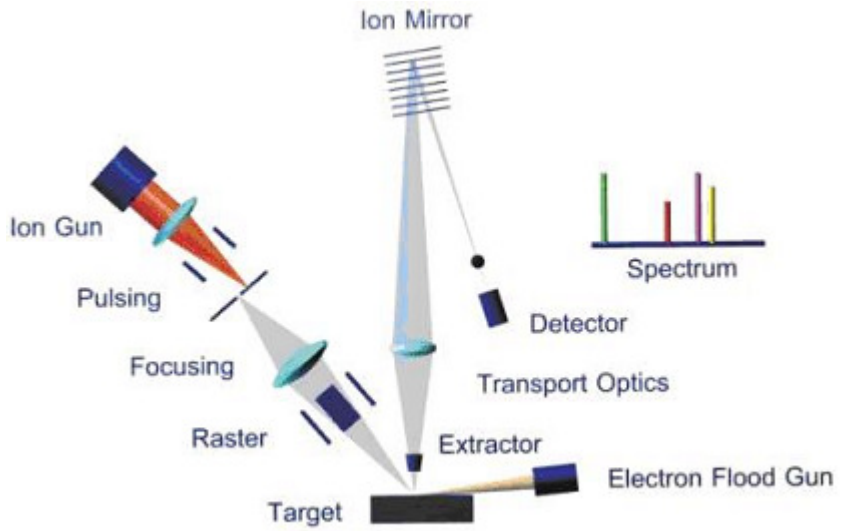

Fig. II-2: Schematic illustration of the working principle of a TOF-SIMS instrument. Figure from ION-TOF GmbH.

The TOFIII instrument is equipped with a docking station for the UHV suitcase and a universal sample holder for the transfer of the collectors used in the Storing Matter instrument. The base pressure in the analysis chamber is approximately $5 \cdot 10^{-9}$ mbar.

II.2. (b) The TOF5 instrument by ION-TOF

A TOF5 instrument (ION-TOF GmbH, Münster, Germany) is available at SAM only since April 2011, therefore only a limited number of analyses could be carried out with this instrument. It is equipped with a cluster LMIG (liquid metal ion gun) with a Bi source, a dual source column with a C_{60} and a Cs source, and a flood gun for charge compensation. Heating and cooling of the sample stage is possible for temperatures ranging from –130 to +600 °C. The mass resolution achieved by the TOF analyzer is higher than 11 000 (FWHM) at m/z=29 for Bi^+ primary ions. The base pressure inside the analysis chamber is approximately $5 \cdot 10^{-10}$ mbar. The instrument is equipped with a docking station for the UHV suitcase and a universal sample holder for the transfer of the collectors used in the Storing Matter instrument.

For this work, Bi^+ (25 keV impact energy), Bi_3^+ (25 keV) and C_{60}^+ (10 keV) primary ions were used. The pulse widths were bunched down to less than 1 ns. The impact angle of all the ion guns is 45° in the TOF5 instrument and the secondary ions are extracted at 90° from the sample surface with a 2 keV extraction potential.

II.3 Fundamental aspects of molecular secondary ion emission

II.3. (a) Sputtering by ion bombardment

Ion irradiation of a solid surface leads to a series of complex interactions involving the primary ions as well as target particles in the region surrounding the impact point. Depending on the parameters of the primary ion beam and the characteristics of the bombarded solid, these phenomena may lead to sputtering, i.e. the ejection of matter from the sample surface.

II.3. (a) i) Cascade regimes

If the impact energy is high enough, the primary ion penetrates into the solid and undergoes a series of collisions with target atoms. At a certain depth (typically 20 - 50 nm)[30], the projectile has lost all its kinetic energy and remains implanted in the target. The implantation depth of the primary ion and the size of the perturbed volume depend on the bombardment parameters (impact energy, incidence angle, primary ion type and atomic mass) as well as on the nature of the target (atomic mass, density, cristallinity, topography).

The stopping power is defined as the energy lost by length unit in the target and can be decomposed into a nuclear and an electronic contribution (energy loss resulting from elastic binary collisions of the projectile with nuclei, or from electronic excitations). In the case of keV primary ions, the nuclear stopping regime is the predominant mechanism for energy deposition[31].

By colliding with target atoms, the projectile creates recoil atoms that may in turn generate secondary recoils and so forth. Based on the mechanism

of energy deposition in the near-surface region, three sputtering regimes (depending mainly on the impact energy and the nature of the projectile) can be distinguished[32]:

- In the *single-knockon regime*, only a small number of target atoms are set in motion and secondary particles are emitted by a direct recoil process.
- The concept of the *linear cascade regime* was developed by Sigmund[30,32] and Thompson[33] and is characterized by successive binary elastic collisions in the target, leading to a diffusion of the primary ion energy in the near-surface region. In this regime, the collision cascades resulting from different projectile impacts are separated in space.
- This is not the case in the *spike regime*, where overlapping collision cascades generate a considerable volume of excited particles.

Among these models, the linear cascade regime is best suited to describe the emission of secondary particles in static SIMS with keV primary ions where the use of very low primary ion fluences prevents an overlapping of different collision cascades. If an atom or molecule close to the surface receives enough energy and outwardly directed momentum from the collision cascade, it is ejected from the target. The minimum energy required for particle ejection is called the threshold energy for sputtering. Its values are typically some tens of eV and depend on the surface binding energy as well as on the ion beam parameters[34].

The concept of linear collision cascade sputtering described above was initially developed for atomic solids, but it can be adapted to describe the emission of fragments and intact molecules from molecular solids[35]: during the first stages of the collision cascade, the impacting primary ion causes fragmentation by breaking bonds in the directly hit molecules. These fragments then collide with their neighbour molecules and possibly cause these to break up too. As soon as the kinetic energy of a generation of recoils becomes

comparable to the binding energies (i.e. a few eV), intact molecules can be set in motion without being fragmented.

II.3. (a) ii) Sputter yields

The sputter yield is defined as the number of sputtered atoms divided by the number of primary ions:

$$Y = \frac{\text{number of sputtered atoms}}{\text{number of primary ions}} \qquad \text{(Equation II-5)}$$

The sputter yield depends on several parameters related to the primary ion beam (energy, incident angle, mass and atomicity) and the sample characteristics (atomic mass, chemical bonds, cristallinity, density and topography).

MD (molecular dynamics) simulations by Delcorte illustrate how the collision cascade inside a PS tetramer solid is affected by an Ar^+ projectile's impact energy (Fig. II-3)[36]. With 10 keV impact energy a large sample volume is perturbed, and the tracks of several recoil atoms intercept the sample surface, which results in sputtering. For an impact energy of 1 keV, there are less recoils, their tracks are shorter, and sputtering is much less efficient.

The sputtering yield initially increases with the impact energy, reaches a maximum somewhere between 10 and 100 keV, and then decreases again because the projectile's energy is deposited too deep into the sample surface[37] (Fig. II-4). The impact energy corresponding to the maximal sputtering yield of a material depends on the mass of the primary ion: this maximum is located at lower energies for small primary ions because they penetrate deeper inside the target for a given impact energy. For the same reason, sputtering is more efficient for heavier primary ions. The penetration depth and thus the sputtering yield are also affected by the incident angle of the projectile with respect to the surface normal. The yield increases with the incident angle up to a value situated between 55° and 85° and drastically decreases for more grazing angles where an important part of the primary ion energy is reflected instead of being deposited into the near-surface region of the target[34] (Fig. II-5). The critical incident angle above which the sputtering yield decreases is smaller for low energy primary ions[38].

Since the sputtering yield depends strongly on the density of energy deposited in the near surface region from which particles can be ejected, it is obvious that in addition to the primary ion beam parameters mentioned above, several characteristics of the target itself also play an important role. In general, the denser the target material (i.e. high atomic mass, high atomic density, close-packed structures for crystalline materials), the higher the sputtering yield for a given set of primary ion parameters.

II.3. (a) iii) Characteristics of the emitted particles

The depth of origin of the sputtered particles depends mainly on the atomic density, but the majority of sputtered particles originate from the first monolayer of the target[39-41]. Consequently, SIMS is an extremely surface sensitive technique.

In the frame of the linear collision cascade theory, a cosine-like angular distribution of the emitted particles is predicted (for non-grazing incidence angles):

$$\frac{dY}{d\Omega} \propto \cos^n \alpha \qquad \text{(Equation II-6)}$$

α is the polar angle with respect to the surface normal, Ω is the solid angle of the emitted species, and n is generally between 1 and 2 [42]. At low impact energies, where binary collisions are the main sputtering mechanism (knockon regime), this distribution becomes under-cosine[43]. Fig. II-6 shows the angular distribution of Al^+ ions sputtered from an Al target by 8 keV Ar^+ ions with different incident angles with respect to the target normal. For oblique incidence angles, the preferential emission direction is closer to the specular direction.

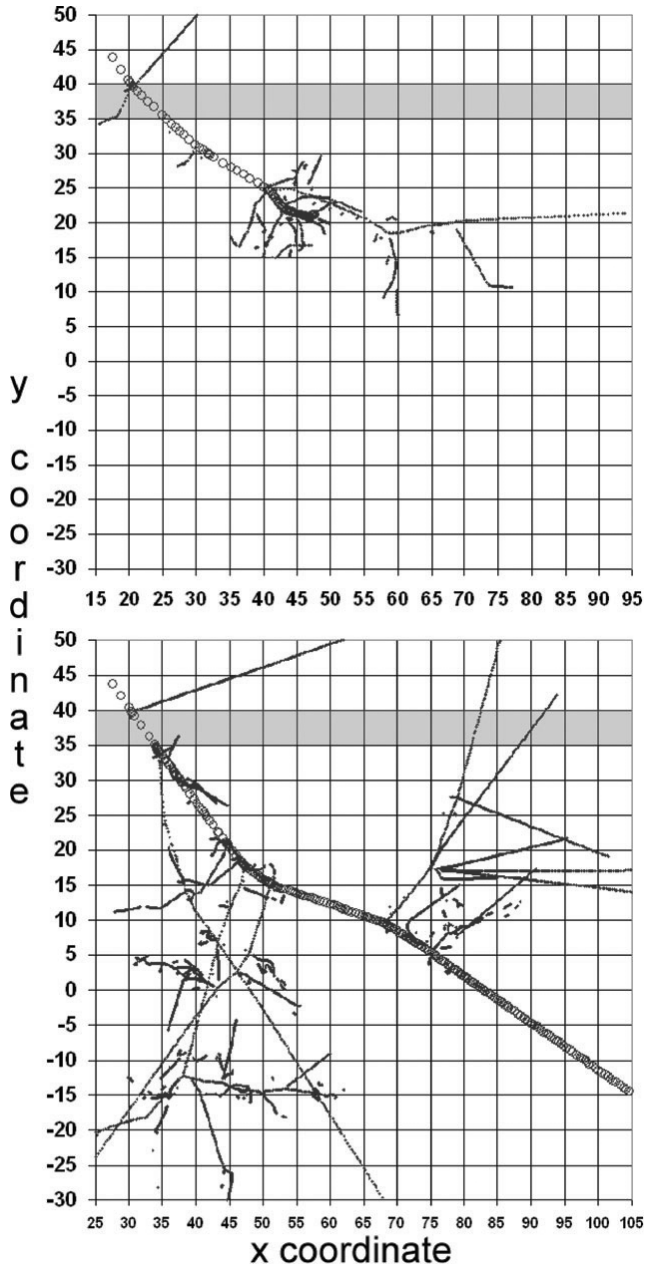

Fig. II-3: Collision trees obtained for 1 keV (top) and 10 keV Ar^+ (bottom) bombardment with 45° impact angle of a PS tetramer solid. The tracks of the projectile atoms and recoils with more than 10 eV kinetic energy are shown for times up to 200 fs. Each square corresponds to an area of 5 · 5 $Å^2$. The gray bar represents the sample-vacuum interface. Figure taken from [36]33.

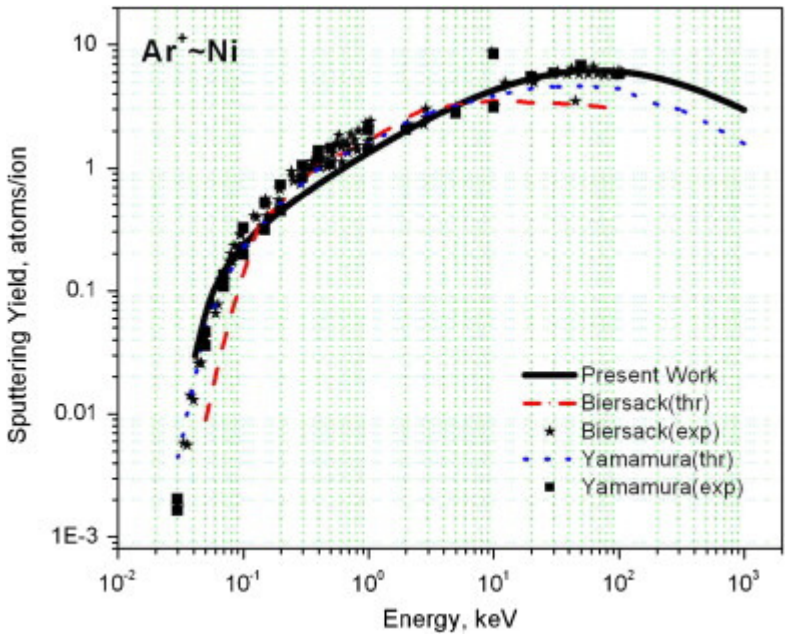

Fig. II-4: Evolution of the sputtering yield of Ni as a function of the impact energy of Ar^+ primary ions at normal incidence from different experimental datasets and theoretical models. Figure from [44].

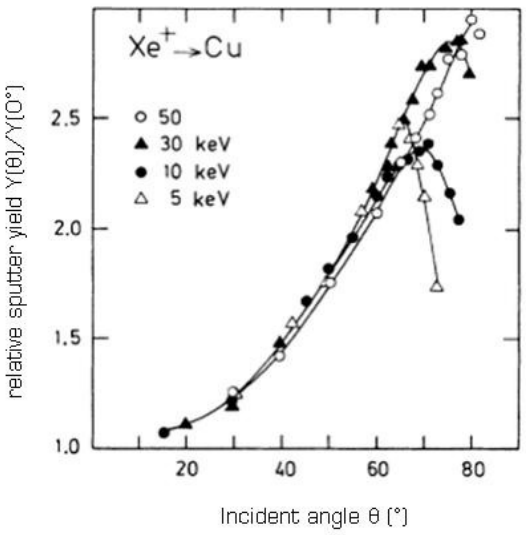

Fig. II-5: Evolution of the relative sputtering yield of a Cu target with the incident angle of Xe^+ primary ions with different impact energies. Figure from [38].

In the linear cascade regime, the kinetic energy distribution (KED) of sputtered atoms is given by the Thompson law[32,33] and is generally characterized by a steep increase for low energies, a maximum at a value of a few eV (corresponding approximately to half of the surface binding energy U_s), and a high energy tail that decreases proportionally to E^{-2}:

$$N(E)dE \propto \frac{E}{(E+U_s)^{3-2m}}dE \qquad \text{(Equation II-7)}$$

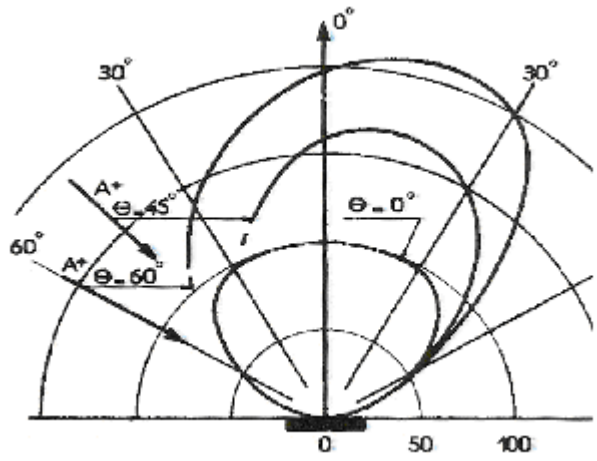

Fig. II-6: Angular distribution of Al^+ ions sputtered from an Al target by 8 keV Ar^+ ions with incident angles θ of 0°, 45° and 60° with respect to the surface normal. Figure from [45].

The value of the parameter m depends on the primary ion energy. For cluster and molecular secondary ions, the energy distributions are narrower, the maxima are situated at lower energies, and the high-energy decrease is sharper[42].

KED measurements of sputtered atoms, molecules or ions are a useful tool to obtain information about sputtering and/or ionization processes.

II.3. (b) Ionization and fragmentation mechanisms

Among the sputtered particles, only less than 1% is ionized. Since only this fraction is accessible by SIMS analyses, it is important to understand the mechanisms leading to the ejection of fragment or molecular ions. A typical S-SIMS mass spectrum of a polymer contains a "fingerprint region" with atomic and small fragment ions, the intermediate mass range contains larger fragment ions or repeat units, and the high mass range consists of intact parent-like molecular ions. A realistic model for molecular ion formation should thus account for these 3 regions.

A model that describes atomic ion formation from materials with (partially) ionic bonding (i.e. salts or metal oxides) is the bond-breaking model proposed by Slodzian[46]: the atoms leave the surface in a neutral but excited and auto-ionizing state and may become ionized via an Auger type de-excitation. The nascent ion-molecule model[47,48] predicts that atomic and molecular fragment ions are formed by dissociation of neutral fragments above the surface.

The first model that was especially dedicated to the explanation of molecular ion emission in static SIMS was Benninghoven's precursor model that was based on mass spectra of amino acids deposited on different metal substrates[49]. This model supposes that preformed ions are already present in the sample before ion irradiation. Around the impact point of the projectile, an energy gradient is formed at the sample surface. The molecules that are very close to the track of the projectile are strongly fragmented, and only atoms or small fragments are emitted from this area. Further away, close to the borders of the excited area, the emission of large preformed molecular ions is possible (Fig. II-7).

The desorption-ionization model developed by Cooks et al.[50,51] predicts that, in addition to the contribution of preformed ions, the mass spectra also contain peaks corresponding to ions formed in the gas phase after ejection, i.e. either in the selvedge (by ion-molecule reactions or ionization by secondary electrons) or via metastable decay reactions in the field free region of the instrument.

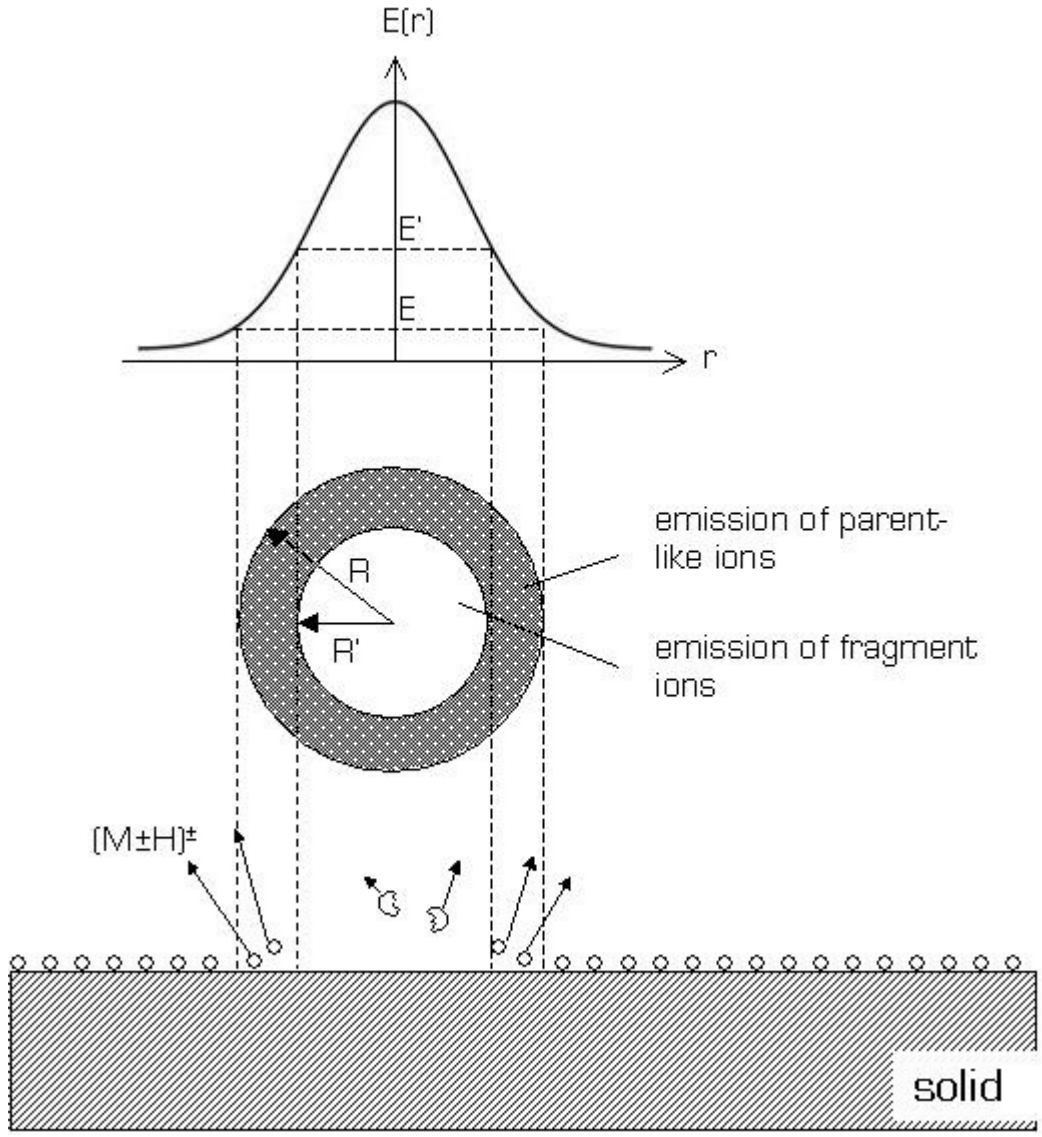

Fig. II-7: Schematic view of the precursor-model for parent-like emission. The function E(r) represents the average energy E transferred to a surface species by the collision cascade at a distance r from the impact point. In the region surrounding the projectile impact point (r<R'), only atoms or small fragments are emitted. Further away (R'<r<R), intact molecular ions can be ejected. Figure adapted from [49].

The contribution of metastable decay reactions to a mass spectrum can be determined by kinetic energy distribution (KED) measurements[52-55]. A molecular secondary ion ejected with an excess of internal energy breaks up into a smaller fragment ion and a neutral particle (unimolecular dissociation). The kinetic energy of the parent ion is then shared between these two species. The newly generated fragment ion will thus be detected with less kinetic energy

than a fragment ion that was formed directly at the surface. The probability of a secondary ion to undergo metastable decay depends on its internal energy content, which is determined by the efficiency of the recoil atoms to convert their translational energy to secondary ion vibrational energy. The contribution of metastable decay reactions to the total intensity in the mass spectrum can be as high as 50% for some secondary ions[53,54].

II.4 Matrix effects

In SIMS, the intensity of a secondary ion is not only related to the concentration of its precursor in the analyzed volume, but it also strongly depends on the matrix, i.e. the chemical environment in the sample. An example of a matrix effect in PS/PMMA blend samples is shown in Fig. II-8: the absolute intensity of the $C_8H_9^+$ ion, which is characteristic for PS, with the PS content in the sample does not increase linearly with the PS content in the sample.

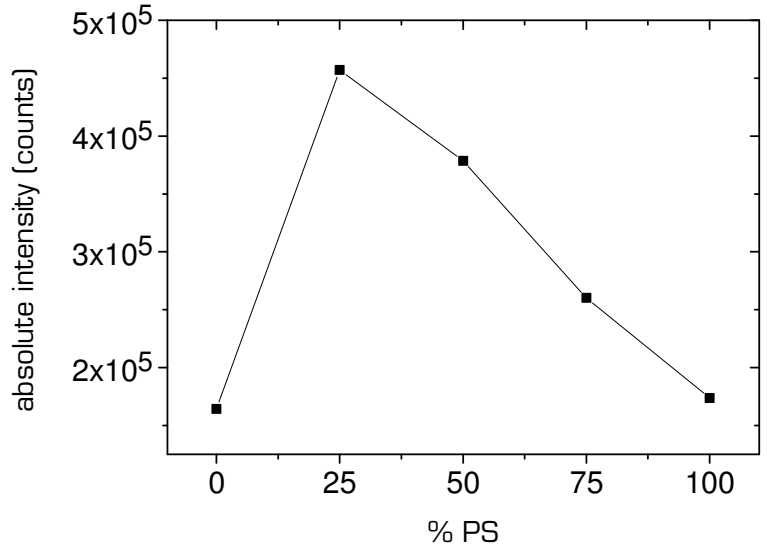

Fig. II-8: Absolute intensity of the $C_8H_9^+$ peak (m/z=105) as a function of the PS content of PS/PMMA blend samples.

Matrix effects in SIMS can be classified into sputter-induced and ionization-induced matrix effects[56]. In the case of molecular secondary ions emitted from multi-component organic samples such as polymer blends or

copolymer systems, an additional contribution by different fragmentation mechanisms needs to be considered. For example, in styrene-butadiene copolymers the characteristic peaks are not unique to one of the components, but they can be formed via different fragmentation pathways from different precursors[57]. This kind of matrix effects in polymer samples can be due to short-range interactions between directly adjacent functionalities (matrix effect of first type, MEI) or long-range interactions between non-covalently bonded groups (matrix effect of second type, MEII)[58]. An example of a MEII is hydrogen bonding between two different functional groups. Hydrogen transfer is one of the main mechanisms that cause this type of matrix effects[59-61]. Vanden Eynde showed that short-range matrix effects can be generated by different end groups of PS chains[62]. In the case of random copolymers, a MEI is often observed: the suppression or enhancement of a characteristic fragment ion of one of the comonomers is related to the statistical distribution of different triad sequences[63].

II.5 Organic secondary ion yield enhancement by ME-SIMS and MetA-SIMS

It has been shown already some time ago that analyzing a thin organic layer on a metal substrate yields high secondary ion intensities, especially for unfragmented parent-like ions[49,64]. The main mechanism at the origin of this observation is an increased near-surface deposition of the projectile's energy due to the high stopping power of the metal substrate, resulting in a higher ejection efficiency of the organic adsorbates as compared to the corresponding bulk organic sample[65]. Metal atoms set in motion by the collision cascade interact collectively with a large organic fragment, thus increasing the chance for the latter to be ejected without fragmentation[66-69].

This method can be linked to a general approach called matrix-enhanced SIMS (ME-SIMS), which is based on the more or less controlled exploitation of matrix effects in view of maximizing the secondary ion intensities[70].

A similar and more recently developed approach is metal-assisted SIMS (MetA-SIMS), which consists in depositing a small amount of metal (most commonly Au or Ag) onto an organic sample prior to a static SIMS analysis[71-74]. Usually the metal is deposited by gas phase evaporation or sputter-coating, or a sub-monolayer of metal nanoparticles is deposited onto the sample[75]. In comparison with pristine organic samples, positive secondary ion yield enhancements of more than two orders of magnitude have been observed for (quasi-) molecular and fingerprint fragment ions[72]. Furthermore, the metallic coating reduces charging effects during the SIMS analysis[72], which makes it possible to obtain molecular information even from thick polymer samples without using an electron flood gun that might significantly damage the sample[76,77]. MetA-SIMS can also be used to improve the sensitivity in molecular imaging of organic surfaces[72].

A comparison of the efficiency of different metals for MetA-SIMS is not straightforward since the magnitude of yield enhancement depends on the sample[72,74,78], on the considered secondary ion[73], on the primary ion[65,79-82], and on the layer thickness and the surface coverage of the metallic layer on the organic material[79,83].

A significant added value in MetA-SIMS as compared to traditional S-SIMS measurements of organic samples is the possibility of detecting metal-cationized fragments (positively charged cluster ions consisting of one or more metal atoms and an organic fragment)[78,84]. The formation of such organometallic complexes can be explained by an interaction between the d-orbitals of the metal atom (or ion) and the π-orbitals in the organic molecule. Grade and Cooks already observed the attachment of metal ions to organic molecules in 1978[85]. In MetA-SIMS mass spectra, the intensities of metal-cationized ions are often found to be higher than those of the corresponding organic ions[74].

It was shown that small amounts of noble metals deposited onto organic substrates form nano-islands on the surface[81,83] because the binding forces among the metal atoms are stronger than those between a metal atom and the organic material[86]. There seems to be either a diffusion of metal particles

into the bulk or a migration of small organic molecules over the metal clusters[71]. The high stopping power of the metal islands and the resulting increase in near-surface energy deposition by the primary ion enhance the efficiency of molecular ejection. It has been shown in recent molecular dynamics (MD) simulations that the projectile's efficiency in desorbing a large quantity of organic matter strongly depends on the position of its impact point with respect to the metal islands[87,88]. Therefore the interfacial area is believed to be a crucial parameter in MetA-SIMS experiments[89]. In this context it is important to mention that very different trends for yield enhancement have been observed with mono- and polyatomic projectiles (see next section). In addition to changes in sputtering mechanisms before and after metal deposition, the ionization efficiencies are also affected, probably by changes in work functions and because the metal plays the role of an external ionizing agent[71].

II.6 Effect of the primary ion type on organic secondary ion emission

During the last decade, cluster polyatomic primary ions such as C_{60}^+, Bi_3^+, Au_n^+ or more recently Ar_n^+, have caused an increasing interest in the organic SIMS community. The use of cluster projectiles for a wide range of static and dynamic SIMS applications is mainly due to higher sputter yields compared to monatomic beams and a decreased tendency to create chemical damage in organic samples. Molecular depth profiling has become possible for many polymers and organic materials.

The increase in sputter yield with clusters is non-linear, i.e. the yield per atom is higher for cluster primary ions than for monoatomic projectiles[90-93]. This may be explained by the near-surface energy dissipation in the solid. When a cluster projectile hits the sample surface, it breaks up into its constituting atoms, each of them keeping a fraction of the initial energy. A C_{60}^+ ion accelerated to 15 keV is thus equivalent to 60 carbon atoms with 250 eV per atom. Compared to the impact of a monoatomic ion with 15 keV impact energy, more collision cascades are generated and they extend less deep into

the substrate, creating a high energy density region (collisional spike regime) in the near-surface region surrounding the impact point[36,94].

In the case of an atomic projectile, a significant fraction of the energy is wasted because it cannot contribute to the sputtering of sample material, but it rather damages the chemical structure in the sub-surface region. Delcorte simulated collision cascades caused by Ar^+ and C_{60}^+ impacts with 45° incident angle in a PS tetramer solid[36]. In the case of 10 keV C_{60}^+ bombardment the collision tree is very dense and located in the near-surface region, while for Ar^+ much less recoil atoms are generated and only few of them reach the sample-vacuum interface.

The increase in secondary ion yields from thick organic samples when clusters such as Bi_3^+, SF_5^+ or C_{60}^+ are used instead of atomic primary ions can reach 3 orders of magnitude[95-97]. The use of massive Au or Ar clusters seems very promising. A single impact of a Au_{400}^{4+} cluster was found to generate in average 12.5 secondary ions from a glycine target via a multi-ion emission process, and the damage cross-section was reported to be very low for these projectiles[98]. Very high secondary yields and virtually no fragmentation were also observed for massive Ar cluster bombardment of organic samples[99-102]. The angular distribution of sputtered matter under massive Ar cluster bombardment at normal incidence does not follow the cosine-like distribution observed for monoatomic Ar projectiles, but lateral sputtering is preferred, which leads to pronounced smoothing of the bombarded surface[103].

The situation is different if the organic material is applied as a thin overlayer on a metallic substrate, or if the organic material is covered with small amounts of a noble metal (MetA-SIMS). Czerwinsky[104] and Postawa[105] found that a C_{60} projectile hitting an organic overlayer on an Ag substrate generates a collective large-scale process involving several carbon atoms of the projectile and creating a shockwave in the substrate. Intact molecules are then ejected by a "catapulting mechanism", but the enhancement of molecular ejection compared to a Ga impact is much weaker than for bulk organic samples. Fig. II-9 shows a cross-sectional view of a collision event of a 15 keV Ga versus a 15 keV C_{60} projectile on an Ag substrate covered with a three layer benzene system[105].

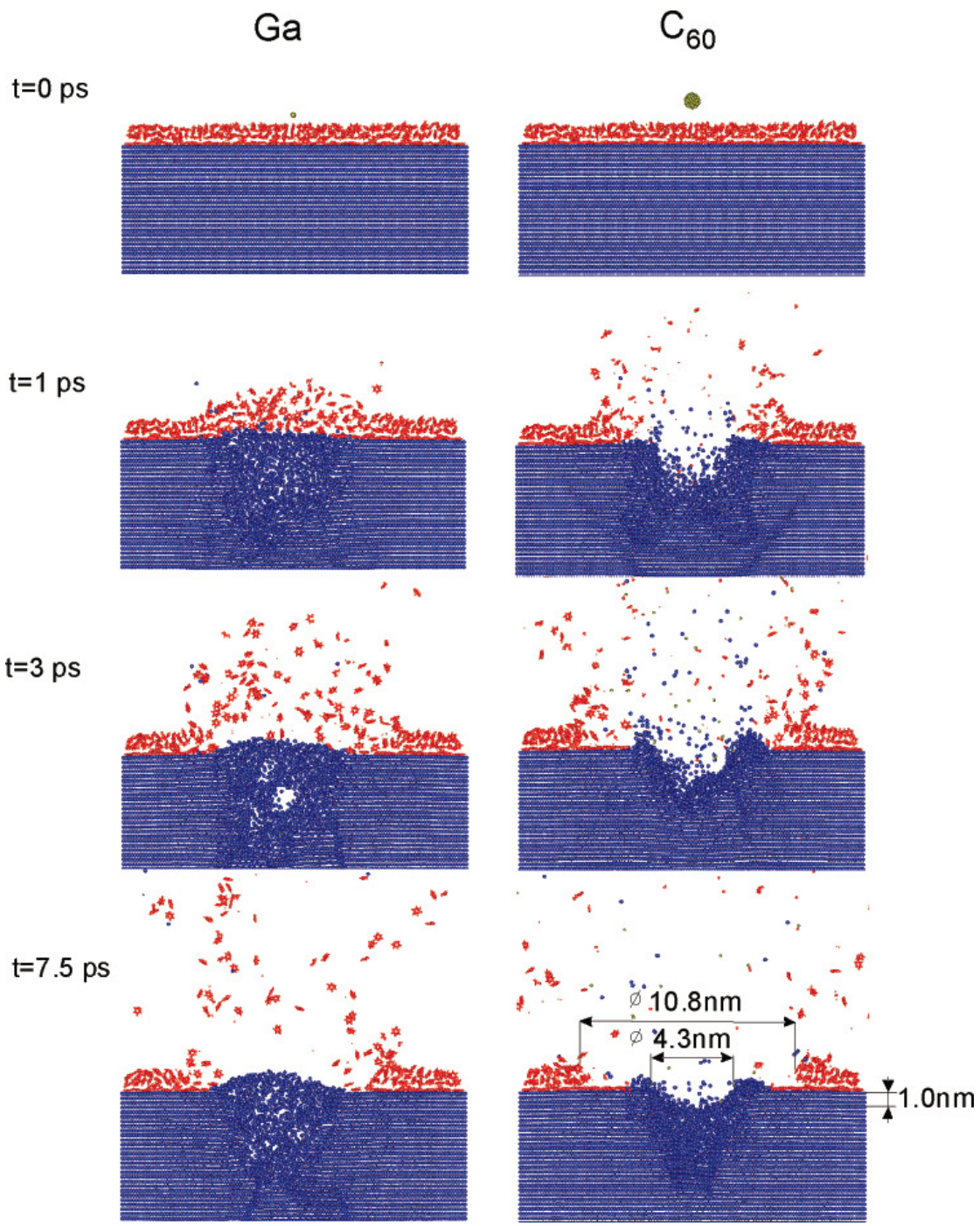

Fig. II-9: Cross-sectional view of the time evolution of a collision event of a 15 keV Ga and a 15 keV C_{60} projectile (in yellow) on an Ag substrate (in blue) covered with a three layer benzene system (in red). Figure from [105].

MD simulations by Ward[106] show that the area over which the energy is distributed for a monolayer of biphenyl molecules on Cu and Si substrates increases when going from a Xe^+ projectile to SF_5^+, but the relative increase of

the energy density area is more pronounced for the Si substrate. The reason is that the cluster projectile breaks up inside the Si surface but on top of the Cu substrate due to the higher mass of Cu atoms.

Several authors have reported experimental observations in agreement with these simulations. Kudo[107] and Heile[65] analyzed thin polymer layers deposited on silicon and metal substrates with different mono- and polyatomic primary ions and observed that the cluster projectiles only cause a yield enhancement in the case of Si substrates. Delcorte[108] found that the deposition of 2 nm of Au onto an Irganox1010 film enhances the yield of the molecular ion by a factor 678 compared to the pristine sample when Ga^+ projectiles are used. In the case of C_{60}^+ bombardment, the molecular ion yield slightly decreased. Delcorte[79] and Heile[80,81] analyzed organic samples covered with various amounts of Au and both observed that the secondary ion yield under polyatomic ion bombardment decreased with increasing gold deposition while the opposite behavior was observed for monoatomic projectiles. Heile concluded that the combination of different yield enhancing methods is not necessarily successful if they are based on the same mechanism, i.e. an increased near-surface energy deposition.

Recent MD simulations by Restrepo[87,88] show that the molecular ion yield of a polyethylene (PE) surface covered with Au cluster islands depends on the impact point of the projectile (in the middle of the cluster, on its periphery, near the Au-PE interface, or on the pristine PE). The yield enhancement tendencies are very different for C_{60}^+ and Ga^+ primary ions. A Ga^+ impact on an Au cluster generates Au recoil atoms that cause the ejection of many organic fragments, while a C_{60}^+ projectile breaks the Au cluster apart and mainly causes the ejection of Au atoms.

In several studies a decrease in fragmentation of the organic molecules has been observed for cluster beams. For example, Weibel showed that the yield enhancement for several organic samples when moving from 12.5 keV Ga^+ to C_{60}^+ projectiles of the same impact energy was more pronounced for ions in the high mass range than for the smaller fragments[97]. This tendency was also observed by other authors[96,109]. However, higher fragmentation has

also been reported for polyatomic ions[110-112], and MD simulations have shown that C_{60}^+ bombardment of benzene breaks numerous C-C and C-H bonds in the near surface region, most of which are directly ejected[79]. It seems that the fragmentation behavior with cluster primary ions is strongly sample dependent[113].

It was also observed that cluster beams create much less chemical damage than monoatomic projectiles[114], even after high fluences. The development of cluster ion sources has thus opened the door to the field of organic depth profiling. A basic requirement for successful molecular depth profiling is that the damaged sample volume is removed fast enough so that the damage will not accumulate and cause a loss of molecular signal even after fluences far above the static limit. Since cluster projectiles generate higher sputter rates and less chemical damage than monoatomic beams, this condition is often fulfilled, but it is strongly dependent on the sample. Organic materials can be divided into two categories according to their behavior under ion beam irradiation[113]:

- Type I or cross-linking type: these molecules tend to undergo cross-linking. Examples of this category are PS, PVC and Alq_3[115].
- Type II or degrading type: chain scissions are predominant. PMMA is a typical example.

The transition between the two types is rather smooth because there is always a competition between chain scission and cross-linking, and the predominant mechanism may change as a function of fluence. Furthermore the irradiation behavior can be influenced by different experimental parameters such as temperature, the molecular weight of a polymer sample, or by the presence of O_2[113].

One of the first depth profiles of a polymer sample was presented by Gillen et al. in 1998[94]. They used SF_5^+ primary ions for depth profiles of a 50 nm PMMA layer on Si. The characteristic fragment ion at m/z=69 could be detected until the Si interface was reached, which was not possible with Ar^+ ions. Since then, a wide range of organic materials has been successfully depth profiled.

Depth profiling with retention of molecular signal is generally possible for type II polymers, but it can also be successful for cross-linking polymers if the experimental conditions are chosen carefully (i.e. the nature primary ion, the beam angle and energy, and the sample temperature)[113]. PS, a type I polymer, has been depth-profiled with massive Ar clusters[116]. An alternative to cluster beams is the use of low energy reactive primary ions, typically Cs^+. Cs is supposed to deactivate free radicals, thus preventing the accumulation of chemical damage by cross-linking as the fluence increases[117].

II.7 Conclusions

SIMS is a very sensitive analysis technique that can be applied to a large variety of samples for surface analysis, depth profiling, imaging, or 3D-reconstruction of a small sample volume. In the particular case of organic samples, where the retention of molecular information is necessary for an unambiguous identification of the sample material(s), the use of TOF-SIMS instrumentation and static bombardment conditions are common practice. However the interpretation of mass spectra is not straightforward since matrix effects and fragmentation mechanisms need to be taken into account.

Over the last decades, several approaches such as MetA-SIMS or the use of polyatomic primary ions have been studied with regard to their potential of maximizing the secondary ion intensities in TOF-SIMS analyses of organic samples, especially for parent-like ions that reflect the analyte's molecular structure. However, the complex interplay of sputtering, fragmentation and ionization mechanisms is still not completely understood. The quest for a deeper insight into these phenomena is carried on by a large variety of experimental, numerical, and combined studies.

Chapter III. Sample preparation and characterization

III.1 Silicon wafers

Silicon wafers of (111) orientation from Siltronix were used as substrates for the metallic and organic layers prepared in this work. In order to remove surface contaminations before coating, the wafers were immerged during 15 minutes subsequently in demineralized water, acetone and ethanol in an ultrasonic bath. TOF-SIMS analyses show that especially organic contaminants are partially removed by this cleaning protocol (Fig. III-1). The Na^+ peak (m/z=23) however is higher after cleaning. The native oxide layer was not removed by this procedure.

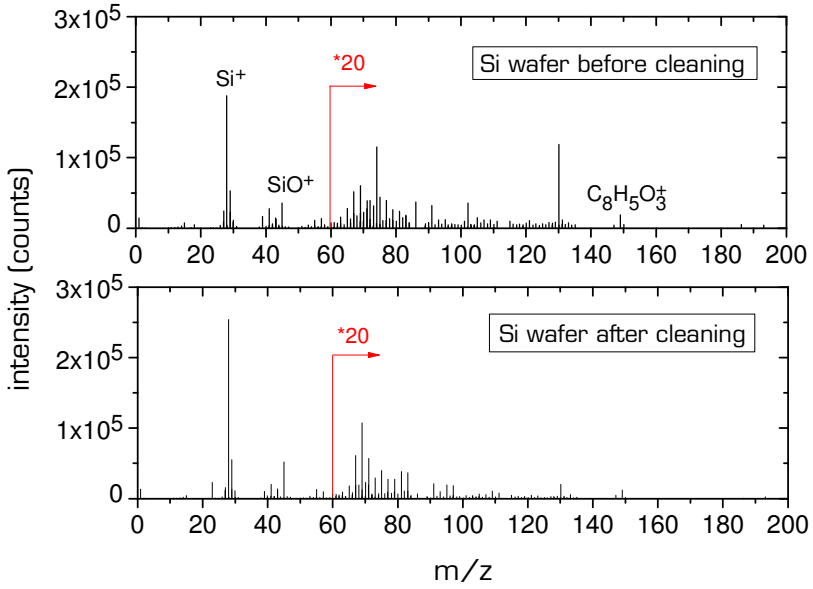

Fig. III-1: Positive mass spectra (Ar^+, 10 keV) of a silicon wafer before and after cleaning.

III.2 Polymer samples

The polymers used for this work were polystyrene (PS), poly(methyl methacrylate) (PMMA), and polyvinyl chloride (PVC). They were purchased as

powders from Sigma Aldrich. The molecular structure of the repeat units as well as the average molecular weights of the used polymers are given in Fig. III-2.

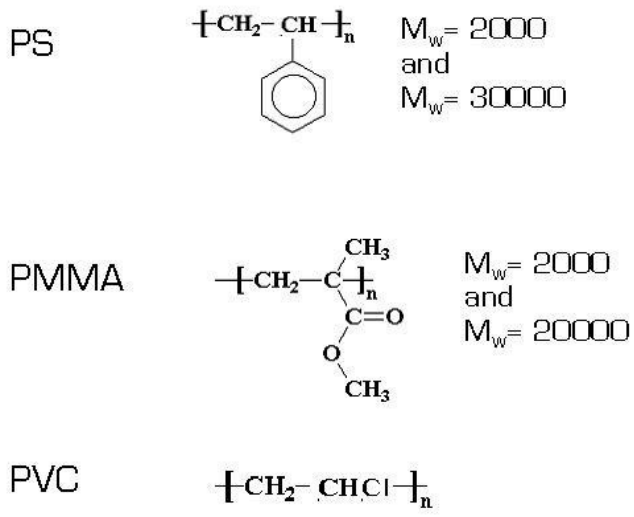

Fig. III-2: Repeat units and average molecular weights of the polymers used in this work. For PVC, no information about molecular weight was provided.

Thin polymer films were obtained by spin-coating. This technique consists in depositing a small volume of a solution of a polymer in a volatile organic solvent onto a solid substrate, which is then spun at high speed during typically one minute. Under the influence of the centrifugal force, the major proportion of the solvent is immediately evacuated over the substrate's borders. This results in an increasing viscosity of the solution on the substrate. After evaporation of the remaining solvent, a thin polymer film is formed. Spin-coating is known for producing very flat and homogenous films on condition that the solvent is well-chosen[118-120]. The obtained film thickness for a given polymer increases with the concentration of the solution and is inversely proportional to the square root of the rotation speed[121].

For this work a Single Wafer Spinner SPIN150 (APT) was used. The wafers were spun with an acceleration of 10 000 rpm/s and a rotation speed of 3 000 rpm during one minute. Toluene (Sigma Aldrich) was used as a solvent for PS and PMMA, and PVC was dissolved in tetrahydrofuran (Sigma Aldrich). The concentrations were 2 wt% for PMMA and PS and 1.5 wt% for

PVC. Under these experimental conditions, the films are estimated to be between 40 and 80 nm thick[89,120]. This thickness is large enough to eliminate substrate effects[89], but still small enough to avoid charging effects during ion bombardment. Indeed, all the analyses presented in this work could be carried out without charge compensation.

III.3 Alq_3 samples

Aluminium tris(8-hydroxyquinoline) (Alq_3) is a commonly used material in the emerging domain of organic optoelectronic devices. Its molecular structure is presented in Fig. III-3. Alq_3 samples were prepared by K.Q. Ngo at the Department of Materials Science and Engineering of the University of Michigan. Thin layers of 50 nm were deposited onto cleaned silicon wafers at room temperature using vacuum thermal evaporation of Alq_3 powder at 10^{-6} mbar. The deposition rates were measured with a precalibrated quartz crystal monitor and varied between 1.2 and 1.7 Å/s.

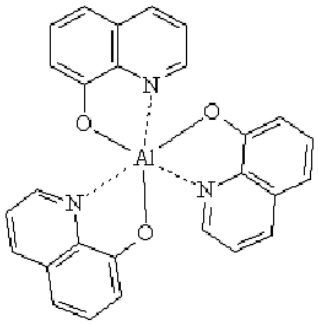

Fig. III-3: Molecular structure of Alq_3.

III.4 Metallic collectors

Metallic layers of Ag, Au or Cu were deposited onto Si wafers by EBE-PVD (Electron Beam Evaporation – Physical Vapour Deposition) in the collector coating chamber of the Storing Matter instrument. A detailed description of the installation has been given in Chapter I. Metal pellets of 99.99% purity (Kurt J. Lesker Company Ltd) were evaporated and deposited onto silicon wafers at a rate of 0.1 nm/s. A nominal layer thickness of 30 nm was chosen

for the preparation of the noble metal collectors. For this thickness the static SIMS collision cascade should be confined to the metallic layer and not penetrate into the Si substrate. This was confirmed by SRIM (Stopping and Range of Ions in Matter) calculations[122]: the mean longitudinal range of 10 keV Ar^+ ions with 45° impact angle averaged for 100 000 trajectories in Au (5.8 nm), Ag (6.1 nm), or Cu (5.0 nm) surfaces was significantly inferior to 30 nm.

The growth mode of noble metals on Si substrates follows the Volmer-Weber model[123-125]. Since the cohesive interactions among metal particles are stronger than the adhesion forces between a silicon atom and a metal atom, 3-dimensional islands of metal clusters are formed during the first steps of the deposition process in order to minimize the surface free energy[123]. As the metal accumulates, the islands grow and finally coalesce into a continuous film. Several authors have shown that small amounts of noble metals evaporated onto Si form 3-dimensional island-like structures at nanometer-level[73,79,126].

AFM (Atomic Force Microscopy) measurements showed that the metallic collector surfaces are very flat. An AFM image of an Au collector is shown in Fig. III-4. The high peaks in the image probably correspond to dust particles on the surface. The RMS (root-mean-squared) roughness calculated for a sub-area of 63 μm^2 of this surface was 1.2 nm.

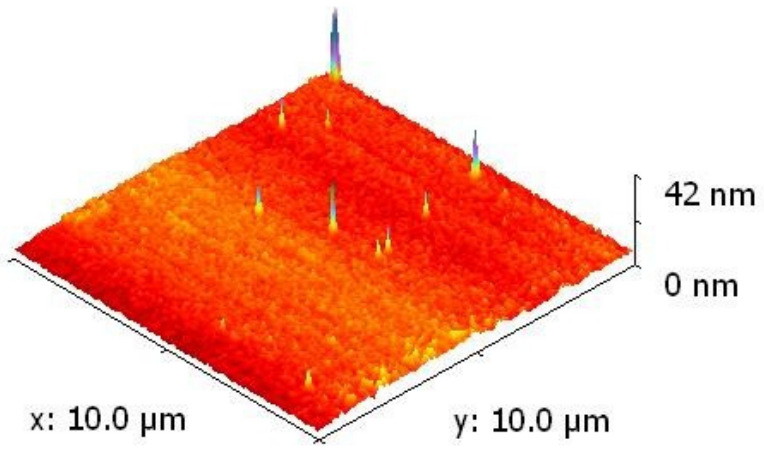

Fig. III-4: AFM image of an Au collector. The high peaks are probably due to dust particles.

Positive TOF-SIMS mass spectra of the metallic collectors (Fig. III-5) showed that the Si substrate was entirely covered by the noble metal since no significant Si^+ signal (m/z=28) was detected. In the case of Au, the positive peaks in the low mass range corresponding to hydrocarbons and nitrogen-containing fragments are extremely high compared to those on the Ag and Cu substrates although the 3 samples were prepared and analyzed under exactly the same conditions. This observation suggests that the Au surface is highly contaminated, which would be surprising because the metallic films were all obtained from very pure metal pellets and transferred to the TOF-SIMS instrument without breaking the UHV conditions.

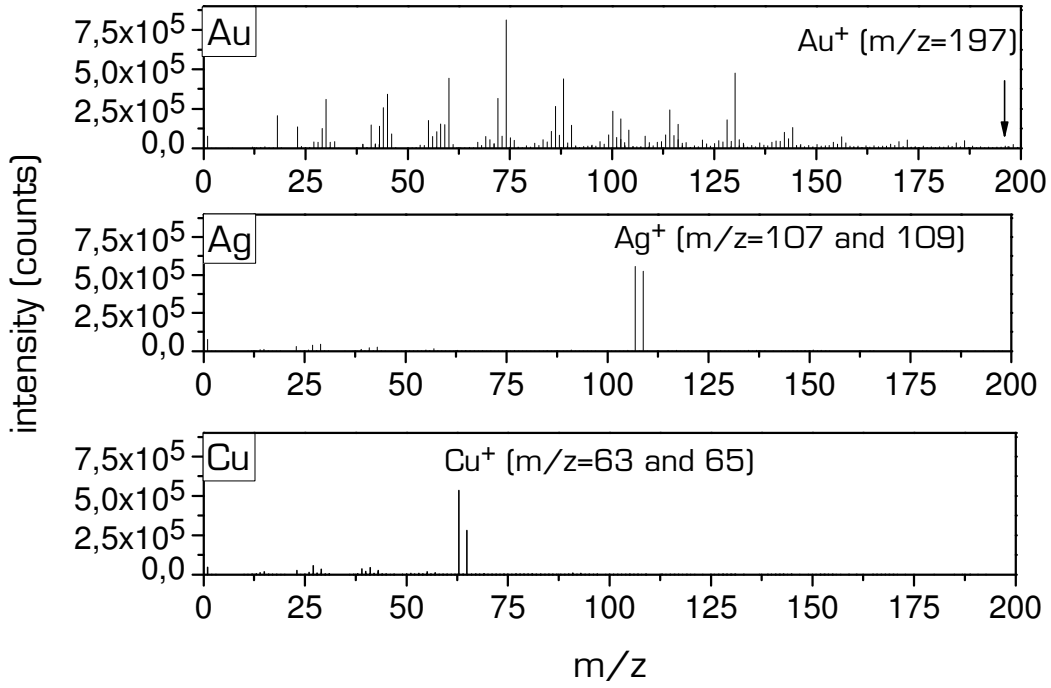

Fig. III-5: Positive mass spectra (Ar^+, 10 keV) of Au, Ag and Cu films prepared in the collector coating chamber.

Negative mass spectra of the 3 collectors show an opposite trend (Fig. III-6): here the Au spectrum looks "cleaner", F^- (m/z=19) and CN^- (m/z=26) being the only significant peaks along with Au^-. The O^- peak is very weak. The negative spectra of Cu and Ag are however dominated by O^- (m/z=16), CN^- and Cl^- (m/z=35 and 37). Especially on the Ag substrate a series of nitrogen-containing hydrocarbon peaks is present.

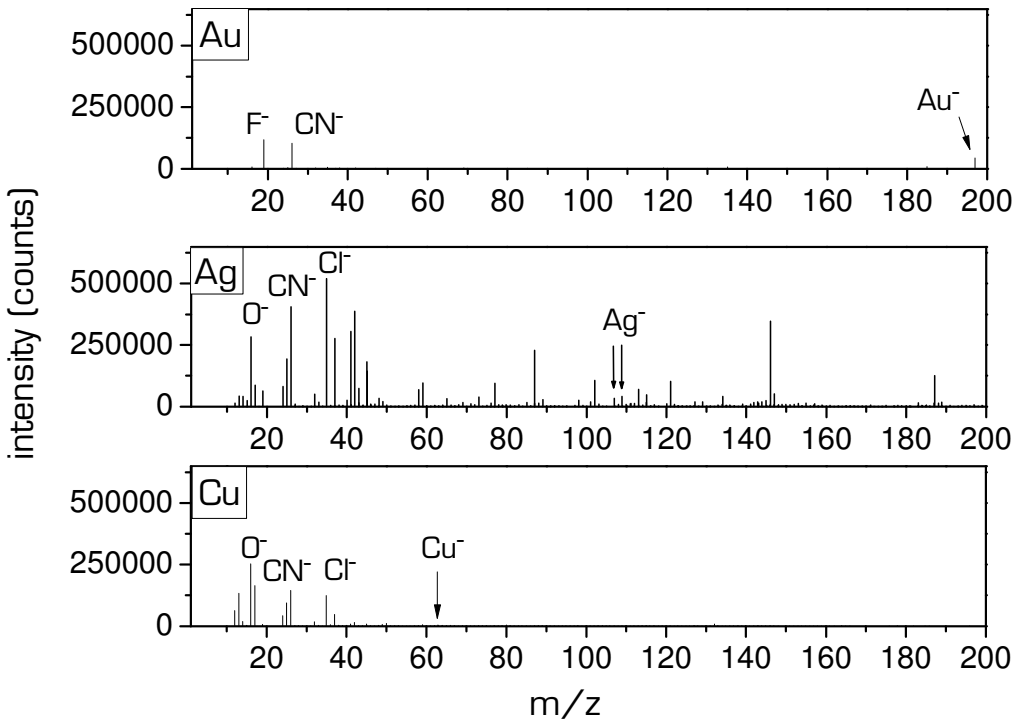

Fig. III-6: Negative mass spectra (Ar^+, 10 keV) of Au, Ag and Cu films prepared in the collector coating chamber.

Since these metal surfaces are destined to serve as collectors for Storing Matter deposits of organic samples, it is important that the pristine collectors should be as clean as possible. It will be shown in chapter IV that the intense organic peaks in the positive mass spectrum of Au represents a disturbing background signal when a Storing Matter deposit of an organic polymer has to be identified on an Au collector. In order to determine the exact origin and to reduce the amount of organic contaminants, several approaches were adopted:

- The collector coating chamber was baked at 100 °C during 12 hours in order to reduce the amount of residual gases.
- The chamber walls were cooled with liquid nitrogen during metal evaporation. This resulted in a basic pressure in the chamber of $5 \cdot 10^{-11}$ mbar instead of 10^{-9} mbar.
- High purity Au pellets from other suppliers (American Elements, Goodfellow) were tested.

- Inside the electron beam evaporator, the Au pellets were placed in a molybdenum crucible liner instead of the initially used amorphous carbon liner.

All these approaches did not lead to any significant changes in the positive or negative mass spectra of the 3 metal coatings. Mass spectra taken directly on a gold pellet are virtually identical with those of the Au collectors. It seems thus that the organic species are naturally present on the metal surfaces and that their presence on the collector surfaces cannot be avoided by the available means.

TOF-SIMS depth profiles (dual beam depth profiling with C_{60}^+ sputtering and Bi^+ analysis gun) of an Au and an Ag collector showed that the organic contaminants are only present on the top layer(s) of both metallic samples and on the interface between the metal and the Si substrate. The depth profile of the Au collector is displayed in Fig. III-7. For Ag the intensity evolutions were qualitatively very similar, but the initial intensity of the hydrocarbon contaminants was much lower than on Au.

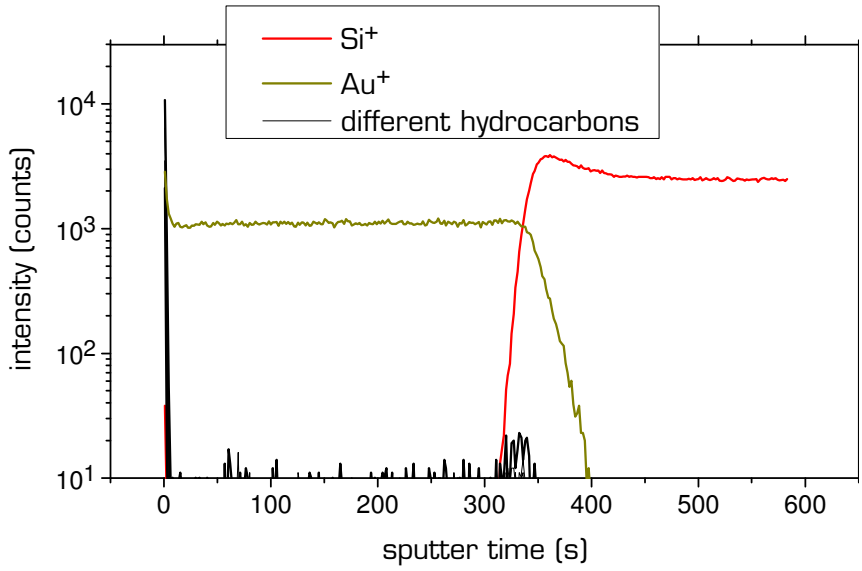

Fig. III-7: TOF-SIMS depth profile of an Au collector (positive mode).

For both samples, the kinetics of hydrocarbon adsorption were qualitatively studied. A large crater of 600 · 600 μm^2 was sputtered until approximately the middle of the metallic layer was reached. Immediately a first

mass spectrum with Bi^+ primary ions, a raster size of 50 · 50 μm^2 and 100 s acquisition time was recorded inside this crater. After 2 and 20 minutes, two more such mass spectra were taken, each at a different spot inside the sputter crater. The absolute intensities of the hydrocarbon contaminants as a function of time (t=0 corresponds to the moment when the C_{60}^+ sputtering was stopped) are compared in Fig. III-8.

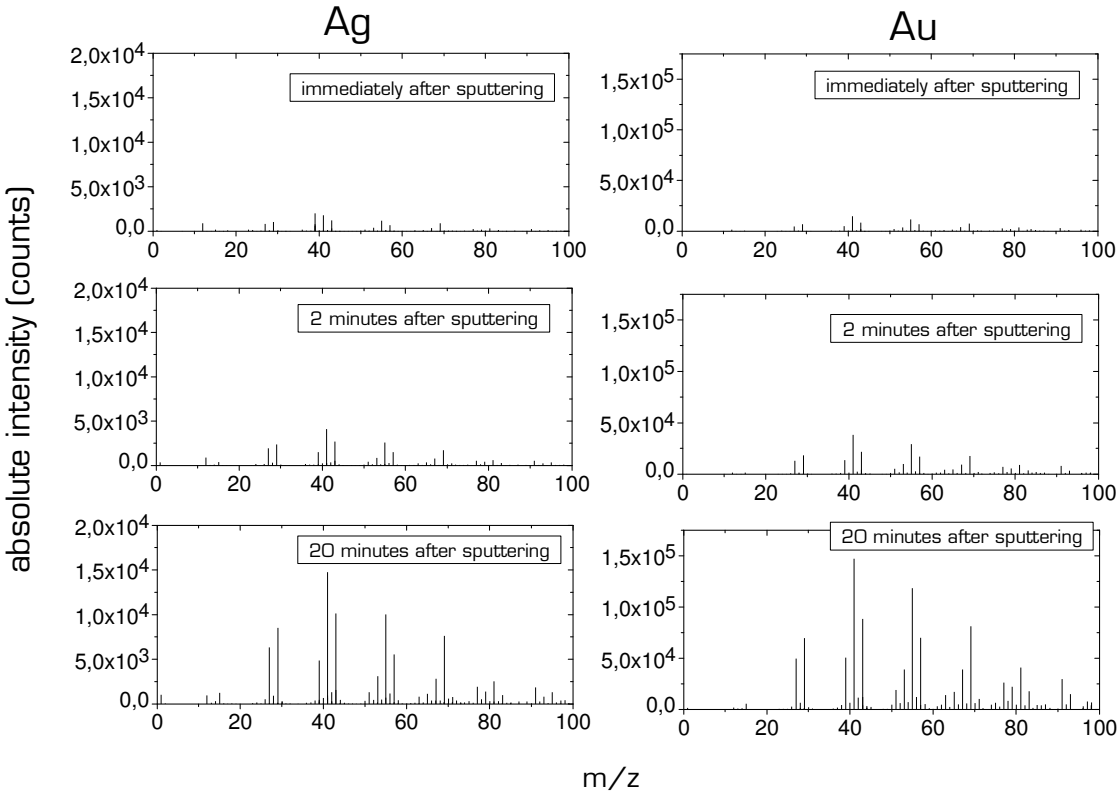

Fig. III-8: Positive mass spectra recorded on Ag and Au at different moments after sputtering with C_{60}^+. Note the different intensity scales for Ag and Au.

Even immediately after sputtering, the hydrocarbon peak intensities on the Au collector are almost 10 times higher than on Ag. As a function of time, the hydrocarbon peaks on both materials increase, and after 20 minutes there is still a factor 10 between the intensities measured on Ag and Au. This intensity ratio was also determined from the spectra taken on the surfaces of the metal collectors (Fig. III-5). Since this intensity ratio stays constant with time, it can be considered that both metals have a similar affinity towards the hydrocarbon contaminants present in the residual gas inside the analysis chamber, but that Au enhances their positive intensities more than Ag.

In order to obtain quantitative information about the surface contaminants, an Au and an Ag collector were analyzed by XPS (X-ray Photoelectron Spectroscopy)[127,128]. XPS is a quantitative and surface sensitive technique, but with a poor detection limit (0.1 – 1 at%) compared to SIMS. The principle of XPS is based on the photoelectric effect: the sample is irradiated by X-rays and the emitted photoelectrons are energy-analyzed. The obtained kinetic energy (*KE*) spectrum gives information about the binding energy (*BE*) of the detected core electrons according to Equation III-1. *hv* represents the energy of the photon and Φ is the work function of the spectrometer. The binding energy of a photoelectron allows to deduce the element (from Li to U) from which it was emitted as well as the chemical state of this element.

$$KE = h\upsilon - (BE + \phi) \qquad \text{(Equation III-2)}$$

After correction by a sensitivity factor, the XPS peak intensities are directly related to the relative concentration of each element inside the analyzed sample volume. The penetration depth of the X-rays is in the micrometer range[127], but only photoelectrons emitted from the top 10 nanometres can be detected. In a first approximation, the value of the sampling depth depends on the density of the analyzed material and on the kinetic energy of the considered photoelectron. It is defined as the depth up to which 95% of the detected photoelectrons are emitted and is equal to 3 times the inelastic mean free path of the electron in the solid. For example, the inelastic mean free path of the C 1s electron is 1.691 nm in Ag and 1.408 nm in Au according to the TPP-2M formula[129], which corresponds to sampling depths of 5.1 nm in Ag and 4.2 nm in Au for this photoelectron.

The metallic collectors were transferred with the UHV suitcase to the ThermoVG Microlab 350 instrument and analyzed with an AlK_α X-ray source with a photon energy of 1486.6 eV. For each metal, an analysis point on the surface and one after sputtering with an Ar^+ beam (3 keV impact energy, 2 µA current, 45° incident angle, 10·10 mm^2 rastered area) during 400 s were chosen. The only detectable elements were Au and Ag respectively, and oxygen and carbon. The considered photoelectrons were Ag $3d_{5/2}$ (369 eV), Au 4f (88 eV), O 1s (531 eV) and C 1s (284.5 eV). The calculated relative concentrations on the surface and after sputtering are given in Table III-1.

	Au sample			Ag sample		
	O	C	Au	O	C	Ag
surface	<1%	1.2	98.8	4.1	3.9	92.0
after sputtering	<1%	<1%	99.7	2.9	<1%	96.7

Table III-1: Relative atomic concentrations of oxygen, carbon, and gold or silver obtained by XPS measurements for an Au and an Ag collector.

These values indicate that the surface of the Au collector is much less contaminated than the Ag sample. Furthermore, the organic contaminants seem to have accumulated on the surface only after preparation of the metallic layers since the atomic concentration of C significantly decreases after only 400 s of sputtering.

It can be concluded from these XPS measurements that the striking differences observed in the SIMS spectra of the 3 noble metals are due to matrix effects and do not reflect the real degree of contamination of these surfaces. Changes in the surface work function are frequently made responsible for matrix effects in SIMS[9,130]. Indeed Au has a higher work function (5.10 eV) than Ag (4.26 eV)[131], which is probably part of the reason why the organic contaminants are more easily cationized on Au than on Ag and Cu.

Chapter IV. Study of the key parameters of the Storing Matter technique in the case of organic samples

IV.1 Introduction

This chapter deals with the fundamental aspects of the sputter-deposition of organic samples and the TOF-SIMS analysis of these deposits. The key parameters of the Storing Matter technique are studied in detail for the particular case of organic samples. The knowledge about the impact of these parameters on the final mass spectra is a prerequisite for a reasonable choice of experimental conditions for a given organic sample with regard to an efficient detection of the Storing Matter deposit and reduced fragmentation of the organic molecules.

During sputter-deposition, atoms and organic fragments of different sizes are emitted with a certain angular distribution that depends on the bombardment conditions, on the sample and on the desorbed particle. The Storing Matter deposits are thus non-uniformly spread over a certain area of the collector. In order to illustrate the distribution of an Alq_3 deposit on an Ag collector, several TOF-SIMS analysis points were chosen along a diameter of the collector (Fig. IV-1). As an example, Fig. IV-2 shows the evolution of the absolute intensity of a characteristic Alq_3 fragment (Alq_2^+, m/z=315) as a function of the position on the collector. A clear maximum can be identified at a distance of around 1 mm from the border of the collector. This analysis point also corresponds to the position where other characteristic fragments of Alq_3 are detected with maximum intensity. This indicates that the angular distributions of these fragments (or their precursors) during the sputter-deposition step are similar.

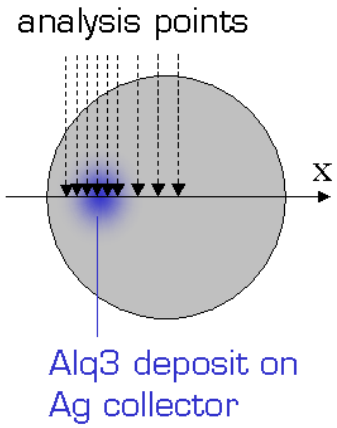

Fig. IV-1: TOF-SIMS analysis points along a diameter of the collector. The raster size was 100·100 μm^2 and the distance between 2 points was 0.5 - 2 mm. The collector diameter was 1" (2.54 cm).

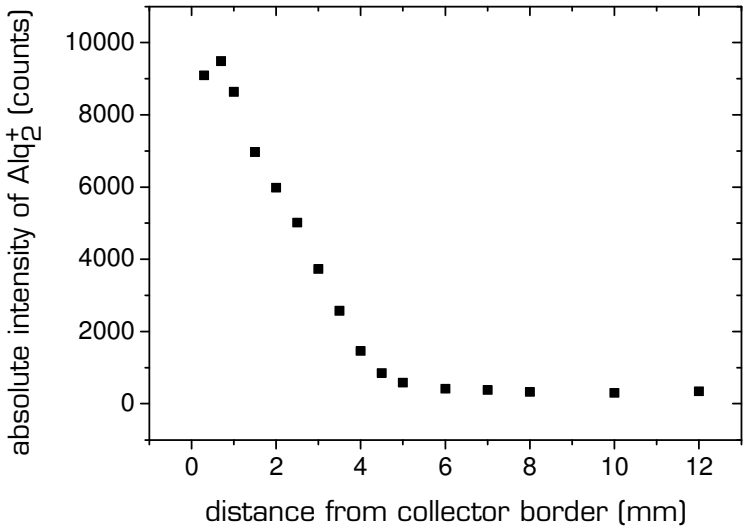

Fig. IV-2: Absolute intensity of the Alq_2^+ peak as a function of the position on the collector.

It should be mentioned that it would be possible to obtain Storing Matter deposits further away from the collector border by moving the collector closer to the nose of the ion gun, but this is only possible if the collector is placed several mm higher above the sample surface than in the usual configuration

shown in Fig. I-4. In that case the deposit would be significantly more diluted (because of the solid angle of the emitted matter) and thus more difficult to detect. For all the Storing Matter deposits presented in this work, the collector was placed in approximately the same horizontal plane as the nose of the ion gun (5 mm above the sample surface) and as close as possible to the latter (Fig. I-4).

IV.2 Experimental conditions

The sputter-deposition conditions in the Storing Matter instrument were chosen as follows (unless mentioned otherwise):

- Ar^+ bombardment, 10 keV impact energy, 45° incident angle
- 1.8 nA primary ion current
- $1.5 \cdot 1.5$ mm^2 raster size.

In order to accumulate a sufficient amount of organic matter on the collector while still keeping the primary ion fluence below the static limit, the sample stage was moved during the sputter-depositions as described in Fig. I-5. The speed of this translation was 0.15 mm/s unless mentioned otherwise. Considering that the raster size was $1.5 \cdot 1.5$ mm^2, each point was irradiated during 10 s, which corresponds to a fluence of $5 \cdot 10^{12}$ ions/cm^2. The total length scanned in this manner was 16 cm for each deposit (8 parallel lines of 2 cm length each), which is equivalent to an irradiated area of 2.4 cm^2 and a total of $1.2 \cdot 10^{13}$ primary ions. The typical sample size used for these experimental conditions was $3 \cdot 3$ cm^2.

For the analysis of all the Storing Matter spectra discussed in this work, TOF-SIMS linescans were carried out as described above. The spectrum acquired on the point corresponding to the maximal intensity of characteristic fragments will be designated as the “Storing Matter spectrum”. The presented mass spectra were, unless mentioned otherwise, analyzed in the TOFIII (Ion-TOF) instrument with the following conditions:

- Ar^+ primary ions, 10 keV impact energy, 45° incident angle
- 0.5 pA pulsed current

- $100 \cdot 100\ \mu m^2$ raster size
- 3 minutes acquisition time for each spectrum.

The resulting primary ion dose was $5.6 \cdot 10^{12}$ ions/cm^2.

IV.3 Identification of Storing Matter deposits on Ag collectors

In the next pages, positive Storing Matter spectra of the 4 studied organic samples on Ag collectors will be presented and discussed. The organic samples and the collectors were prepared as described in Chapter III (pages 54-55).

IV.3. (a) PVC sample

IV.3. (a) i) Positive secondary ions

Fig. IV-3 displays positive mass spectra taken directly on the spin-coated PVC sample, in the centre of the Storing Matter deposit of PVC on an Ag collector, and on the pristine Ag collector. The positive PVC reference spectrum is dominated by peaks in the low-mass region corresponding to saturated hydrocarbon fragments of the type $C_nH_{2n-1}^+$ and $C_nH_{2n+1}^+$. These fragments mirror the structure of the polymer's backbone. Several chlorine containing hydrocarbons, which are more specific for PVC since they also contain information about the functional group, are also detected, e.g. $C_2H_2Cl^+$ (m/z=61) or $C_3H_4Cl^+$ (m/z=75).

Apart from the Ag^+ and Ag_n^+ peaks, the signal on the pristine Ag collector is low, as already discussed in Chapter III. The positive Storing Matter spectrum of PVC on an Ag collector shows a similar distribution for the low mass hydrocarbon peaks as the reference spectrum. The absolute intensities are around 3 times lower than those measured directly on the PVC sample.

This is not surprising because the Storing Matter deposit consists of only a sub-monolayer of PVC fragments.

As a comparison, the positive mass spectra of a very thin PVC layer spin-coated onto an Ag substrate and of the PVC sample covered with 2nm Ag (MetA-SIMS) are shown in Fig. IV-4. These spectra were acquired on the same day and under the same experimental conditions as the spectra in Fig. IV-3, thus the absolute intensities can be directly compared. The highest hydrocarbon peak intensities in the low mass range are obtained for the PVC thin layer on an Ag substrate, followed by the PVC sample covered with 2 nm Ag and finally the Storing Matter spectrum. For the Storing Matter spectrum to compete with the other spectra in terms of absolute intensities, it would probably be necessary to accumulate more matter on the collector (i.e. to irradiate a larger sample area for sputter-deposition).

Chlorine containing fragments are however not detected at all in the Storing Matter spectrum. This may be due to the double fragmentation during the sputter-deposition and the analysis step. The C-Cl bond constitutes the weak point of the chain. The bond strengths for the covalent bonds in the chloroethane molecule are given in Table IV-1.

In the positive Storing Matter spectrum, the only evidence of the chlorine atoms of PVC is provided by the $AgCl_2^+$ peak series around m/z=251. These peaks together with the series of saturated hydrocarbon fragments thus make it possible to associate this Storing Matter spectrum to a chlorinated hydrocarbon molecule, even without previous knowledge about the sample.

The relatively high Na^+ peak (m/z=23) in the Storing Matter spectrum is due to a Na contamination on the Ag collector. In the high mass range (m/z > 300), the only significant peaks correspond to Ag_n^+ clusters and to short Ag-cationized hydrocarbon fragments of the type $(AgC_nH_{2n})^+$ with n ranging from 2 to 8. These are also the only Ag-cationized fragments detected for the thin PVC layer on Ag and for the PVC sample covered with 2 nm Ag (Fig. IV-4).

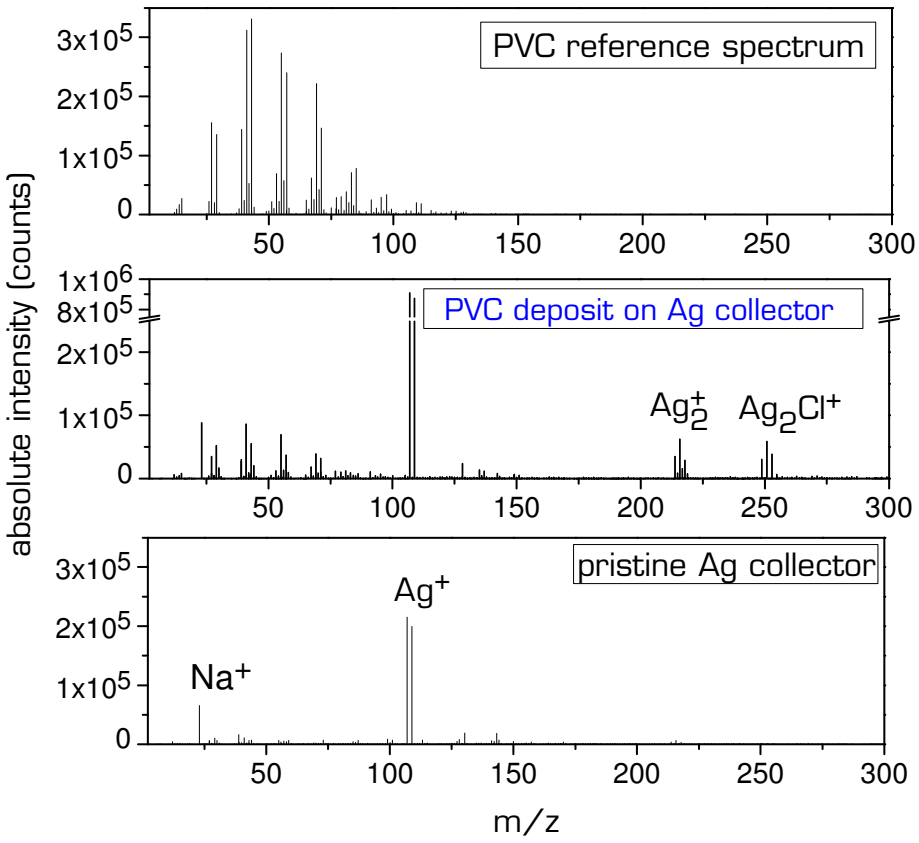

Fig. IV-3: From top to bottom: positive mass spectrum of the PVC sample, positive Storing Matter spectrum of PVC on an Ag collector, and positive reference spectrum of the pristine Ag collector. The same primary ion fluence was used for all the spectra.

It is interesting to note that the Ag^+ and Ag_n^+ peaks are significantly higher in the centre of the Storing Matter deposit than on the pristine Ag collector, although the Ag surface is partly "hidden" by the presence of the deposit. The ratio of the intensities in the deposit compared to those on the pristine collector is around 4 for Ag^+ and 10 for Ag_3^+. This effect was also observed for the other polymers. There seems to be a mutual yield enhancing effect between the organic deposit and the Ag particles.

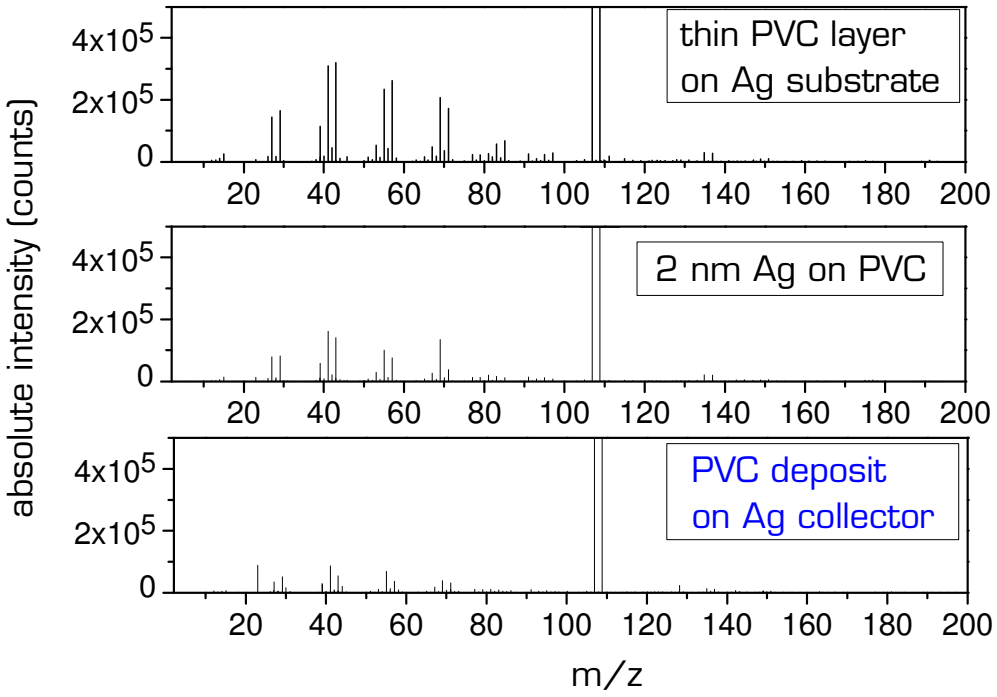

Fig. IV-4: From top to bottom: positive mass spectra of a thin PVC layer on Ag, of a 2 nm Ag overlayer on PVC, and the positive Storing Matter spectrum of PVC on an Ag collector. Note: the $^{107}Ag^+$ intensities in the 3 spectra are $8.7 \cdot 10^5$, $7.3 \cdot 10^5$ and $9.1 \cdot 10^5$ counts, respectively.

C-C	C-H	C-Cl
375,4	406,6	354,1

Table IV-1: Average bond energies (in kJ/mol) for the different covalent bonds in the chloroethane molecule. Values from [132].

IV.3. (a) ii) Negative secondary ions

Negative mass spectra taken directly on the PVC sample, in the centre of the Storing Matter deposit of PVC on an Ag collector, and on a pristine Ag collector are displayed in Fig. IV-5.

The negative Storing Matter of PVC does not differ much from the spectrum taken on the pristine Ag collector, except for the $AgCl^-$ and Ag_2Cl^- peak series. No information about the hydrocarbon backbone is obtained. The negative PVC reference spectrum is also quite unspecific since it does not contain any chlorinated hydrocarbon peaks.

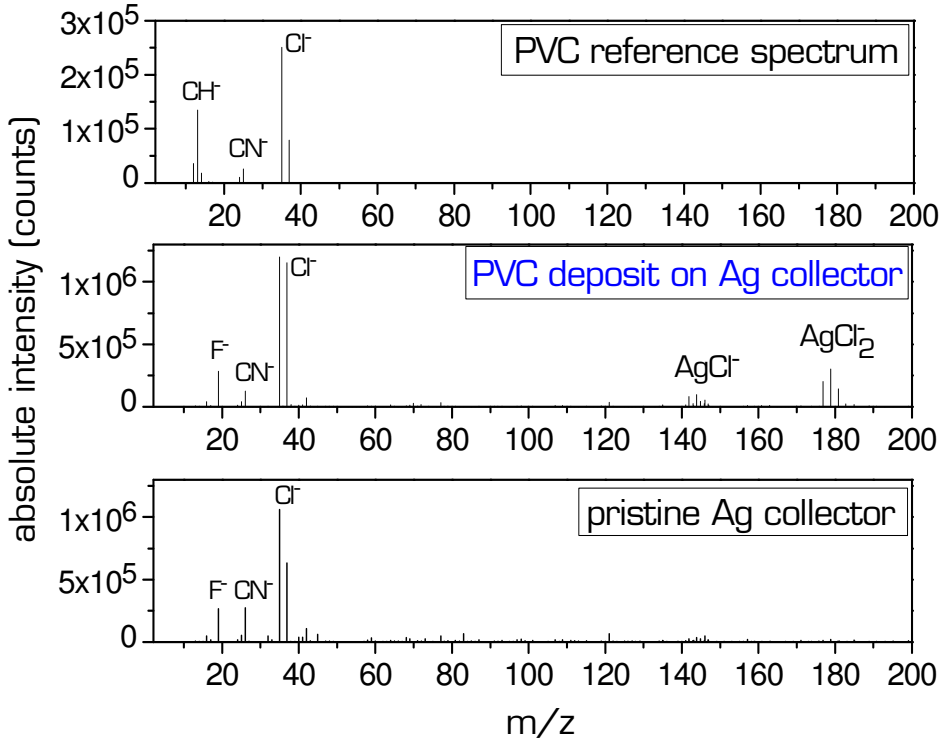

Fig. IV-5: From top to bottom: negative mass spectrum of the PVC sample, negative Storing Matter spectrum of PVC on an Ag collector, and negative reference spectrum of the pristine Ag collector.

IV.3. (b) PS samples

IV.3. (b) i) Positive secondary ions

In the positive mass spectrum of the PS30000 sample (first spectrum in Fig. IV-6), it can be observed that the positive intensities are globally very weak compared to the positive PVC reference spectrum (Fig. IV-3), although the analysis conditions were identical. Charging effects can however be excluded since in negative mode the overall intensities are comparable to those obtained on the other studied polymer samples.

PS has a much lower sputter rate than for example PMMA[133]. This means that for the same number of primary ions used for sputter-deposition, there will be significantly less material on the collector in the case of PS. This explains why the characteristic PS peaks in the Storing Matter spectrum (Fig.

IV-6) are more difficult to distinguish from the collector "background signal" than for example the hydrocarbon peaks in the PVC deposit (Fig. IV-3).

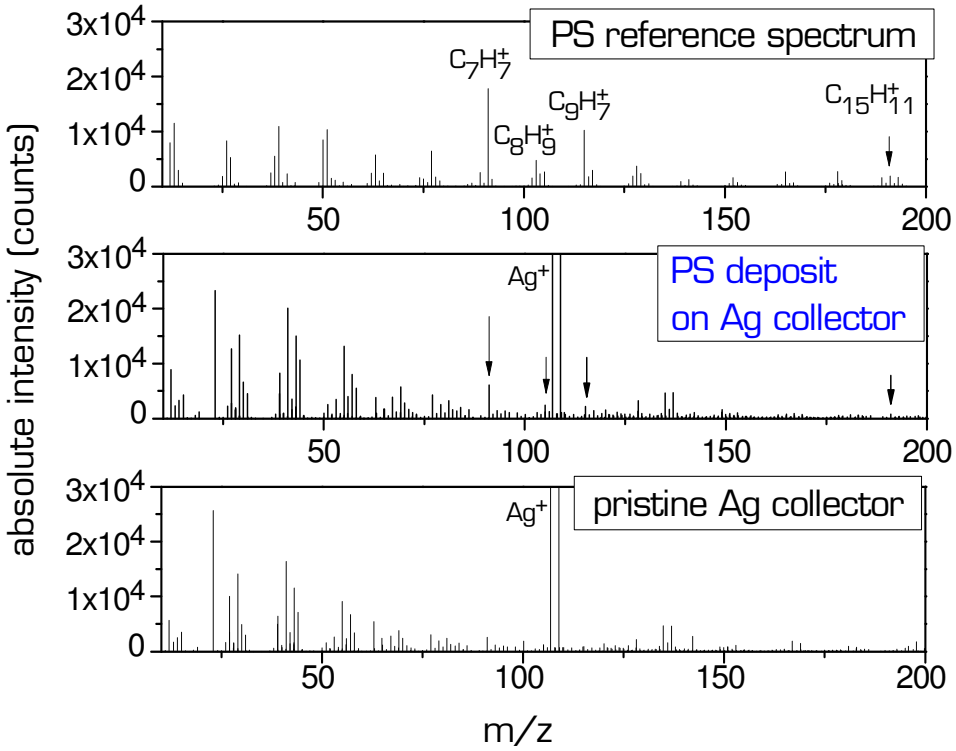

Fig. IV-6: From top to bottom: positive mass spectrum of the PS30000 sample, positive Storing Matter spectrum of PS30000 on an Ag collector, and positive reference spectrum of the pristine Ag collector.

Note: for a better visibility of the low mass peaks, the Ag^+ peaks are not displayed entirely. The $^{107}Ag^+$ intensities in the 2 last spectra are $5.1 \cdot 10^5$ and $4.3 \cdot 10^5$ counts, respectively.

However some characteristic PS peaks are significantly more intense in the deposit centre than on the pristine Ag collector. Among them are $C_7H_7^+$ (m/z=91), $C_8H_9^+$ (m/z=105), $C_9H_7^+$ (m/z=115), $C_9H_9^+$ (m/z=117), $C_{10}H_{11}^+$ (m/z=131), $C_{14}H_{11}^+$ (m/z=179), and $C_{15}H_{11}^+$ (m/z=191). The exact structures of these ions have been described in [134].

Furthermore, Ag-cationized fragments are detected in the Storing Matter spectrum: $AgC_nH_{2n}^+$ with n between 2 and 5, and the only characteristic fragment is $AgC_7H_8^+$ (m/z=199 and 201). It is important to mention that the spectra shown in this section were obtained from a PS of relatively high

average molecular weight (30000 Da). It will be shown in section IV.5. (b) that large characteristic fragments are detected in the Storing Matter spectrum of a low molecular weight PS.

Again, the Ag_n^+ peaks are higher in the centre of the PS deposit than on the pristine collector (increase by a factor 1.2), but the difference is smaller than for the PVC deposit.

For the PS deposit analyzed in positive mode, identification is possible, but not as straightforward as for PVC. Due to the lower sputter yield of PS, it might be necessary to collect matter from a larger total area during the sputter-deposition step in order to get higher PS-characteristic peaks in the Storing Matter spectrum. Another approach consists in using preparation methods inspired from the domain of MetA-SIMS and ME-enhanced SIMS for the PS sample. The results of these experiments will be presented in section IV.5. (b) .

IV.3. (b) ii) Negative secondary ions

The only significant peaks in the negative reference spectrum of PS (Fig. IV-7) are of the type C_n^-, C_nH^-, and $C_nH_2^-$, with n varying from 1 to 6. The negative Storing Matter spectrum (not shown) cannot be distinguished from the negative spectrum of the pristine Ag collector. Hence the analyses in negative mode do not provide any specific information about this polymer.

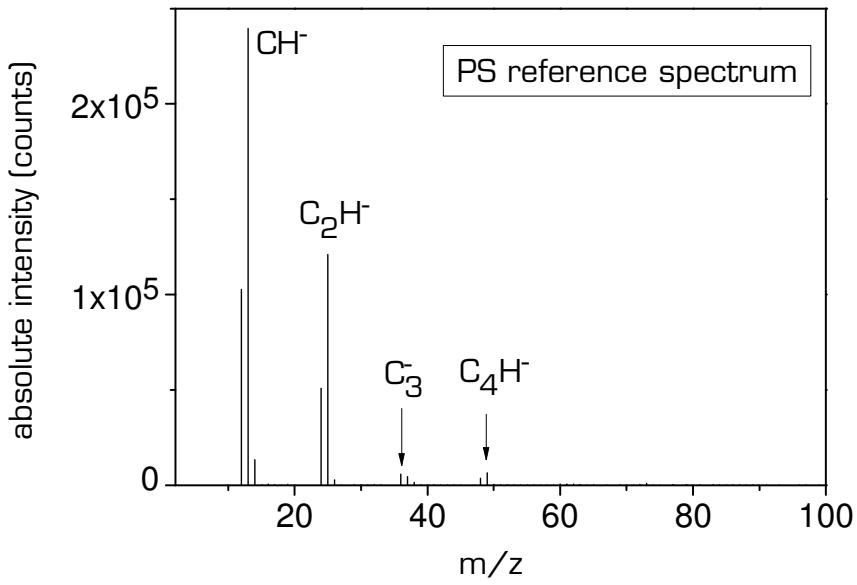

Fig. IV-7: Negative reference spectrum of a PS30000 sample.

IV.3. (c) PMMA samples

IV.3. (c) i) Positive secondary ions

The low mass range of the positive PMMA20000 reference spectrum (first spectrum in Fig. IV-8) contains several peaks that are characteristic for this polymer. Among them are hydrocarbon fragments reflecting the backbone structure (e.g. $C_3H_5^+$ at m/z=41 or $C_4H_7^+$ at m/z=55) and more specific oxygenated fragments like for example $C_2H_3O_2^+$ and $C_3H_7O^+$ at m/z=59, $C_4H_5O^+$ at m/z=69, as well as the protonated monomer unit $C_5H_9O_2^+$ at m/z=101. Structural assignments for these characteristic peaks have been proposed by Leeson et al.[135]

The hydrocarbon peaks can be easily recognized in the Storing Matter spectrum, but only few oxygen containing fragments are detected and their intensities are quite small. This suggests that, like for the C-Cl bonds in the case of PVC, the carbon-oxygen bonds tend to be destroyed by double fragmentation. In the higher mass range (not shown), only unspecific Ag-cationized fragments of the type $AgC_nH_{2n}^+$ are detected.

The Ag^+ intensity is more than 3 times higher in the Storing Matter spectrum than in the spectrum taken on the pristine Ag collector.

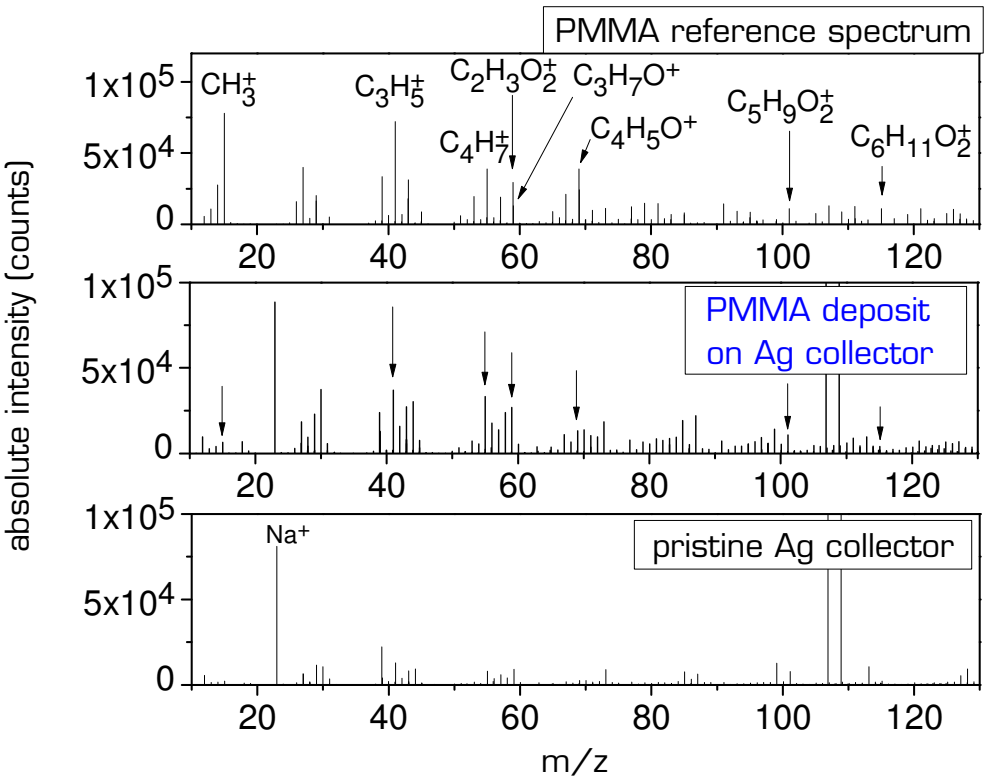

Fig. IV-8: From top to bottom: positive mass spectrum of the PMMA20000 sample, positive Storing Matter spectrum of PMMA20000 on an Ag collector, and positive reference spectrum of the pristine Ag collector. Note: The $^{107}Ag^+$ intensities in the 2 last spectra are $6.6 \cdot 10^5$ and $2.8 \cdot 10^5$ counts, respectively.

IV.3. (c) ii) Negative secondary ions

The negative reference spectrum of PMMA20000 (Fig. IV-9) is dominated by the O^- and CH^- peaks, but many characteristic fragments are detected. The most intense peaks correspond to CH_3O^- (m/z=31), C_2HO^- (m/z=41), $C_3H_3O^-$ (m/z=55), $C_4H_5O_2^-$ (m/z=85), $C_8H_{13}O_2^-$ (m/z=141), and $C_9H_{13}O_4^-$ (m/z=185). Structural assignments for these characteristic peaks have been proposed by Leeson et al.[135] In the negative Storing Matter spectrum however, the intensities of these peaks are hardly higher than the "background signal" from the pristine Ag collector.

For the 3 studied polymers, negative Storing Matter spectra did not provide any valuable information. This is not very surprising since the choice of the Ag collector was made with regard to a yield enhancement in positive analysis mode. In section IV.5. (a) the particular importance of the collector surface will be studied in detail.

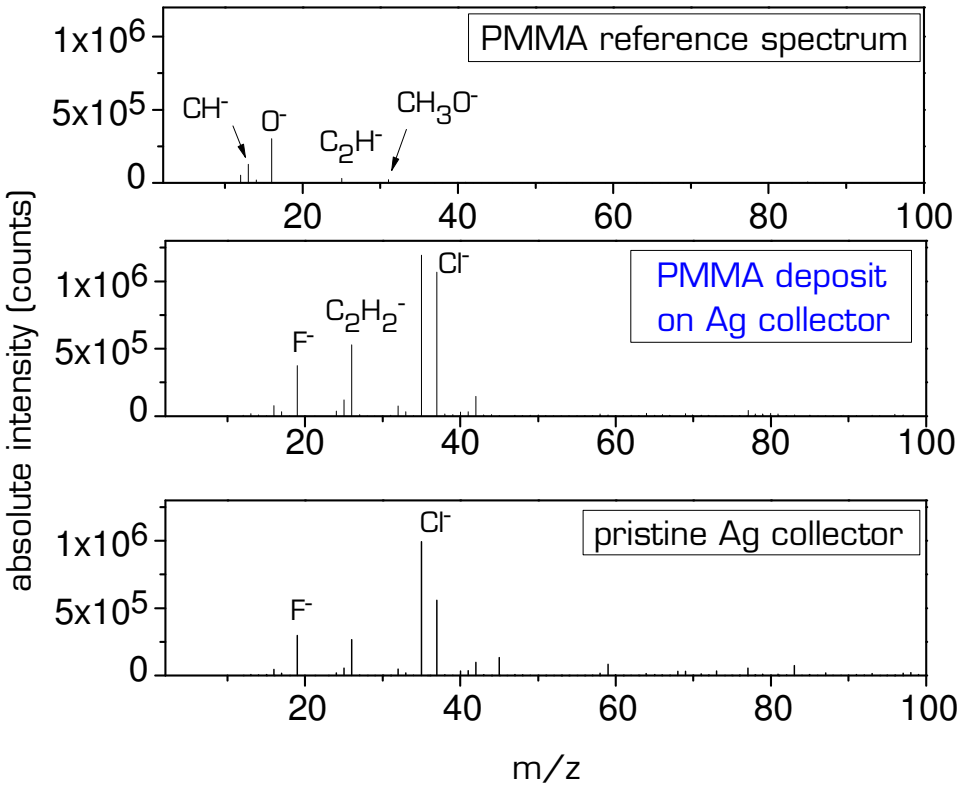

Fig. IV-9: From top to bottom: negative mass spectrum of the PMMA20000 sample, negative Storing Matter spectrum of PMMA20000 on an Ag collector, and negative reference spectrum of the pristine Ag collector.

IV.3. (d) Alq_3 sample

The characteristic peaks of Alq_3 in positive analysis mode[115] are Al^+ (m/z=27), $(Alq)^+$ (m/z=171), $AlqH^+$ (m/z=172), $AlqOH^+$ (m/z=188), Alq_2^+ (m/z=315), and $Al_2q_3O^+$ (m/z=502) (Fig. IV-10). In the Storing Matter spectrum, all these peaks are detected, and their intensity ratios are very similar to those in the reference spectrum (Fig. IV-11). Contrarily to PVC and PMMA, Alq_3 does not seem to undergo significant double fragmentation. No Ag-cationized fragments were detected in the Storing Matter spectrum.

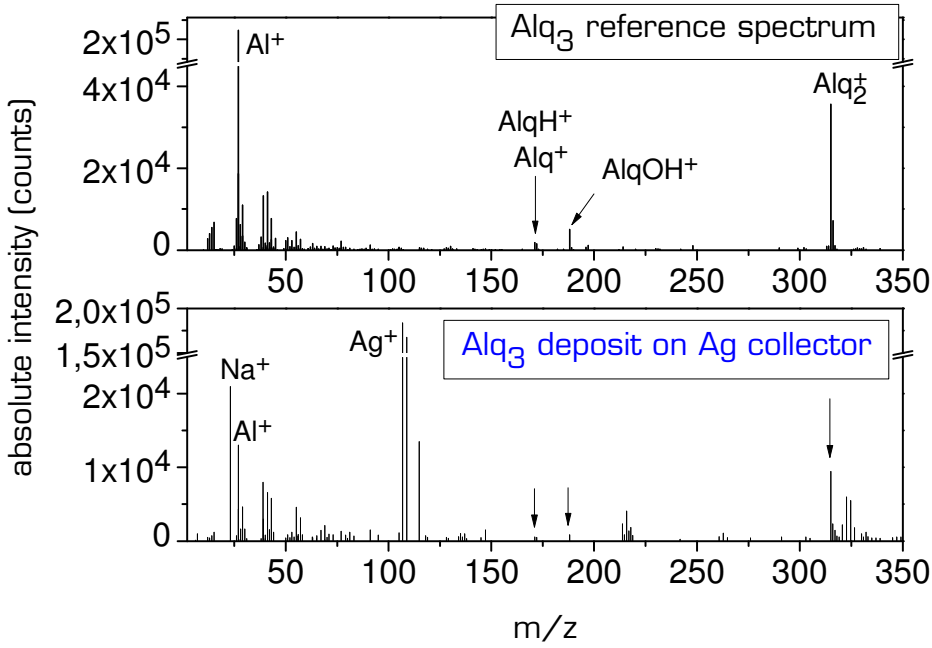

Fig. IV-10: From top to bottom: positive mass spectrum of the Alq_3 sample and positive Storing Matter spectrum of Alq_3 on an Ag collector.

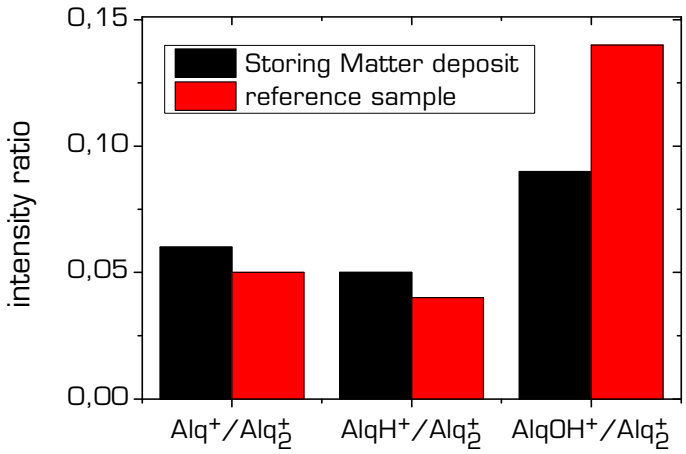

Fig. IV-11: Absolute intensity ratios of characteristic peaks in the Storing Matter spectrum of Alq_3 on an Ag collector and in the Alq_3 reference spectrum.

IV.3. (e) Conclusions

In this section, TOF-SIMS reference spectra as well as Storing Matter mass spectra on Ag collectors were presented for PS, PMMA, PVC and Alq_3 samples. The characteristic peaks of each sample were pointed out, and it was shown that it is possible to identify the 4 organic samples studied in this work by their Storing Matter deposits.

A surprising observation was that the Ag^+ peak is higher in the centre of a Storing Matter deposit than on the pristine Ag collector. This will be discussed more in detail in section IV.5. (c) .

IV.4 Biasing of the sample-holder during sputter-deposition

During the sputter-depositions described above, the polymer sample and the Ag collector were both grounded. In order to get information about the fragmentation and ionization mechanisms involved in the Storing Matter technique, Storing Matter deposits of PVC with different sample potentials (0 V, -100 V and +100 V) were compared. The Ag collectors were always grounded.

When the PVC sample is biased at –100 V, the potential difference between sample and collector prevents cations from being deposited onto the collector. In this case, only neutral and negatively charged particles can be deposited. When the sample voltage is +100 V, only neutrals and anions will be collected. In the usual experimental setup of the sputter-deposition step (collector and sample grounded) the velocities of all the emitted particles (charged and neutral) correspond to their kinetic energy distribution (KED) upon sputtering. The KEDs of fragments and fingerprint ions sputtered from a polymer sample cover a few eV[136,137]. It is possible that some fragments have a kinetic energy that is slightly above the threshold energy for sputtering[138]. Re-sputtering on the collector of already deposited matter by incoming particles may be possible, but it should not be significant because the sputtering yields for such low impact energies would be very low. A potential difference of ±100 V between collector and sample does not affect the velocities of the sputtered neutrals, but the kinetic energies of the positive or negative ions are increased by 100 eV. The resulting impact energy is certainly high enough to cause some re-sputtering on the collector. But since only less than 1% of the particles impacting on the collector are charged, and because the sputtering yield should be very low, re-sputtering should also be negligible in this case.

The 3 Storing Matter deposits of PVC were analyzed in positive and negative mode, and no significant changes in the mass spectra for each polarity were observed for the different sample potentials applied during sputter-deposition. This means that a Storing Matter spectrum mainly consists of fragments that (or whose precursors) were previously deposited as neutrals onto the collector. Consequently the peak distribution in a Storing Matter

spectrum is not necessarily identical with that measured in a direct TOF-SIMS spectrum of the sample.

Moreover the similarity of the Storing Matter spectra obtained for deposits prepared with different bias voltages confirms that re-sputtering on the collector can be neglected.

IV.5 Study of the key parameters of the Storing Matter technique for organic samples

IV.5. (a) The collector surface

The collector surface is one of the most important parameters of the Storing Matter technique. During the analysis step, it constitutes the common matrix for all the deposited particles. The collector surface should thus be well chosen as a function of the organic sample and the desired analytical information.

For inorganic samples, a detailed study about the influence of the collector's work function on the useful yields of Au^-, Ge^-, and In^+ has been carried out at SAM during the last years[139,140]. For organic samples, noble metal collectors should be an appropriate choice since they are successfully used in the MetA-SIMS and ME-SIMS domains to enhance positive secondary ion yields (section II.5). In this section, Storing Matter deposits on Au, Ag, Cu, Si and Cs collectors will be presented.

Assessing the performance of a collector material for an organic material is not straightforward, since many peaks that are characteristic for the studied samples are also present in the mass spectra of the pristine collector, especially hydrocarbon fragments in the low mass range. The "visibility" of a given fragment ion on a collector can be evaluated by calculating the ratio of its intensity measured in the centre of the deposit and on the pristine collector. This ratio will be referred to as "Storing Matter sensitivity" and denoted S_{Stomat} (of course this is not equivalent to the definition of sensitivity in a traditional SIMS analysis):

$$S_{Stomat} = \frac{I(\text{deposit centre})}{I(\text{pristine collector})} \quad \text{(Equation IV-1)}$$

It is important to stress out that S_{Stomat} is not a fixed characteristic value for a given secondary ion/sample/collector combination, but that it depends

on both the sputter-deposition (e.g. amount of deposited matter) and analysis conditions (e.g. primary ion dose).

For a given polymer, the more easily its characteristic peaks can be distinguished from a collector's background signal, the better this collector material is suited for the analysis of this particular Storing Matter deposit in the chosen secondary ion polarity. The use of S_{Stomat} also has the advantage of accounting for changes in absolute intensity due to instrumental variations when deposits analyzed on different days (and even in different instruments) need to be compared.

If S_{Stomat} of a given secondary ion is very different for the same Storing Matter deposit on different collectors, 3 possible reasons can be considered:

- the sticking coefficient of the emitted particles is different for both materials and the amount of deposited matter is significantly different,
- the detection efficiency (resulting from the combination of sputtering, fragmentation, and ionization) of the considered ion during the analysis of the deposit is enhanced by one of the collector materials compared to the other one,
- or the intensity of this ion on the pristine collectors is different.

The last point is related to the main drawback associated with the above definition of S_{Stomat}: indeed this value is affected by variations of the absolute intensity of the considered ion measured on the pristine collector, especially if this intensity is low. In order to minimize this issue, the collectors used for a given experimental series (i. e. when a direct comparison of S_{Stomat} for different deposits was required) were prepared within a few hours and analyzed on the same day (usually the day after their preparation).

For most deposits, the mass spectrum corresponding to the "pristine collector" was actually taken on the collector with the Storing Matter deposit, but at the side opposed to the deposit. It cannot be excluded that in some cases this spectrum contains some fragments resulting from the deposit (due to diffusion processes for example).

IV.5. (a) i) Sample preparation and experimental conditions

Ag, Au and Cu collectors were prepared by electron beam evaporation as described on page 55.

Cs coated collectors were prepared by deposition onto cleaned silicon wafers in the neutral Cs evaporation chamber developed at SAM[27]. Since the sticking factor of Cs on Cs is very low, the coverage is in the (sub-) monolayer range[141-146]. It should also be considered that the Cs covered surface has a high affinity towards oxygen from the residual gas ("getter effect"). Therefore the Cs coated collectors were transferred towards the Storing Matter instrument under UHV conditions.

Alq_3 samples were obtained by vacuum thermal evaporation (page 55), and polymer layers were spin-coated onto silicon substrates (page 54).

The experimental conditions for sputter-deposition and analysis of the deposits described in this section are indicated on pages 65 and 65.

IV.5. (a) ii) Ag vs. Si collector for Alq_3 deposits

In order to investigate the interest of using noble metal collectors for organic samples, Ag and Si collectors were compared in the case of an Alq_3 deposit.

The positive Storing Matter spectra of Alq_3 deposits on an Ag and a Si collector are compared in Fig. IV-12. The absolute intensities of all the characteristic Alq_3 peaks are higher on the Ag collector than on Si. The Alq_2^+ fragment, which provides the most valuable molecular information about the molecular structure, is extremely well visible in the Storing Matter spectrum on Ag. The Storing Matter sensitivities of the characteristic Alq_3 peaks are represented in Fig. IV-13. For the considered positive secondary ions, S_{Stomat} is 4 (for Alq^+) to 81 (for Al^+) times higher for the Ag collector as compared to Si.

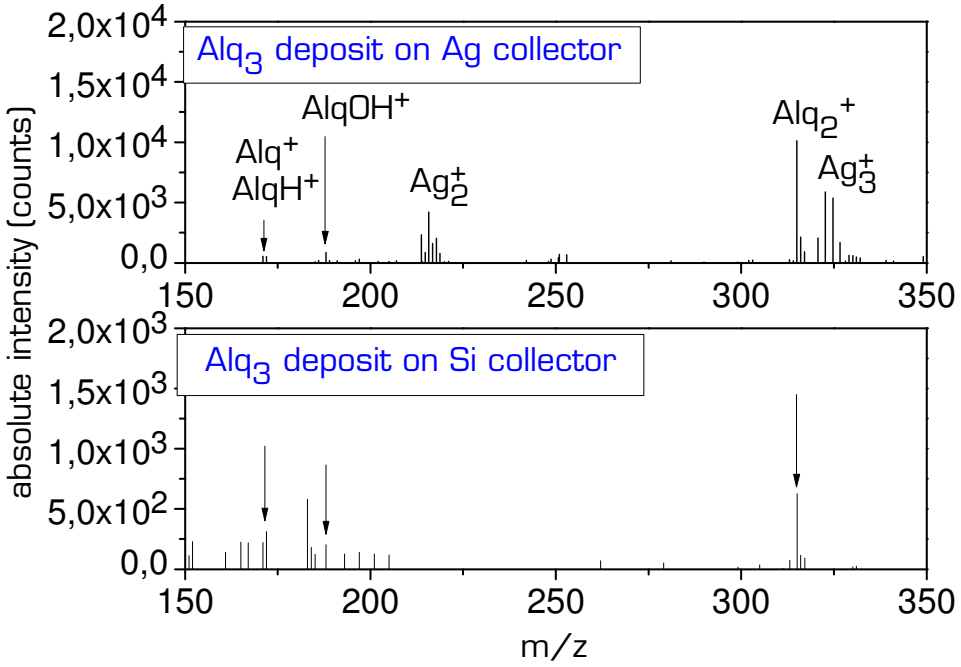

Fig. IV-12: Positive Storing Matter spectra of Alq_3 deposits on an Ag and a Si collector.

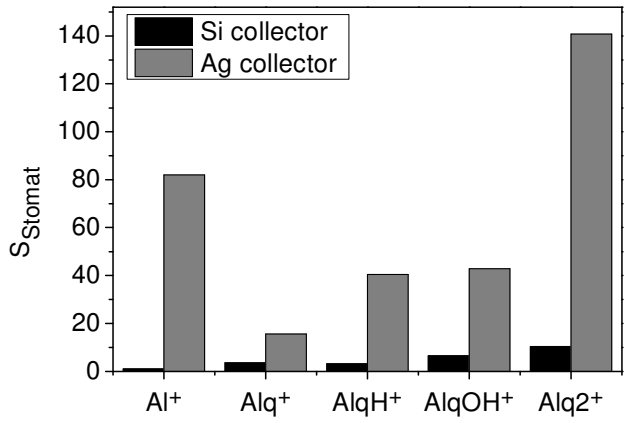

Fig. IV-13: Storing Matter sensitivities of some positive secondary ions for Alq_3 deposits on an Ag and on a Si collector.

The Storing Matter sensitivity of Al^+ on the Si collector is 1, which means that the intensity measured on the deposit is equal to that recorded on

the pristine collector. This might be due to the much higher Al^+ intensity (10^5 counts) on the pristine Si collector (probably due to contaminations) than on the pristine Ag surface (200 counts).

In addition to sputtering/ionization mechanisms, the collector surface may also have an effect on the fragmentation of the deposited particles during the analysis step. For the Storing Matter deposits of Alq_3, some intensity ratios of characteristic fragment ions were calculated for Si and Ag collectors (Fig. IV-14). These values give an indication about the degree of fragmentation of the Alq_3 molecule (assuming that the differences in sticking coefficient and in sputtering/ionization efficiencies between the two collector surfaces affect all the considered fragments in the same way). For the Ag collector, the ratios are similar to those measured directly on the Alq_3 reference sample (Fig. IV-11). The proportion of smaller fragments is higher on the Si collector, suggesting that fragmentation is more important in this case. This might be explained by the increased near-surface energy deposition in the case of the Ag collector: several Ag atoms are set in motion by the collision cascade and can contribute to a collective uplifting of large fragments[67]. Furthermore, the large Ag atom can interact with several atoms of the organic molecule at a time and may thus enhance the desorption of large fragments[66]. Possible bonds and chemical interactions between the deposited particles and the collector surface can also influence the fragmentation mechanisms during the analysis step: a high reactivity of a collector material towards the deposited Alq_3 fragments would favour the breaking of intramolecular bonds[66].

These results illustrate that using an Ag collector instead of Si for a Storing Matter deposit of Alq_3 influences the sputtering/ionization processes during the analysis step in a beneficial way and reduces the fragmentation of the molecule. However, a difference in sticking efficiency of Alq_3 fragments on Ag and Si collectors cannot be excluded.

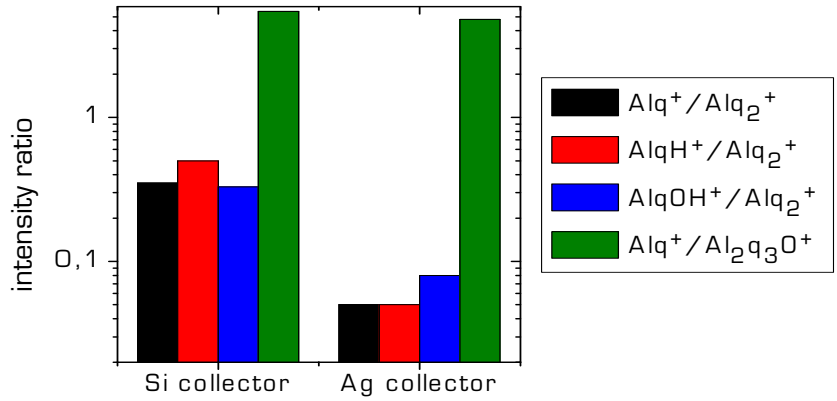

Fig. IV-14: Intensity ratios of characteristic fragments for the positive Storing Matter spectra of Alq_3 on Si and Ag collectors.

IV.5. (a) iii) Comparison of Au, Ag and Cu collectors for a PVC deposit

The positive mass spectra of Storing Matter deposits of PVC on Au, Ag and Cu collectors are displayed in Fig. IV-15. The Storing Matter spectra on the Ag and Cu collectors show a similar hydrocarbon peak series in the low mass range as the PVC reference spectrum, while the peak distribution on the Au collector is totally different. As shown in Chapter III, the positive mass spectrum of the pristine Au collector contains many intense peaks corresponding to organic species. This strong "background signal" makes it impossible to identify a Storing Matter deposit on an Au collector by only looking at the spectra.

The Storing Matter sensitivities of some characteristic PVC peaks for the 3 collectors are displayed in Fig. IV-16. The sensitivities for hydrocarbon fragments are by far the highest on the Ag collector. Here again the question is whether this is due to a difference in sticking coefficients or in desorption and/or ionization yields during the analysis step. For comparison purposes, ME-SIMS (polymer on metal) and MetA-SIMS (metal on polymer) experiments were also carried out for PVC in combination with the 3 noble metals.

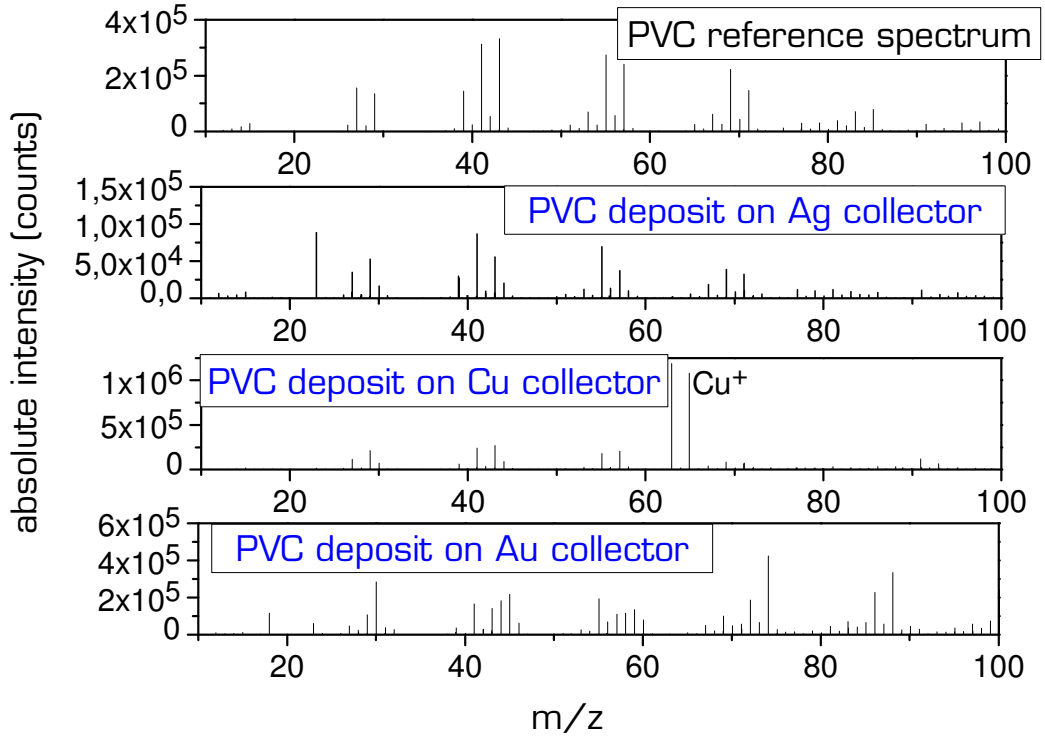

Fig. IV-15: From top to bottom: positive reference spectrum of the PVC sample, positive Storing Matter spectrum of PVC on Ag, Cu, and Au collectors.

ME-SIMS samples were prepared by spin-coating thin layers of PVC from a 0.1 wt% solution in THF onto metal substrates prepared in the collector coating chamber (30nm nominal thickness on cleaned Si wafers) and positive mass spectra were acquired. For an easier comparison with the Storing Matter results, the ME-SIMS sensitivity $S_{ME\text{-}SIMS}$ was defined as the ratio of the absolute intensity of a peak in the ME-SIMS spectrum divided by its intensity on the pristine noble metal. This ratio indicates how easily a characteristic peak of the polymer can be distinguished from the "background signal" of the pristine metal surface. The obtained values are represented in Fig. IV-17. For all the considered fragment ions, the Au substrate provides the highest ME-SIMS sensitivities, while Cu and Ag give similar and very low values. The differences observed for the 3 substrates may be due to one or more of the following parameters:

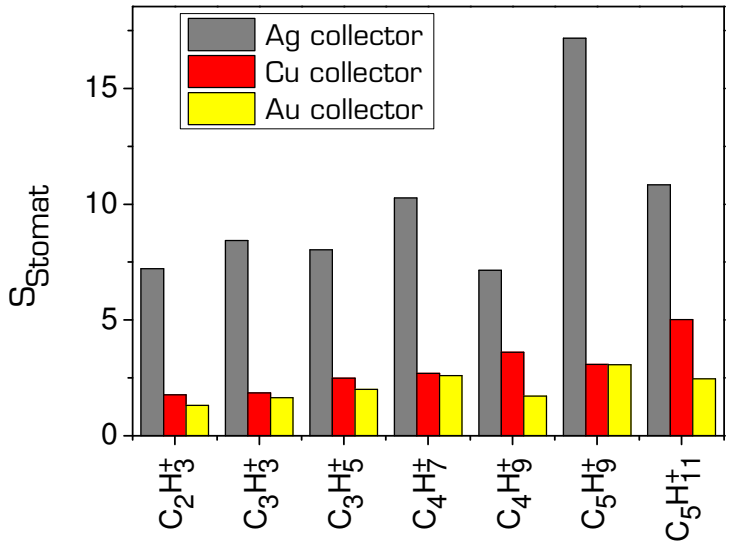

Fig. IV-16: Storing Matter sensitivities of some characteristic positive ions of PVC deposits on Ag, Cu and Au collectors.

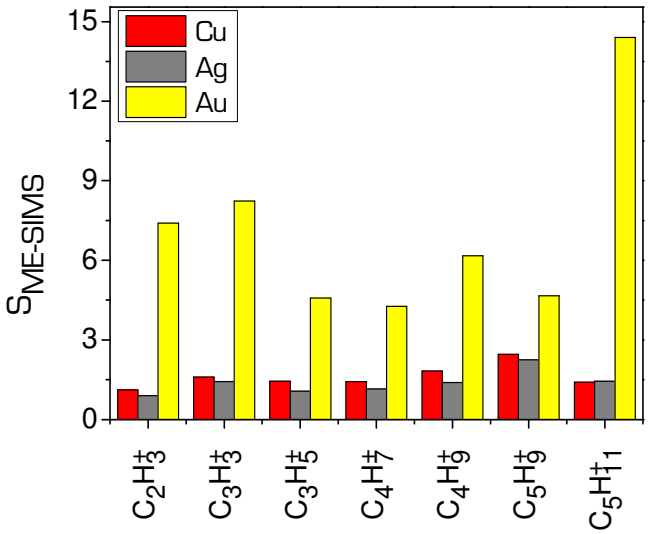

Fig. IV-17: ME-SIMS sensitivities of characteristic PVC for thin PVC layers spin-coated on Cu, Ag and Au substrates. $S_{ME-SIMS}$ is defined as the ratio of the absolute intensity of a peak in the ME-SIMS spectrum divided by its intensity on the pristine noble metal.

(1) Sputtering: due to its large atomic radius, Au has a higher stopping power and thus reflects the projectiles' kinetic energy more efficiently towards the sample surface, causing an increase in sputtering yield of the organic particles on the surface. It is however unlikely that this is the only reason for the above observations, because in that case there should also be a significant difference between the Cu and Ag substrates.

(2) Ionization: the differences observed between the 3 substrates might also be related to the ability of each metal to provide a positive charge to an organic fragment.

(3) Coverage of the metal surface by PVC: although the spin-coating parameters were identical for the 3 noble metal substrates, differences in the structure and coverage of the thin PVC layers depending on the interactions between the metal surface and the polymer solution cannot be excluded.

For ME-SIMS, the use of an Au substrate seems thus to be the best choice for PVC, while Ag seems more beneficial for Storing Matter deposits. This means that changes in ionization probabilities induced by the different noble metals cannot be considered as the only reason for the higher Storing Matter sensitivities obtained with Ag collectors. The different trends observed for the noble metals in Storing Matter and ME-SIMS are either due to different degrees of coverage of the metal surface by the polymer (due to different sticking coefficients in the case of Storing Matter and to different interactions between the polymer solution and the metal surface in the case of ME-SIMS), or the mechanisms that govern the secondary ion emission are fundamentally different in ME-SIMS and in Storing Matter. A Storing Matter deposit consists of polymer fragments of different sizes, while in the ME-SIMS configuration the metal surface is covered with long polymer chains. The comparison of secondary ion formation from a Storing Matter deposit and a ME-SIMS sample is thus not straightforward since the starting materials are very different. Moreover, the deposition methods (sputter-deposition and spin-coating) are different and may also influence the way the polymer or the organic fragments

interact with the metallic substrate. From this point of view, the different trends observed for the noble metals in the case of Storing Matter and ME-SIMS seem less contradictory. Furthermore, variations in surface coverage from one noble metal to another cannot be ruled out for the Storing Matter deposits and for the ME-SIMS samples.

For complementary MetA-SIMS experiments, 3 PVC samples were covered by 2nm (nominal thickness) of Au, Ag, or Cu in the collector coating chamber and transferred to the TOFIII instrument with the UHV suitcase. For the characteristic peaks already considered in Fig. IV-16, the MetA-SIMS enhancement factor (ratio of the intensity measured on the metal coated PVC sample as compared to the PVC reference sample) was calculated for each noble metal (Fig. IV-18). These enhancement factors should be considered with caution because the metallization procedure introduces also organic contaminants that might contribute to the hydrocarbon peak intensities in the low mass range. It is thus possible that the enhancement factors for the hydrocarbon cations are overestimated. The observed yield enhancements are quite low, and for some peaks the signal seems even to be suppressed by the presence of the Ag or Cu overlayer ($C_3H_3^+$, $C_4H_7^+$, and $C_5H_9^+$). Due to the non-negligible contribution of organic contaminants to the positive MetA-SIMS mass spectra, it would be risky to draw any conclusions from these experiments. Furthermore, it would be necessary to analyze samples covered with various amounts of noble metals since this parameter has a significant influence on the yield enhancement.

Ag and Au collectors were also compared for Storing Matter deposits of PS. Except for $C_7H_7^+$, the sensitivities of the considered characteristic ions are higher on the Ag collector (Fig. IV-19). The difference between the 2 metals is however smaller than for the PVC deposits.

It can thus be concluded that Ag collectors are well suited for Storing Matter deposits of organic materials if the deposits are analyzed in the positive secondary ion polarity.

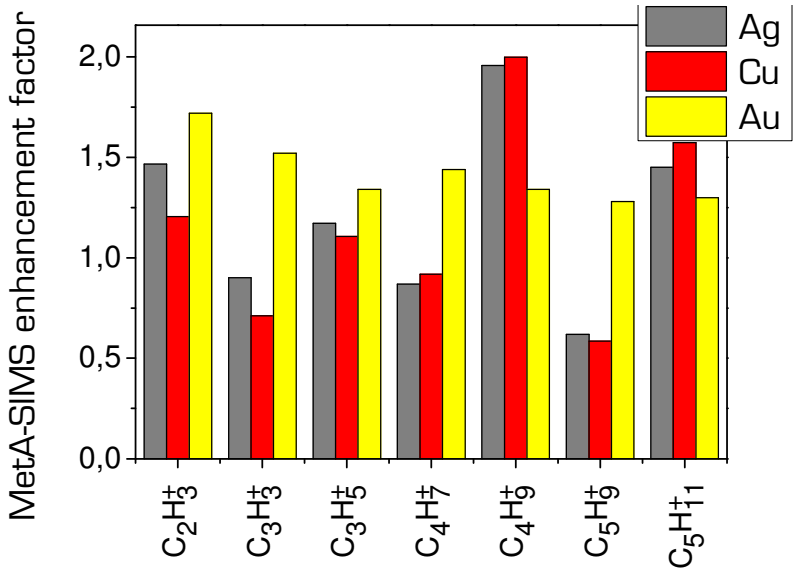

Fig. IV-18: MetA-SIMS enhancement factors of characteristic PVC peaks for Ag, Cu and Au (positive analysis mode).

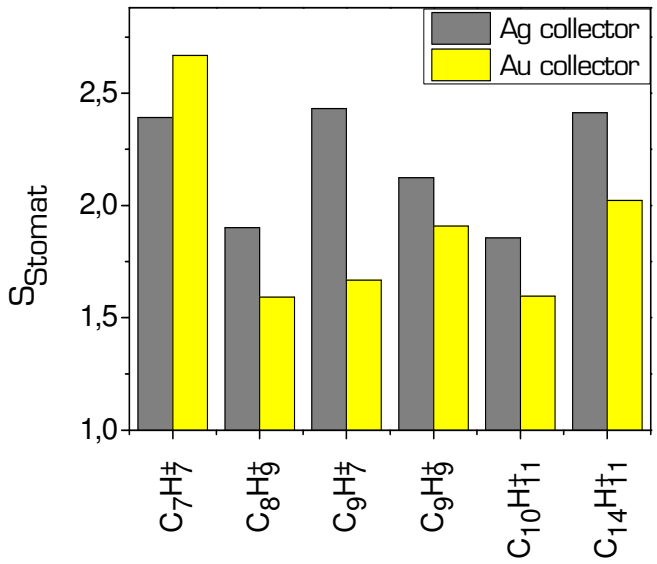

Fig. IV-19: Storing Matter sensitivities of some characteristic positive ions of PS deposits on Ag and Au collectors.

IV.5. (a) iv) Cs collectors

Noble metal collectors are the first choice for Storing Matter deposits of organic samples if the deposit is analyzed in positive mode. The use of Cs

coated collectors might be interesting for negative analysis, because Cs has a low work function and therefore enhances the negative ionization yields[9,147]. Cs is also the most electropositive element and thus a good electron donor. Furthermore, it has been shown that Cs forms positively charged clusters with organic fragments (MCs_x^+)[23,148,149] and that it reduces the formation of chemical damage during ion irradiation of polymers[117].

Storing Matter deposits of PMMA were prepared on a Cs collector and on an Ag collector. Fig. IV-20 shows the Storing Matter sensitivities of several negatively charged characteristic PMMA fragments. More different O-containing fragments are detected on the Cs collector than on Ag. This means that either the double fragmentation is reduced in the case of the Cs collector, or that oxygen-containing fragments are more easily detected on a Cs surface. The latter option is more likely since the oxygenated fragments that were detected on both collectors have a higher S_{Stomat} on the Cs collector. For negative analysis mode, Cs collectors are thus better suited than Ag.

In the positive mass spectrum (not shown here) of the PMMA deposit on Cs, two characteristic MCs_x^+ ions were detected: $Cs_2CH_3O^+$ (m/z=297) and $Cs_2C_4H_5O_2^+$ (m/z=351). These clusters consist of two Cs^+ cations combined with CH_3O^- and $C_4H_5O_2^-$, respectively. These two anions are the most intense oxygen-containing peaks in the negative reference spectrum of PMMA. Hence the PMMA deposit can also be identified in the MCs_x^+ mode.

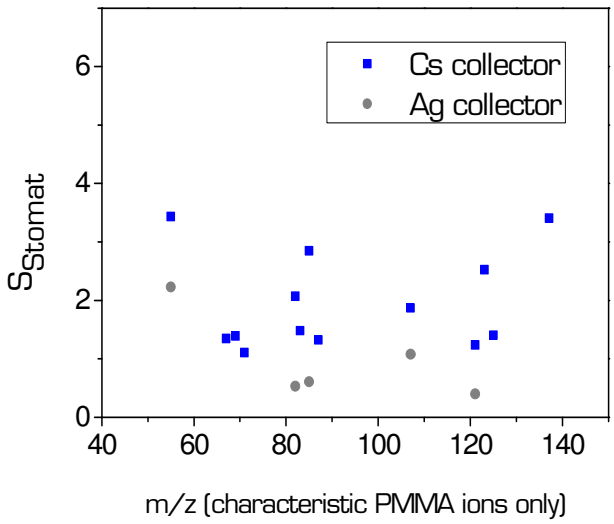

Fig. IV-20: Storing Matter sensitivities for characteristic negatively charged fragments for a PMMA deposit on an Ag and on a Cs collector.

IV.5. (a) v) Importance of UHV transfer of the deposits

In order to highlight the importance of keeping the collectors under UHV conditions during the entire experiment (from the preparation of the collectors until the analysis of the deposit), a pristine Ag collector was first analyzed by TOF-SIMS after UHV transfer from the Storing Matter prototype, then exposed to air during 3 minutes, re-introduced into the instrument and analyzed again under the same conditions. 3 minutes would be approximately the time required for a transfer under atmospheric conditions of the collector between 2 instruments.

The low and high mass range of the positive mass spectra recorded before and after air exposure is shown in Fig. IV-21 and Fig. IV-22, respectively. Exposing the Ag collector to air has striking consequences:

- The total intensity of all the positive peaks is increased by a factor 10 (from $3.4 \cdot 10^5$ to $3.1 \cdot 10^6$ counts).
- The hydrocarbon peaks in the mass range m/z<100 show an average increase by a factor 8.

- Oxygen containing peaks are particularly enhanced by air exposure. For example, the CHO^+ (m/z=29) intensity becomes 20 times higher and Ag_3O^+ increases by a factor 57.
- The Ag_n^+ peaks are 5 to 17 times higher. The mechanisms leading to this somewhat surprising signal increase are probably similar to those that cause the Ag_n^+ peaks to be higher in a Storing Matter spectrum than on the pristine Ag collector.
- Small Ag-cationized hydrocarbon fragments of the type $AgC_nC_{2n}^+$ are enhanced by one order of magnitude.

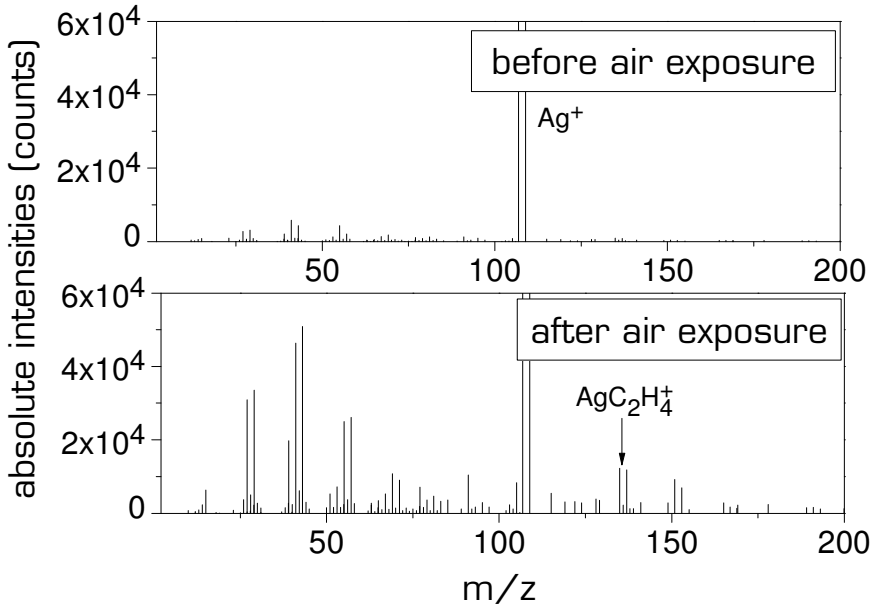

Fig. IV-21: Positive mass spectra (low mass range) of a pristine Ag collector before and after air exposure. The absolute intensity of the $^{107}Ag^+$ peak is $1.2 \cdot 10^5$ counts before air exposure and $1.2 \cdot 10^6$ counts after air exposure.

The Ag surface is thus highly altered by adsorption of organic and inorganic (especially oxygen) species after 3 minutes in air. The resulting higher peak intensities of inorganic and especially organic contaminants on the pristine collector would represent a disturbing background signal for the analysis of a Storing Matter deposit on this collector and the Storing Matter sensitivities would decrease. Vacuum transfer of the collectors between the different chambers (from the collector coating chamber to the sputter-deposition

chamber and then to the analytical instrument) is thus extremely important and was carried out for all the Storing Matter deposits presented in this work.

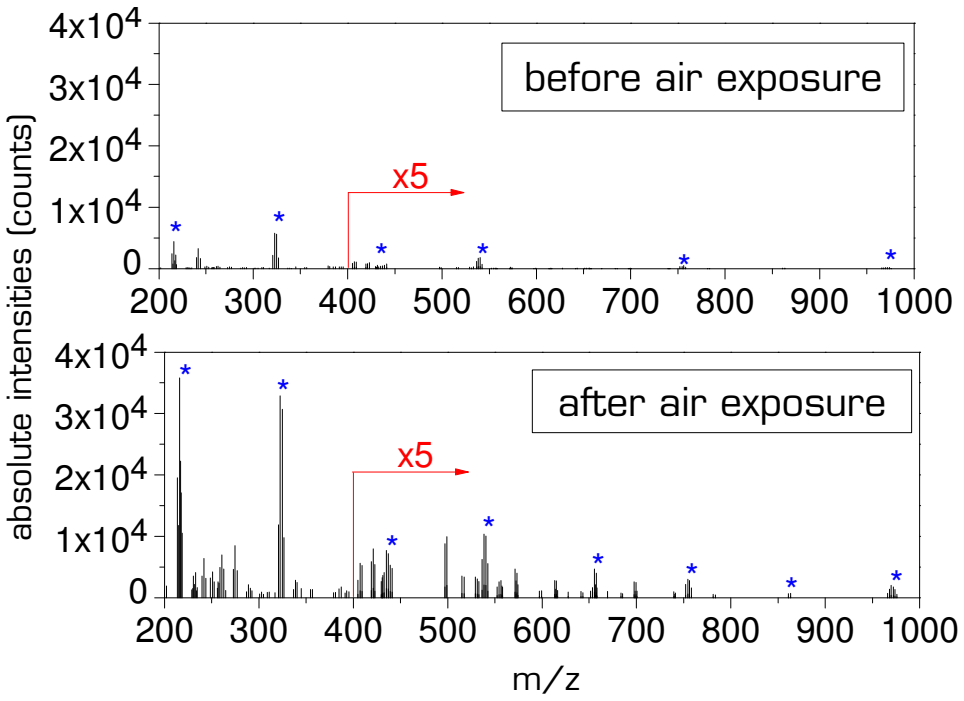

Fig. IV-22: Positive mass spectra (high mass range) of a pristine Ag collector before and after air exposure. Ag_n^+ peaks are marked with blue asterisks.

IV.5. (b) Sample preparation methods to enhance Ag-cationization for Storing Matter deposits of PS

IV.5. (b) i) Introduction

One of the reasons for using noble metal collectors is that, in addition to the fingerprint ions in the low mass range, metal-cationized fragments providing valuable molecular information may be detected in the positive Storing Matter spectra. However, for the deposits presented in the previous section only small and unspecific metal-cationized fragments, such as $AgC_2H_4^+$ or Ag_2Cl^+, have been detected. The same observation has been made for the MetA-SIMS and ME-SIMS results presented above. This absence of high mass fragments is probably due to the relatively high chain lengths of the polymers

used for these experiments. It is likely that chain entanglement prevented the emission of large fragments composed of several monomer units.

IV.5. (b) ii) Sample preparation

In order to further investigate Ag-cationization in Storing Matter, low molecular weight PS (3700 Da) was used for the experiments presented in this section. Moreover, different methods for metal-cationization used in traditional SIMS were combined with the Storing Matter technique. The samples used for sputter-deposition were prepared as follows:

- PS sample: a PS layer was spin-coated onto a cleaned Si wafer from a 2 wt% solution in toluene.
- Ag on PS sample: the same PS sample was covered with a small amount of Ag (2 nm nominal thickness) in the collector coating chamber.
- PS on Ag sample: a thin layer of PS was spin-coated on an Ag substrate from a very diluted solution of PS in toluene (0.1 wt%).
- PS/AgTFA sample: AgTFA (silver trifluoroacetate, formula shown in Fig. IV-23) was added to a solution of PS in THF (tetrahydrofuran) which was then spin-coated onto a cleaned Si wafer. The solution concentrations were 1 mg/mL for PS and 1 mg/mL for AgTFA, which corresponds to one Ag atom for 2 styrene monomer units. AgTFA is commonly used for sample preparation in MALDI-MS (Matrix-Assisted Laser Desorption/Ionization Mass Spectrometry) experiments and has also been found to enhance cationization in SIMS measurements[70,150].

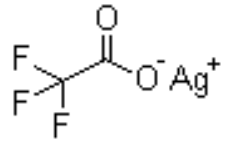

Fig. IV-23: Molecular structure of AgTFA.

These 4 samples were sputter-deposited onto Si and Ag collectors under identical conditions (page 65). The Storing Matter deposits, as well as

the PS-based reference samples, were analyzed in positive mode (analysis conditions described on page 65).

IV.5. (b) iii) Results and discussion

Fig. IV-24 shows the positive reference spectra of PS, Ag on PS, PS on Ag, and PS/AgTFA. For the 3 Ag-containing samples, some Ag-cationized peak series were detected in the high mass range: Ag-cationized styrene oligomers $[Ag(C_8H_8)_n]^+$, Ag-cationized oligomers with a butyl chain end and an extra proton $[C_4H_9(C_8H_8)_nHAg]^+$, and the latter fragments with loss of a C_7H_6 fragment $\{[C_4H_9(C_8H_8)_nHAg]\text{-}C_7H_6\}^+$. These 3 peak series mirror the structure of the styrene monomer unit and of the butyl chain end group. They are very valuable from an analytical point of view since the mass spectrum of the pristine PS sample does not contain any oligomer fragments.

In the mass spectrum of the PS/AgTFA sample, $[C_4H_9(C_8H_8)_nHAg]^+$ peaks are visible up to m/z=2 000, but the $\{[C_4H_9(C_8H_8)_nHAg]\text{-}C_7H_6\}^+$ series is absent. This suggests that the interaction of the Ag atoms with the polymer chains is different for this sample type than for the Ag on PS and PS on Ag sample configurations. Ag_n^+ peaks with n ranging from 2 to 5 were also detected. This indicates that the Ag atoms form clusters on the PS/AgTFA sample surface[70,150]. The absolute intensities of the Ag-cationized fragments detected for this sample are in average one order of magnitude lower than for the PS on Ag sample, which is in agreement with results reported by Delcorte[150].

The mass spectra of Ag on PS and of PS on Ag are qualitatively very similar, but the intensities of the Ag-cationized fragments are up to 3 times higher for the latter sample. This is in agreement with previous results obtained by Delcorte[74]. Since the PS layer on the Ag substrate is very thin, chain entanglement is reduced. The Ag substrate below the thin PS layer seems to favour the emission of large fragments. This desorption mechanism might also play a role for the Ag-covered PS sample if one assumes that the PS macromolecules diffuse over the Ag islands, but in this case only a fraction of the PS molecules on the surface are in contact with Ag clusters. In the PS/AgTFA sample, the presence of the large Ag atoms probably also influences the sputtering mechanisms, but to a lesser extent than for the two other samples.

The fact that the Ag on PS3700 and the PS3700 on Ag mass spectra contain large Ag-cationized fragments, while this was not the case for the PS samples of higher molecular weight used in section IV.3. (b) , suggests that polymer chain length is a crucial parameter in metal-cationization experiments. Shorter chains are less entangled and can more easily diffuse on metallic clusters (or vice versa). This argument is supported by a study by Delcorte et al. on the diffusion of PS chains over Au clusters[71]. They concluded that the diffusion speed is of the order of some µm per hour for PS700, and at least 10 times slower for PS2180. They also found that for an Au-covered PS sample, Au-cationized oligomers larger than 3 000 Da could not be detected, while fragments of up to 10 000 Da were detected on thin PS overlayers on Au substrates. These findings suggest that the diffusion process of oligomers larger than 3 000-4 000 Da over the Au islands is not efficient enough to give rise to large Au-cationized fragments.

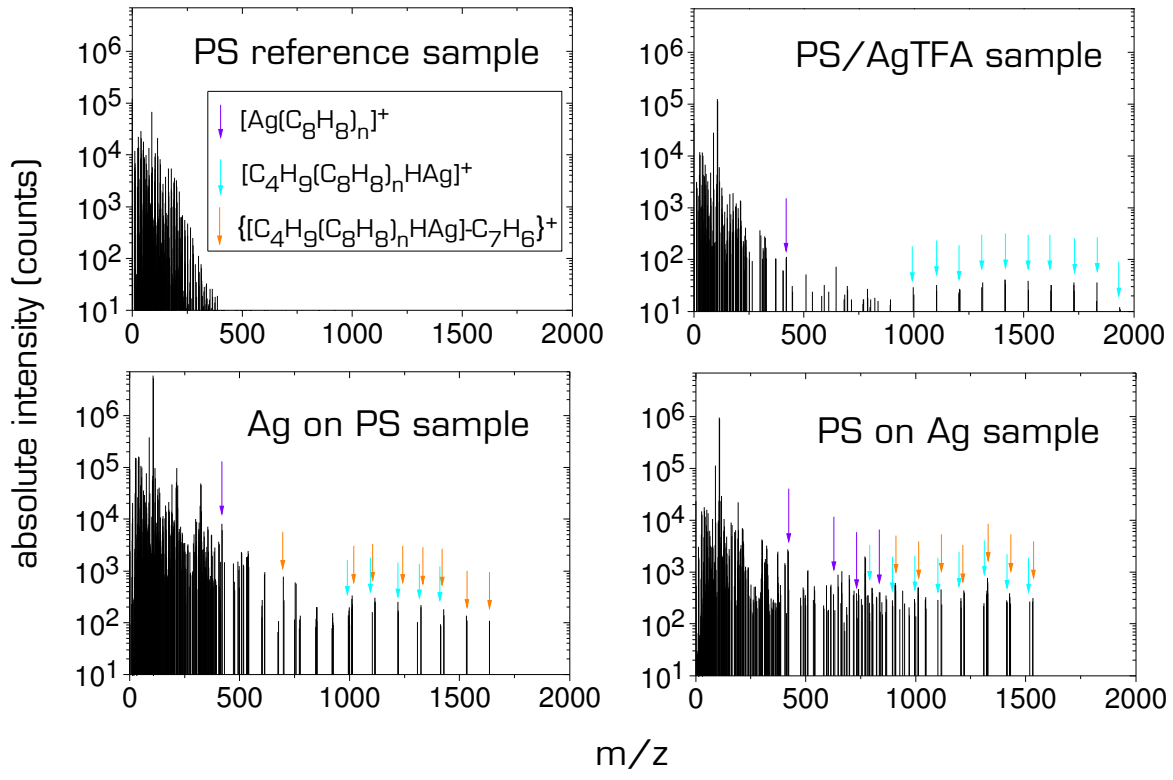

Fig. IV-24: Positive mass spectra of the PS reference sample, the Ag on PS sample, the PS on Ag sample, and the PS/AgTFA sample.

Fig. IV-25 represents the positive Storing Matter spectra obtained on the deposits of the 4 samples on Si and Ag collectors. For the deposit of the Ag-covered PS on a Si collector, some Ag-cationized fragments were detected, but their intensities were very low. It is possible that these adducts were already generated in the sputter-deposition step or that they are only formed on the Si collector surface when an organic fragment and an Ag atom that were deposited independently enter in contact. Since the deposit is very dilute, the latter option seems rather unlikely, except if the diffusion processes were very efficient.

The 4 Storing Matter deposits on Ag collectors all present at least some ions of the 3 Ag-cationized peak series that were already observed for the Ag-containing reference samples in Fig. IV-24. The Storing Matter spectrum of the pristine PS sample on the Ag collector contains the least Ag-cationized fragments. There is thus an additional benefit for the high mass range of the Storing Matter spectra if Ag is already present in the sample used for sputter-deposition. The deposit obtained from a thin PS layer on an Ag substrate yields the most numerous and most intense Ag-cationized ions. These adducts may be formed via 2 different mechanisms: (1) the Ag atom originates from the initial sample and the adducts were not destroyed during the analysis step, or (2) the Ag-cationized fragments result from the recombination of an organic fragment with one of the Ag atoms that constitute the collector surface. Mechanism (1) alone seems unlikely because in that case the Ag-cationized fragments should also be easily detected in the Storing Matter deposits of Ag-containing PS samples on Si collectors. (2) is very probable because all the deposited fragments are in contact with the Ag collector. In the case of the pristine PS deposit on the Ag collector, (2) is the only possible mechanism. For the Storing Matter deposits obtained from Ag-containing PS samples, a combination of (1) and (2) seems most likely.

The high mass ranges of the Storing Matter spectra on Ag collectors are qualitatively and quantitatively very similar to those of their respective reference sample shown in Fig. IV-24. Fragmentation and ejection mechanisms are the determining parameter for the sputter-deposition step, while for the analysis step sputtering and ionization play a role (and possibly further fragmentation, but this was obviously not significant in the case of the large

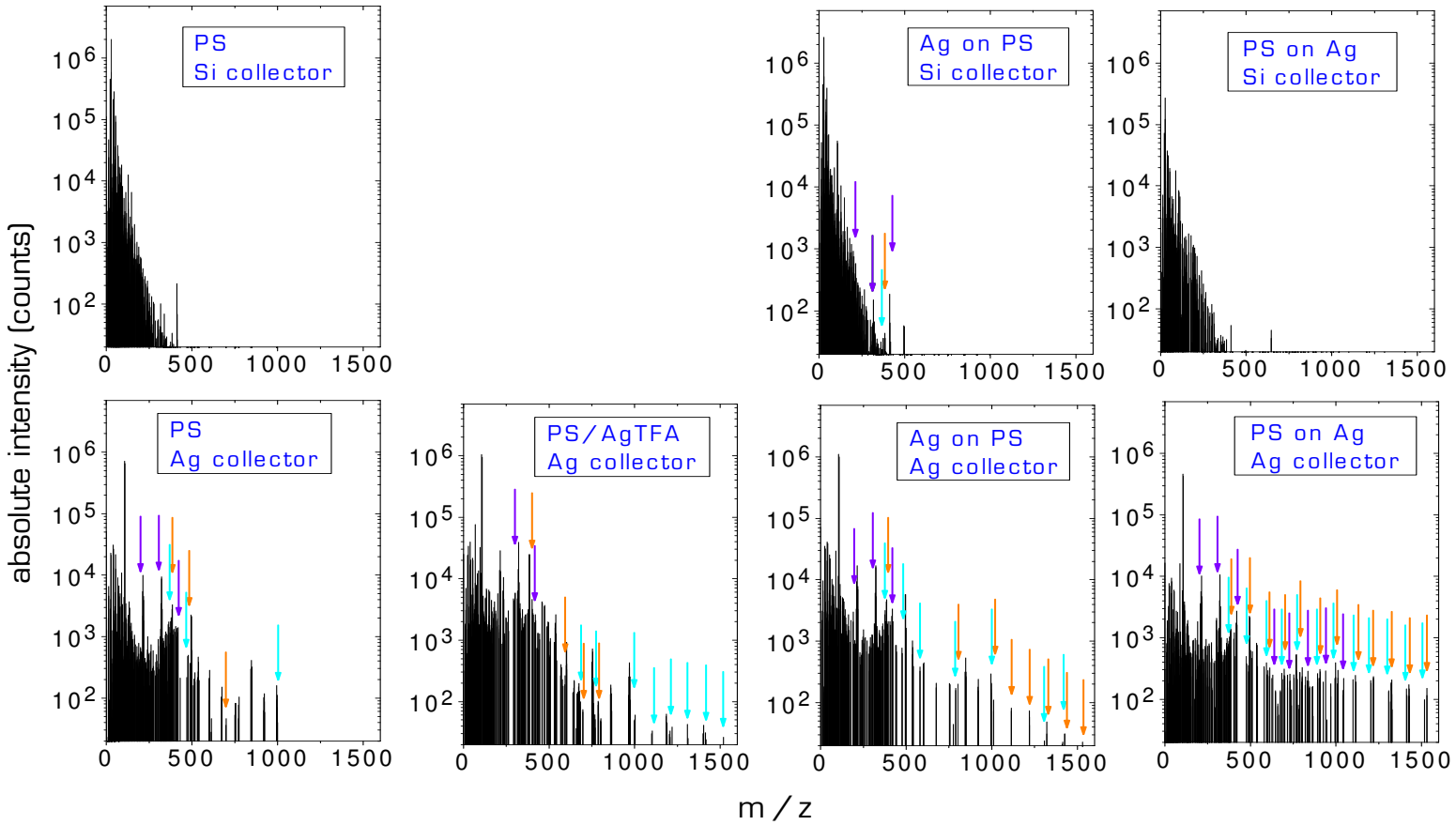

Fig. IV-25: Positive Storing Matter spectra for deposits of PS, Ag on PS, PS on Ag, and PS/AgTFA on Si and Ag collectors. The signification of the coloured arrows is the same as in Fig. IV-24.

fragments detected in the Storing Matter spectra). The conditions for sputtering and ionization of a fragment from a given collector surface are identical for all the deposits on Ag collectors, consequently the differences in the high mass range of the Storing Matter spectra of the 4 PS-containing samples are essentially due to fragmentation and ejection probabilities of large fragments during the sputter-deposition step. This explains the similarity of the high mass range of the reference spectra and the Storing Matter spectra.

There are three basic requirements for the lift-off of large chain fragments from a polymer sample surface: (1) the part of the polymer chain containing the considered fragment should be localized inside the sputter crater, but not in the central region where most bond scissions take place; (2) the chain entanglement and other inter- or intramolecular interactions should be weak in order to allow the extrication of the fragment from the polymer matrix; (3) the emission mechanism of the fragment should be gentle enough to avoid further bond scissions. According to the intensities of the Ag-cationized fragments in the Storing Matter spectra (Fig. IV-25) as well as in the reference spectra (Fig. IV-24), the efficiency of large fragment ejection can be classified as follows: PS sample < PS/AgTFA < Ag on PS < PS on Ag. This order seems quite logical: for the PS on Ag sample, the increased near-surface energy deposition in the Ag substrate and the lower degree of chain entanglement both facilitate the emission of large fragments. The Ag cluster islands on the surface of the Ag on PS sample provide a similar but less pronounced effect, while the Ag atoms (and clusters) present in the PS/AgTFA sample probably have a significantly smaller influence on the sputtering efficiencies. Chain entanglement in these 2 samples is probably more important than for the PS on Ag sample.

The Storing Matter sensitivities of the $C_7H_7^+$ ion calculated for the deposits of different PS-containing samples on Ag and Si collectors are shown in Fig. IV-26. The values are 2 - 3 times higher on the Ag collectors than on Si. For $C_7H_7^+$, the evolution of S_{Stomat} of the 4 deposits on the Ag collectors is slightly different from that of the intensities of the Ag-cationized fragments (the order of PS/AgTFA and the Ag on PS samples is switched). The similarity between reference and Storing Matter spectra is thus restricted to the high mass range, which contains only fragments that do not suffer significant double

fragmentation. On the contrary, small fingerprint fragments like $C_7H_7^+$ can be formed via many different pathways, as well directly in the sputter-deposition step as during the analysis (by double fragmentation of larger chains). Moreover, contrarily to the Ag-cationized fragments, the formation of fingerprint ions does not require the proximity of Ag atoms. It is thus not surprising that the behaviour of a small fragment is different from that of large Ag-cationized oligomers.

In addition to the use of Ag collectors, Ag-cationization of PS oligomers with the Storing Matter technique can be further enhanced by adding Ag in any form to the sample used for sputter-deposition. The best results are obtained in the case of the PS layer on an Ag substrate, which is also the sample that yields the highest intensities in the reference spectra. However the only method that is applicable to real-world samples is the evaporation of small amounts of Ag onto the organic sample's surface since the other preparation routes require the analyte to be solubilized for spin-coating.

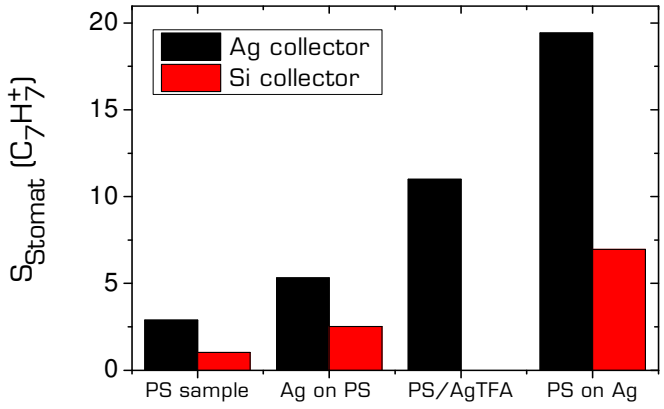

Fig. IV-26: Storing Matter sensitivity of the $C_7H_7^+$ ion for deposits of different PS-containing samples on Ag and Si collectors.

IV.5. (c) The amount of matter deposited on the collector

IV.5. (c) i) Introduction

The amount of organic matter deposited onto the collector is one of the key parameters of the Storing Matter technique: there should be enough particles on the collector to allow an efficient detection during the static SIMS analysis, but the coverage should be inferior to one monolayer so that all the deposited particles are in contact with the same matrix (i.e. the collector surface).

The amount of deposit on the collector depends on three factors:

- the sputtering yield of the organic sample,
- the sticking factor of the emitted particles on the collector,
- and the total number of primary ions used for the sputter-deposition step.

For a given polymer/collector combination and fixed ion beam conditions (impact energy and angle, primary ion type, fluence), only the last parameter can be experimentally controlled.

IV.5. (c) ii) Experimental conditions

PS2000 samples were sputter-deposited onto Ag collectors with varying total numbers of primary ions, thus forming deposits with different degrees of coverage. In order to keep the sputter-deposition fluence constant ($5 \cdot 10^{12}$ ions/cm^2) for all the deposits, only the size of the total bombarded area was modified while the raster size, the ion current, and the speed of the sample stage were identical (as described on page 65). The values chosen for the sputtered area and the corresponding number of primary ions used for each sputter-deposition are given in Table IV-1. By assuming that the sticking factor does not undergo any significant variations during the sputter-deposition step (i.e. that the sticking coefficient is independent of the amount of deposit already present on the collector, at least for the low degrees of coverage considered

here), it can be considered that the degree of surface coverage by the deposit is proportional to the number of Ar^+ ions used for the sputter-deposition.

IV.5. (c) iii) Results and discussion

For these deposits, the Storing Matter sensitivities for 3 characteristic PS fragments and for the Ag^+ peak are compared in Fig. IV-27 and Fig. IV-28. For PS-characteristic organic fragments such as $C_7H_7^+$ (m/z=91), $C_9H_7^+$ (m/z=115), or $C_{14}H_{13}^+$ (m/z=181), S_{Stomat} increases as a function of the deposit coverage, while the Ag^+ intensity becomes more and more inferior to the value measured on the pristine Ag collector. These observations confirm that the amount of organic fragments on the collector increases and progressively covers the Ag collector.

Deposit	N°1	N°2	N°3	N°4	N°5	N°6
area (cm^2)	0.15	0.60	1.00	2.25	4.29	6.30
primary ions	$7.5 \cdot 10^{11}$	$3.0 \cdot 10^{12}$	$5.0 \cdot 10^{12}$	$1.1 \cdot 10^{13}$	$2.1 \cdot 10^{13}$	$3.2 \cdot 10^{13}$

Table IV-2: Total bombarded area and number of primary ions used for the sputter-deposition of PS2000 samples onto Ag collectors. The fluence was $5.0 \cdot 10^{12}$ ions/cm^2 for all the deposits.

For comparison purposes, thin layers of PS2000 were spin-coated onto Ag substrates from solutions with varying concentrations (0.002 - 0.87 mg/mL) and analyzed by TOF-SIMS. Fig. IV-29 displays the absolute intensity variations of $C_7H_7^+$ and Ag^+ as a function of the concentration of the PS solution. The first point corresponds to the intensity measured on the pristine Ag substrate. With increasing PS concentration, the $C_7H_7^+$ intensity first increases, reaches a maximum somewhere between 0.01 and 0.1 mg/mL, and then decreases again. This decrease can be attributed to the progressive loss of the yield-enhancing effect of the Ag substrate as the PS coverage

increases, and also to an increasing chain entanglement. Qualitatively similar results have been found by Muddiman[151] for thin PS layers on etched silver, and by Wehbe[152] in the case of Au substrates covered with thin PS layers obtained by spin-coating from solutions of varying concentrations.

As can be seen in the second frame in Fig. IV-29, the presence of a small quantity of PS enhances the Ag^+ intensity by one order of magnitude. Even for the highest PS concentration, the Ag^+ signal is still 5 times higher than on the pristine Ag surface. Such a signal enhancement has also been observed for an Ag collector exposed to atmospheric pressure during 3 minutes (section IV.5. (a) v)), and to a lesser extent for Storing Matter deposits on Ag collectors. The Ag^+ intensity is thus influenced by a matrix effect related to the organic sub-monolayer. Schnieders et al. also reported an increase of the Ag^+ peak for sub-monolayer coverages of adenine and β-alanine on Ag[56,153]. With the help of complementary laser-SNMS measurements (no ionization matrix effects), they were able to separate the matrix effect experienced by Ag^+ into sputtering and ionization effects: in presence of the adenine sub-monolayer, the matrix effect of Ag^+ was ionization-induced, while with the β-alanine overlayer there was a sputter-induced matrix effect. On the other hand, the matrix effect experienced by the organic secondary ions was sputter-induced for both materials, and for β-alanine there was an additional contribution by ionization effects. The sputtering enhancement of the organic species can be explained by the high stopping power of Ag. The sputtering-enhancement is thus reciprocal for alanine on Ag, indicating that this molecule, even at sub-monolayer coverage, significantly affects the collision cascades, while this is not the case for adenine. As for the ionization-induced matrix effects, it seems logical that only one of the interacting materials (metallic or organic) can be concerned.

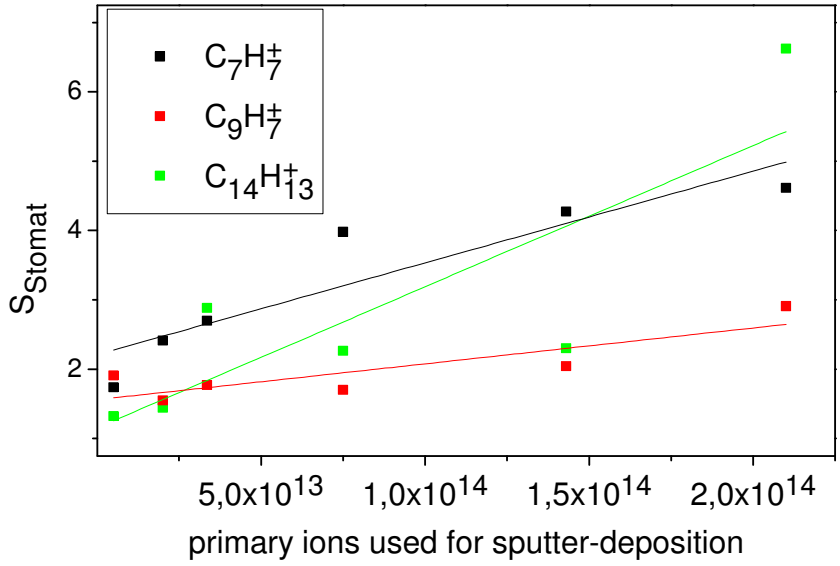

Fig. IV-27: Storing Matter sensitivities of 3 characteristic peaks for PS deposits on Ag collectors prepared with different numbers of primary ions. The straight lines are meant to guide the eyes.

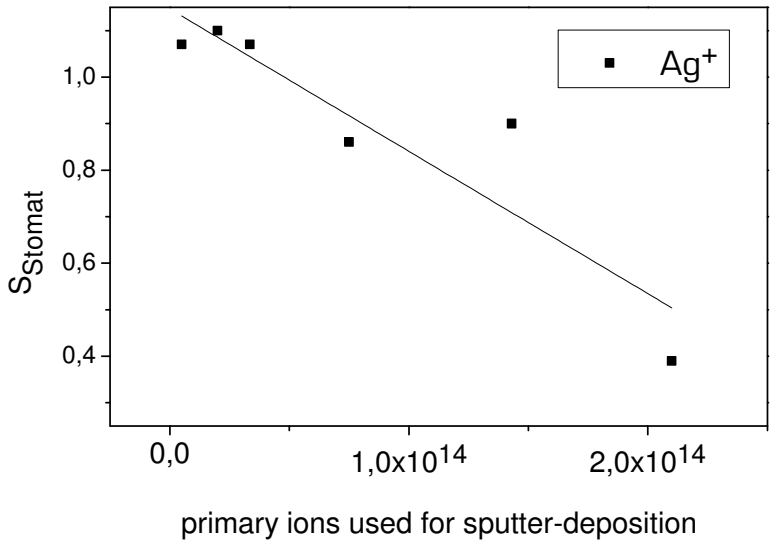

Fig. IV-28: Storing Matter sensitivities of Ag^+ (sum of both isotopes) for PS deposits on Ag collectors prepared with different numbers of primary ions. The straight line is meant to guide the eyes.

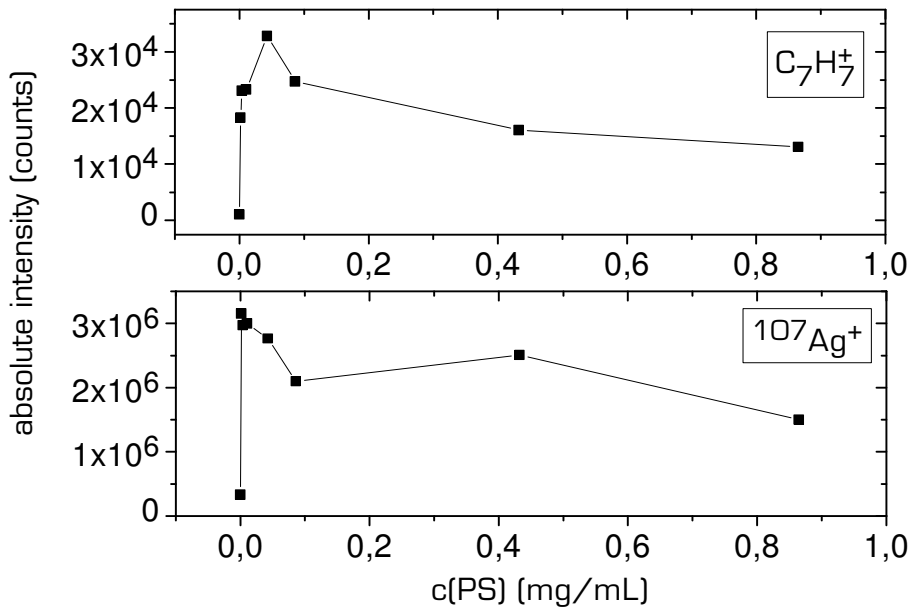

Fig. IV-29: Absolute intensity of the $C_7H_7^+$ and Ag^+ peaks for PS2000 dissolved in toluene at different concentrations and spin-coated on Ag substrates. The first data point corresponds to the intensities measured on the pristine Ag substrate.

Muddiman found that the Ag^+ intensity was constant in the concentration range in which the PS signal increased with coverage and then dropped[151]. This shows that the evolution of the Ag^+ intensity in the low coverage region is determined by 2 competing factors: on one hand the matrix effect (sputter- or ionization effects) induced by the presence of the organic material, and on the other hand the progressive decrease of available Ag surface with increasing coverage by organic material.

The yield enhancement of a metallic cation in presence of an organic sub-monolayer thus depends on the charge transfers taking place between the two materials and on the organic material's ability to influence the collision cascade. The latter factor is probably influenced by the exact arrangement of the molecules on the metallic surface, i.e. whether there is formation of organic islands, diffusion of the molecules over the metal and vice-versa, etc.

IV.5. (c) iv) Conclusions

Since the Storing Matter sensitivities of characteristic PS peaks increase with deposit coverage through the studied range, it can be concluded

that they are quite dilute and that the yield-enhancing effect of the Ag collector is not yet lost, even for the deposit prepared with the highest number of primary ions. For practical reasons, most Storing Matter deposits presented in this work were prepared with 1.0-1.2 · 10^{13} Ar^+ ions. This corresponds to the total sputtered area available on a sample of the same dimensions as the sample-holder of the Storing Matter prototype instrument. The other experimental parameters (raster size, ion current, and the speed of the sample stage movement) were adapted in order to reach a fluence of 5 · 10^{12} ions/cm^2 (i.e. within the static limit) on each point of the sample (page 65).

IV.5. (d) The primary ion fluence used for sputter-deposition

IV.5. (d) i) Introduction

The primary ion fluence is a critical factor for the analysis of organic samples, since ion beam degradation can have important consequences, both qualitative and quantitative, for the mass spectrum of an organic sample[154-157]. Similarly, the fluence used for the sputter-deposition step in the Storing Matter technique can be expected to have a significant impact on the Storing Matter spectra. PVC is known to be a type I polymer (cross-linking type)[113] and is thus very sensitive to the primary ion fluence.

IV.5. (d) ii) Experimental conditions

3 PVC samples were sputtered with the same flux (1.2 · 10^{13} primary ions during 200 s) but the total bombarded sample area was changed by moving the samples at different speeds under the rastering Ar^+ ion beam. This made it possible to reach different primary ion fluences while keeping the total number of primary ions and the sputtering time constant for each deposit:

- deposit 1: fluence: 5 · 10^{12} ions/cm^2, sputtered area: 2.4 cm^2, sample speed: 0.8 mm/s
- deposit 2: fluence: 5 · 10^{13} ions/cm^2, sputtered area: 0.24 cm^2, sample speed: 0.08 mm/s

- deposit 3: fluence: $5 \cdot 10^{14}$ ions/cm^2, sputtered area: 0.024 cm^2, sample speed: 0.008 mm/s.

The Ar^+ current was adjusted to 9.6 nA for these sputter-depositions.

These Storing Matter deposits, as well as a PVC reference sample used for comparison purposes, were analyzed by ToF-SIMS in positive mode. The Ar^+ fluence for the analysis step was $5 \cdot 10^{12}$ ions/cm^2 for all the samples.

IV.5. (d) iii) Results and discussion

Fig. IV-30 compares the positive mass spectra recorded in the centre of each deposit as well as a positive reference spectrum recorded directly on a PVC sample. The low mass range (m/z < 100) of these spectra mainly contains peaks that are characteristic of the hydrocarbon backbone of PVC, such as $C_3H_5^+$ at m/z = 41 or $C_4H_7^+$ at m/z = 55. The higher mass range (not shown) of the PVC reference spectrum contains only very weak peaks, while the spectra of the Storing Matter deposits show different series of relatively high peaks corresponding to Ag_n^+ clusters, Ag_2Cl^+, and small Ag-cationized fragments such as $Ag\ C_4H_8^+$.

From the spectra of the different Storing Matter deposits, it can be clearly seen that the overall peak intensities decrease as the primary ion fluence used for sputter-deposition increases. This can be explained by a decrease in sputtering yield at higher fluences due to an accumulation of chemical damage at the sample surface[133].

Leggett et al. investigated the changes in the positive PVC mass spectrum when the primary ion fluence increases[155]. They observed that the peaks of some aromatic fragments (e.g. $C_7H_7^+$ or $C_{11}H_9^+$) became more dominant as the fluence increased. These fragments mirror the chemical damage that accumulates at the PVC surface. Fig. IV-31 shows the Storing Matter sensitivities for some positive hydrocarbon fragment ions. The sensitivity of the damage-related fragments increases with the sputter-deposition fluence. For the deposit prepared with the highest fluence, the sensitivities of damage-related fragments even overweigh those that are characteristic of the polymer and thus making an identification of PVC by its Storing Matter spectrum impossible.

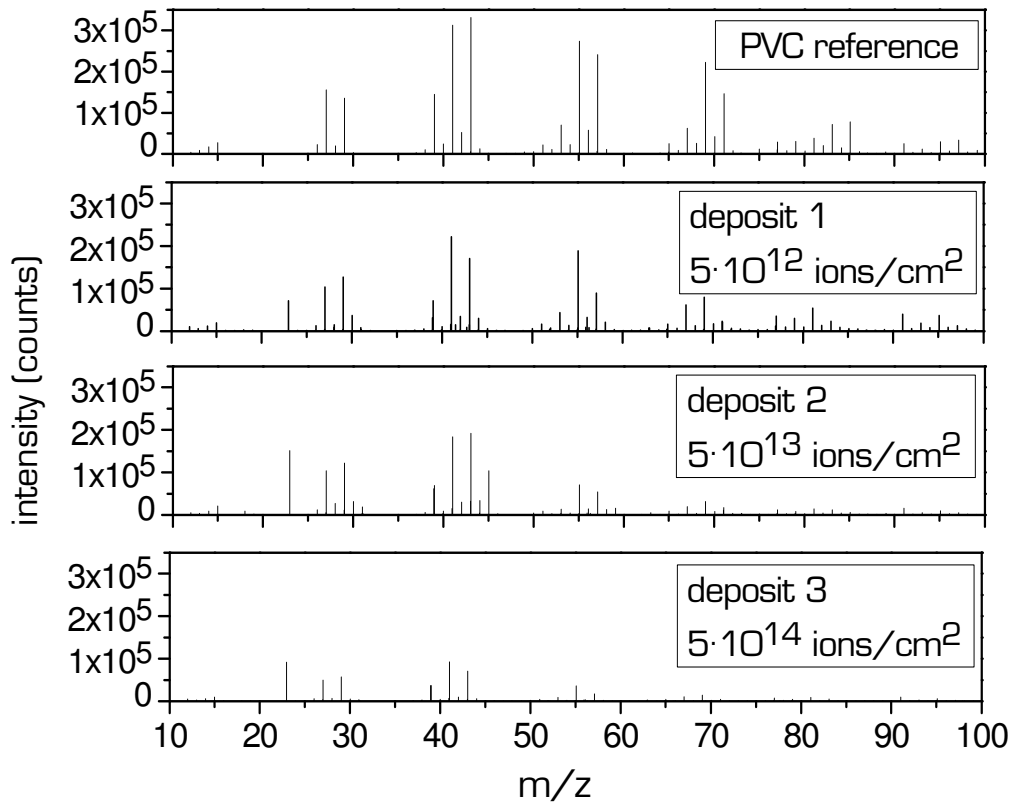

Fig. IV-30: Low mass range of the positive mass spectra recorded on PVC deposits prepared with different PI fluences. The mass spectrum of a PVC reference sample is shown for comparison purposes. The primary ion fluence used for analysis was $5 \cdot 10^{12}$ ions/cm^2 for all the mass spectra.

IV.5. (d) iv) Conclusions

It can be concluded from these experiments that the Storing Matter technique is sensitive enough to observe the well-known quantitative (decrease in sputtering yield) and qualitative (increasing contribution of aromatic fragments) consequences of increasing the primary ion fluence. It is thus important not to exceed the static limit in both steps of the Storing Matter technique since the changes in the mass spectra may easily lead to misinterpretations.

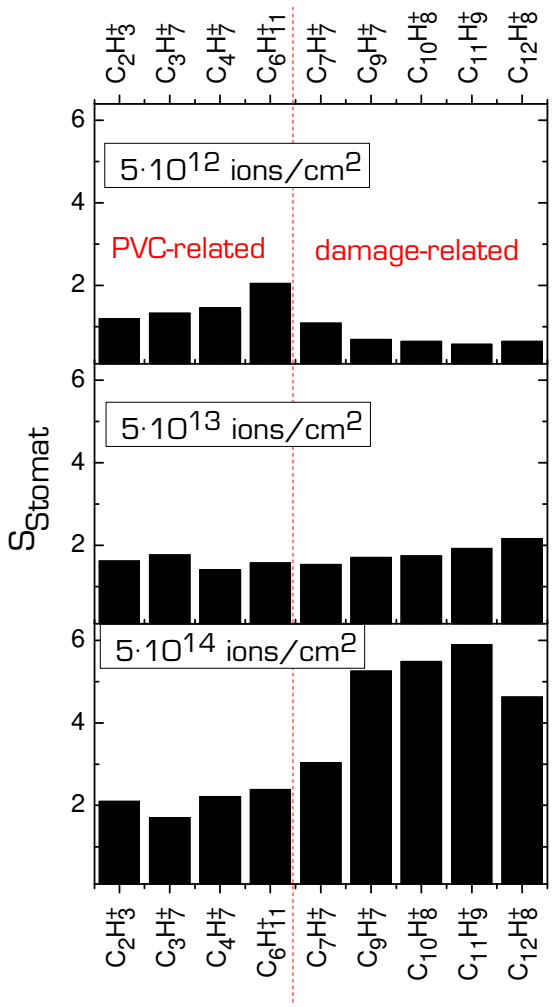

Fig. IV-31: Storing Matter sensitivities of positive hydrocarbon ions for 3 PVC deposits on Ag collectors prepared with different Ar^+ fluences. The dotted red line separates the fragments related to the hydrocarbon backbone of PVC from those that reflect chemical damage in the sample due to ion irradiation.

IV.5. (e) The primary ion energy used for sputter-deposition

IV.5. (e) i) Introduction

For PMMA and PVC samples, the sparseness of oxygen- or chlorine-containing fragments in the Storing Matter spectra compared to the reference spectra has been attributed to double fragmentation during sputter-deposition and the subsequent analysis step (page 67). Indeed all the ions in a Storing

Matter spectrum that originate from the organic sample have been involved in two collision cascades, which is exactly what one tries to avoid in a traditional static SIMS analysis. In this section a possible effect of the primary ion energy used for sputter-deposition on the fragmentation is studied.

IV.5. (e) ii) Experimental conditions

For Storing Matter deposits of PMMA, PVC and Alq_3 the impact energy of the Ar^+ ion beam used for sputter-deposition was varied. For energies lower than 2 keV, the ion gun was used in floating mode as described in Chapter I. The other sputter-deposition parameters (raster size, current etc.) were kept constant. The deposits were all analyzed with 10 keV Ar^+ ions as described on page 65.

IV.5. (e) iii) Results and discussion

Storing Matter deposits of Alq_3 on Ag collectors were prepared with impact energies of 10, 7.5, 5, and 3.75 keV and analyzed in positive mode. For all the deposits, the characteristic fragments identified above (page 75) were detected: $(Alq)^+$ (m/z=171), $AlqH^+$ (m/z=172), $AlqOH^+$ (m/z=188), and Alq_2^+ (m/z=315). Their absolute intensities drop with decreasing impact energy because of the decrease of the sputtering yield. These intensity variations are not proportional for all the considered fragments, which indicates that changes in fragmentation occur. In order to directly compare fragmentation for different energies, the intensity ratios $\frac{I(Alq^+)}{I(Alq_2^+)}$, $\frac{I(AlqH^+)}{I(Alq_2^+)}$, and $\frac{I(AlqOH^+)}{I(Alq_2^+)}$ were calculated for each deposit. The evolution of these ratios with the sputter-deposition energy is represented in Fig. IV-32. As the energy decreases, the smaller fragments become more and more dominant compared to the Alq_2^+ ion, suggesting that the fragmentation during the sputter-deposition step becomes more important at low energies. The fragmentation trends reported in the literature are quite contradictory. Several authors have associated a lower impact energy with less fragmentation[158,159]. Kersting et al.[109] observed that fragmentation of an Irganox1010 layer on LDPE increases with the impact energy of Ga^+, but the opposite was the case for Au^+ and Cs^+ projectiles in the studied energy range, which indicates that the nature of the primary ion seems

to play an important role. They did not present further explanations for these observations. Delcorte et al. observed an increase of the fragmentation of PET (poly(ethylene terephtalate)) with the impact energy of In^+ primary ions[160]. Unfortunately no literature data is available for the particular case of Alq_3 samples and Ar^+ bombardment.

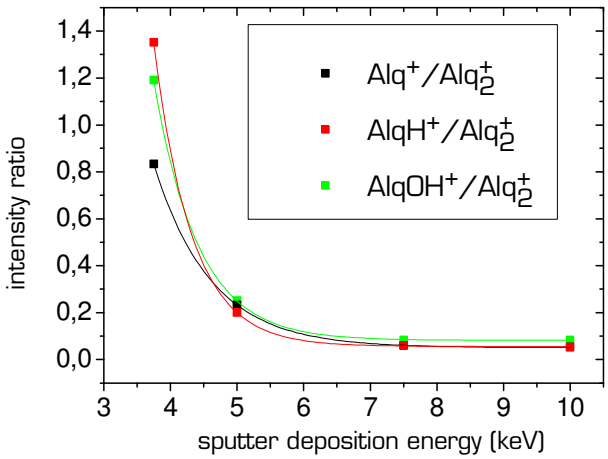

Fig. IV-32: Intensity ratios calculated from the Storing Matter spectra as a function of the impact energy of the Ar^+ beam used for sputter-deposition of Alq_3 samples onto Ag collectors. The curves represent data fits by an exponential decay function.

The damage created by a slower primary ion is more surface-localized, while a faster projectile rather destroys chemical bonds in the sub-surface region. Since the ejected species mainly originate from the top few monolayers of the sample[39,161], the peak ratios in a mass spectrum do not necessarily convey a realistic picture of the global amount of bond-scissions occurring in the sample. Regardless of the global extent of fragmentation caused by the collision cascades, the efficiencies of mechanisms leading to ejection of large intact versus small damaged fragments may also vary as a function of the impact energy. The degree of "fragmentation" that is indicated by peak ratios in a mass spectrum may not reflect the real extent of fragmentation caused by the collision cascades, but it is the combined result of the bond-scissions taking place near the impact point, of the ejection efficiencies of large/small fragments, and of the contribution of metastable decay reactions in the field

free region of the mass spectrometer. Which factor overweighs at a given impact energy probably depends on the sample and the projectile.

The contribution of meta-stable decay reactions during the analysis step of the Storing Matter deposits should be similar for the different deposits since the analysis conditions were identical.

Sputter-depositions with different impact energies in the range of 0.2-10 keV have also been carried out for PVC and PMMA samples (Ag collectors). The positive Storing Matter mass spectra of the low energy deposits (not shown) do not contain any additional chlorine- or oxygen-containing fragments compared to the 10 keV deposit. Lowering the impact energy for the sputter-deposition step does not seem to reduce the double fragmentation for these 2 polymers. However these observations should be relativized because the impact energy used for the analysis step was always 10 keV. Even if sputter-depositions at low energy eject larger fragments, it is possible that the latter are destroyed during the analysis step and cannot be detected in the Storing Matter spectra.

IV.5. (f) Primary ion type used for the analysis step

IV.5. (f) i) Introduction

In section IV.5. (a) , it was shown that the choice of the collector surface is a crucial parameter for the analysis step. The Storing Matter spectra presented above were all analyzed with 10 keV Ar^+ primary ions, which might not be the best option as far as efficient sputtering and reduced fragmentation are concerned.

IV.5. (f) ii) Experimental conditions

Storing Matter deposits of Alq_3, PS and PMMA, as well as of their corresponding reference samples were analyzed with different primary ions (Ar^+ in the TOFIII, and Bi^+ and Bi_3^+ in the TOF5 instrument by Ion-TOF) in order to verify a possible influence of the analysis projectile on the Storing Matter spectra. The analysis conditions are resumed in Table IV-3. The primary ion fluence was similar for all the projectiles.

projectile	Ar^+	Bi^+	Bi_3^+
impact energy (keV)	10	25	25
current (pA)	0.5	0.95	0.65
raster size (μm^2)	$100 \cdot 100$	$100 \cdot 100$	$100 \cdot 100$
acquisition time (s)	180	120	180
fluence (ions/cm^2)	$5.6 \cdot 10^{12}$	$7.1 \cdot 10^{12}$	$7.3 \cdot 10^{12}$

Table IV-3: Analysis conditions used for different primary ion types.

IV.5. (f) iii) Results and discussion: Alq_3 sample

a. Reference sample

The positive mass spectra of an Alq_3 reference sample analyzed with Ar^+, Bi^+, and Bi_3^+ primary ions are shown in Fig. IV-33. The characteristic ions Al^+ (m/z=27), $(Alq)^+$ (m/z=171), $AlqH^+$ (m/z=172), $AlqOH^+$ (m/z=188), Alq_2^+ (m/z=315), and $Al_2q_3O^+$ (m/z=502) are detected in each spectrum, but their absolute intensities vary strongly for the different projectiles. It should be noted that the Ar^+ mass spectrum was recorded in a different instrument and that the absolute intensities should not be directly compared with those measured with the other projectiles.

The highest overall peak intensities are obtained with Bi_3^+ primary ions. The intensity of the Alq_2^+ peak ($2 \cdot 10^6$ counts) corresponds to the number of primary ion pulses used for this analysis, which means that there were probably detector saturation issues for this ion. This is confirmed by the fact that in the Bi_3^+ spectrum the intensity ratio of the Alq_2^+ peak (m/z=315) and the same ion containing one ^{13}C atom (m/z=316) does not correspond to the natural abundance of the ^{13}C isotope. Therefore the intensity of the Alq_2^+ peak measured with Bi_3^+ will not be included in the discussions.

In order to compare the fragmentation obtained with Ar^+ and Bi^+, intensity ratios of different characteristic fragments were calculated for these two projectiles (Fig. IV-34). These ratios are very similar for each projectile, indicating that there is no significant change in fragmentation although a bi atom is 5.2 times heavier than an Ar atom. In general, heavier monoatomic projectiles are associated with less fragmentation[159]. However the impact energy of Bi^+ (25 keV) was higher than that used for Ar^+ (10 keV), which makes it more difficult to directly compare the effect of these two projectiles.

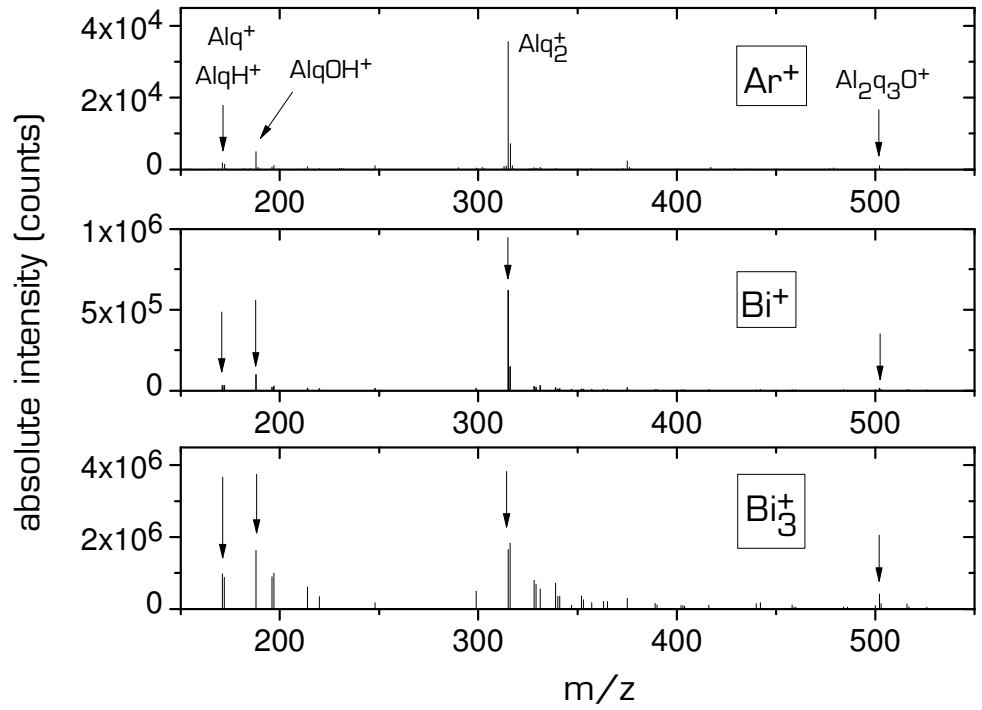

Fig. IV-33: Positive mass spectra of an Alq_3 sample obtained with different primary ion types. Note the different vertical scales.

Due to the detector saturation for Alq_2^+ in the case of Bi_3^+ bombardment, the correct intensity ratios are not known fir this projectile. It is thus not possible from the available data to draw any conclusions about the fragmentation of Alq^3 with Bi_3^+.

Diehnelt[55] analyzed an α-cyano-4-hydroxycinnamic acid sample with Cs^+ and different polyatomic primary ions and found that the intensity ratio of the deprotonated molecular ion by the intensity of a fragment ion was lower for cluster projectiles. These results could be correlated with an increase in decay

fractions with polyatomic ions. The higher fragmentation observed with cluster primary ions is the result of bond breaking by the collision cascades and by further dissociation reactions in the drift region of the instrument. The contribution of metastable decay reactions to the final peak distribution in the mass spectrum depends on the efficiency of the recoil atoms to convert their translational energy into vibrational energy of the ejected fragment ions[55]. For a given projectile type and energy, the relative contribution of fragmentation through metastable decay is sample-dependent, which explains the very different trends observed in fragmentation behaviour with mono- and polyatomic primary ions for various samples.

Fig. IV-35 shows the yield enhancements measured for different secondary ions if the Alq_3 sample is analyzed with Bi_3^+ ions instead of Bi^+. Yield enhancements up to a factor 34 are observed when going from the mono- to the polyatomic projectile.

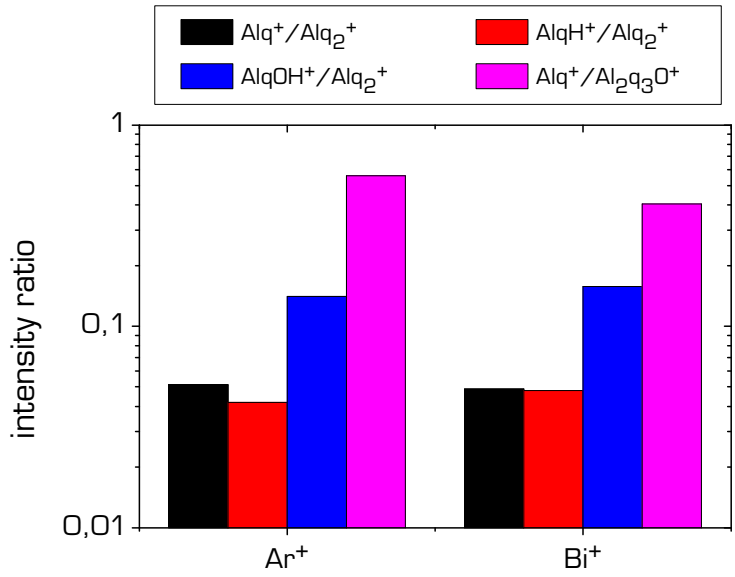

Fig. IV-34: Intensity ratios of characteristic Alq_3 fragments obtained for positive mass spectra of an Alq_3 reference sample recorded with Ar^+ and Bi^+ primary ions.

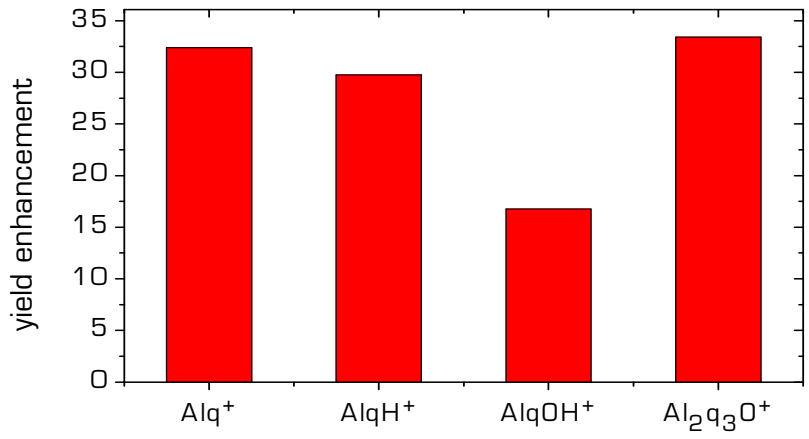

Fig. IV-35: Yield enhancement measured for different characteristic ions if the Alq_3 reference sample is analyzed with Bi_3^+ ions instead of Bi^+.

b. Storing Matter deposit

A Storing Matter deposit of Alq_3 on an Ag collector was prepared with the experimental conditions described on page 65 and the deposit was analyzed with Ar^+, Bi^+ and Bi_3^+ primary ions (experimental conditions given in Table IV-3). The Storing Matter sensitivities of characteristic Alq_3 ions were calculated for each primary ion (Fig. IV-36).

For all the considered peaks, Ar^+ ions yield the highest Storing Matter sensitivities. For Al^+ and the smaller fragment ions, the Storing Matter sensitivities are higher for Bi_3^+ than for Bi^+, but the opposite trend is observed for the 3 largest fragments. For each secondary ion the sensitivities obtained for these two projectiles are very close.

The better results obtained with Ar^+ as compared to Bi_3^+ are not surprising since it is well known that significant secondary yield enhancements with cluster projectiles are rather obtained for bulk organic samples than for thin layers (or a sub-monolayer as it is the case for the Storing Matter deposit) of organic matter on metallic substrates[65,107]. However the difference between Bi^+ and Ar^+ is in contradiction with results published by Heile and co-workers[65], who analyzed a thin layer of polyethylene imine (PEI) on an Ag substrate with monoatomic projectiles of different mass and found that a larger projectile

causes higher secondary ion yields. They observed an almost 4-fold intensity increase for the characteristic ion $C_3H_8N^+$ when going from 10 keV Ar^+ to 25 keV Bi^+ primary ions.

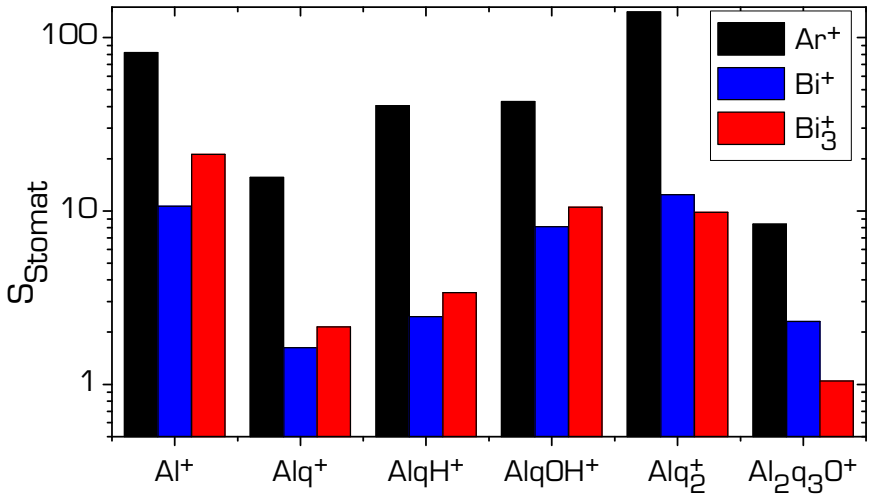

Fig. IV-36: Storing Matter sensitivities of characteristic positive Alq_3 secondary ions for a Storing Matter deposit of Alq_3 on an Ag collector analyzed with Ar^+, Bi^+, and Bi_3^+ primary ions.

In order to study possible changes in fragmentation when the Storing Matter deposit of Alq_3 on an Ag collector is analyzed with Ar^+, Bi^+ and Bi_3^+ ions, intensity ratios of characteristic fragment ions are compared in Fig. IV-37. The proportion of small fragments increases strongly when going from Ar^+ to Bi^+, and then slightly further with Bi_3^+ primary ions. For the Alq_3 reference sample the intensity ratios were very similar for Ar^+ and Bi^+, and one order of magnitude higher for Bi_3^+. The differences in the Storing Matter spectra with these 2 projectiles are thus not related to the material Alq_3 itself, but rather to the fact that Alq_3 (molecules and fragments) is present at sub-monolayer coverage on the Ag collector.

The use of Bi^+ or Bi_3^+ ions for the analysis of an Alq_3 deposit on an Ag collector is thus not recommended because (1) the Storing Matter sensitivities are lower and (2) there seems to be more fragmentation than with Ar^+.

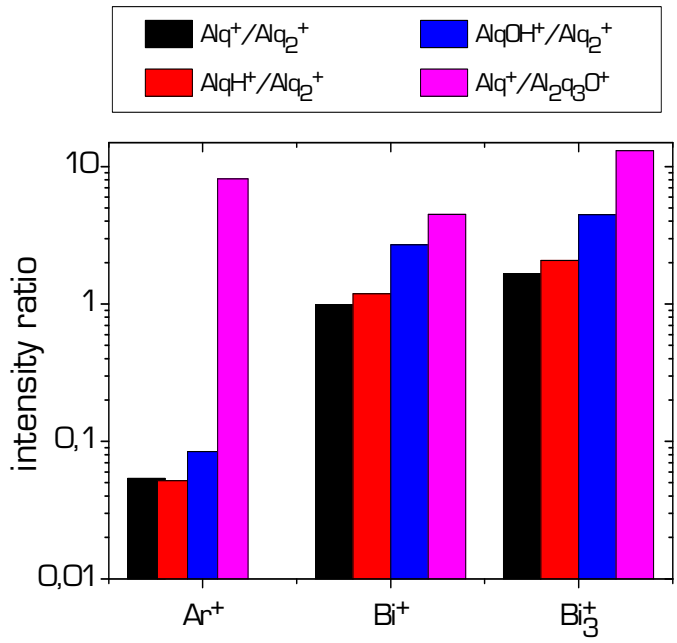

Fig. IV-37: Intensity ratios of characteristic Alq_3 fragments obtained for positive Ar^+, Bi^+ and B_3^+ mass spectra of an Alq_3 Storing Matter deposit on an Ag collector.

IV.5. (f) iv) Results and discussion: PS2000 sample

a. Reference sample

A PS2000 reference sample was analyzed with Bi^+, Bi_3^+ (experimental conditions given in Table IV-3) and C_{60}^+ primary ions (with 10 keV impact energy, 0.4 pA ion current, 100 · 100 μm^2 raster size, 3 minutes acquisition time, 4.5 · 10^{12} ions/cm^2). The yield enhancements obtained by the two polyatomic projectiles were calculated for some characteristic fingerprint ions (Fig. IV-38). The enhancements of the considered fragments are between 2 and 14. Bi_3^+ gives a stronger yield enhancement compared to Bi^+ than C_{60}^+, except for the $C_7H_7^+$ ion. Fig. IV-39 represents the yield enhancement factors for the entire mass spectrum. Bi_3^+ preferentially enhances high mass peaks while the enhancement effect of C_{60}^+ is mainly restricted to the fingerprint region. This can be interpreted as an indication of higher fragmentation with C_{60}^+ and less fragmentation for Bi_3^+ as compared to Bi^+. Increased fragmentation of polymers with C_{60}^+ as compared to monoatomic projectiles have been reported by Wells[110] and Delcorte[79].

b. Storing Matter deposit

Storing Matter deposits of PS2000 were prepared on an Ag and a Si collector according to the experimental conditions described in page 65 and analyzed with Ar^+, Bi^+ and Bi_3^+ primary ions (analysis conditions in Table IV-3). The Storing Matter sensitivities of the PS fingerprint fragment ions $C_7H_7^+$, $C_8H_9^+$, $C_9H_7^+$, and $C_{13}H_9^+$ were calculated for each collector material and each primary ion type (Fig. IV-40).

- For the Si collector, the Storing Matter sensitivities of the 4 considered ions are maximal for Bi_3^+ projectiles followed by Bi^+. This is in agreement with literature results concerning the evaluation of secondary ion yields from organic thin layers or (sub)monolayers on Si/SiO_2 substrates[65,80]: the stopping power of these substrates significantly increases with the mass and atomicity of the primary ion, leading to a smaller penetration depth. The result is a more pronounced near-surface energy deposition that provides higher yields of organic secondary ions.
- On the Ag collector, Ar^+ ions yield the highest sensitivities, except for the $C_7H_7^+$ ion, which has very similar sensitivities with the 3 studied projectiles. The sensitivities with Bi_3^+ are higher than with Bi^+, but this increase is much smaller than for Si collectors. This poor enhancement is in agreement with general trends reported in literature for thin organic layers on metallic substrates[65]: the energy deposited by a monoatomic projectile is already quite surface-localized for these substrates, and the gain obtained with a polyatomic ion is much lower than for silicon substrates.

No Ag-cationized fragments were detected with Bi^+ and Bi_3^+, although some were observed when the deposit was analyzed with Ar^+ (Fig. IV-25). This might be an indication for increased fragmentation of the PS deposit with Bi_n^+ projectiles.

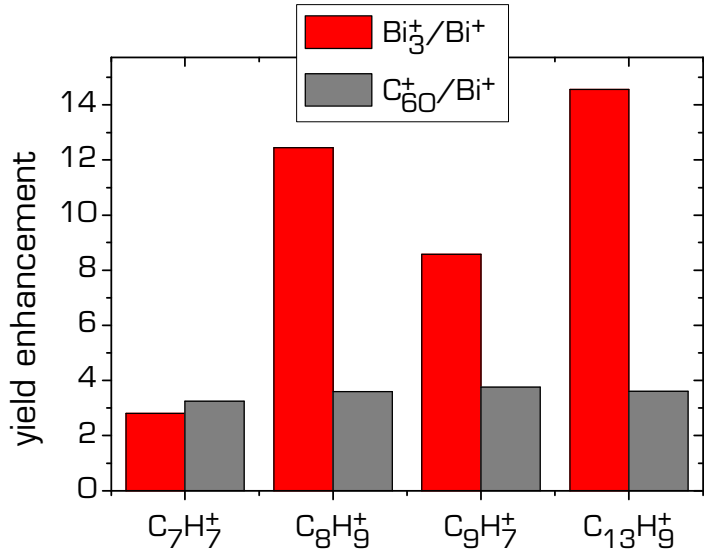

Fig. IV-38: Yield enhancements of some characteristic PS ions obtained from analyzing the PS reference sample with Bi_3^+ or C_{60}^+ instead of Bi^+ ions.

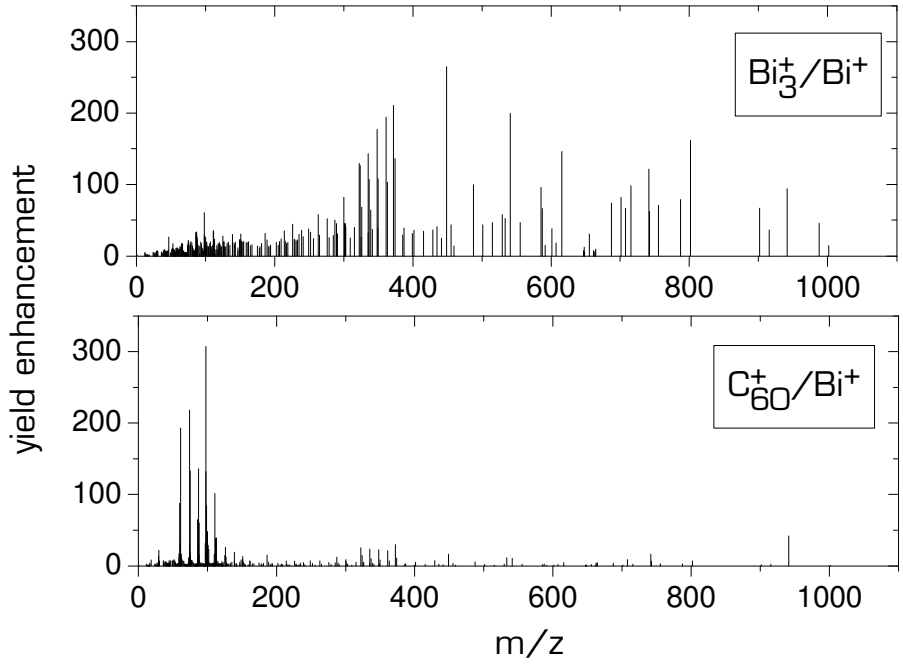

Fig. IV-39: Yield enhancements obtained when analyzing the PS reference sample with Bi_3^+ or C_{60}^+ instead of Bi^+ ions.

It can be concluded from the results presented in this section that small monoatomic primary ions are best suited for the analysis of organic Storing Matter deposits on Ag collectors. In general, they provide higher Storing Matter sensitivities, less fragmentation, and large Ag-cationized fragments in the case of a PS deposit. For Si collectors a cluster projectile is the better option. In the case of Ag collectors, it seems that any method that increases the near surface energy deposition (i.e. the use of polyatomic or larger monoatomic projectiles) reduces the Storing Matter sensitivities of characteristic fragments and increases the fragmentation.

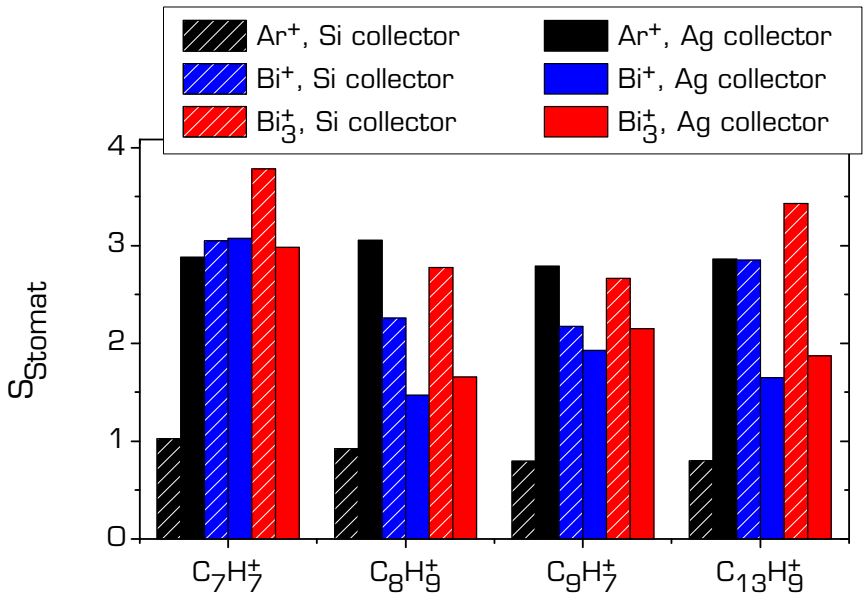

Fig. IV-40: Storing Matter sensitivities of 4 PS fingerprint fragments for Storing Matter deposits of PS on an Ag and a Si collector analyzed with Bi^+ and Bi_3^+ primary ions.

IV.5. (g) Conclusions about the experimental parameters of the Storing Matter technique applied to organic samples

This chapter constitutes a feasibility study of the application of Storing Matter to organic samples. In a first step, it was demonstrated that the 4 investigated organic samples could be identified by their Storing Matter mass spectra on Ag collectors. Then the key parameters of the technique were identified and each studied in detail for one or more organic samples. In particular, it was shown that the collector material is of outmost importance for the analytical step. In general, the highest Storing Matter sensitivities of positive secondary ions were obtained on Ag collectors. Cs coated collectors were found to provide molecular information about PMMA in the negative analysis polarity as well as in the MCs_x^+ mode. Ag collectors are of particular interest when molecular information from large metal-cationized fragments is desired. However this is only the case for relatively short polymers (<4 000 Da), and the presence of Ag already in the sample used for sputter-deposition is required to obtain reasonable yields.

The quantity of matter deposited onto the collector is a crucial parameter: on the one hand there should be enough matter for high Storing Matter sensitivities to be reached, but on the other hand the coverage needs to be in the sub-monolayer regime so that all the deposited particles are embedded in the same matrix.

The sparseness of heteroatom-containing fragments in the Storing Matter spectra of PMMA and PVC was attributed to the double fragmentation during the sputter-deposition and the analysis step. Lowering the impact energy for the first step did not solve this problem; on the contrary, even a higher degree of fragmentation was observed. The primary ion fluence used for sputter-deposition was also found to have a significant impact on the Storing Matter spectra: already for $5 \cdot 10^{13}$ ions/cm^2 an increased contribution of damage-related secondary ions to the Storing Matter spectrum of PVC was observed.

As for the analysis step, the optimal primary ion type with regard to high Storing Matter sensitivities and/or a low degree of fragmentation strongly depends on the collector material. For Ag collectors, a small monoatomic projectile such as Ar^+ gives good results, while for Si collectors a cluster primary ion beam such as Bi_3^+ should be preferred.

A thorough understanding of the influence of each parameter on the final Storing Matter mass spectrum is required for a successful application of the technique to more complex samples.

Chapter V. Application of the Storing Matter technique to PS/PMMA blends

V.1 Introduction

V.1. (a) Context

Applications of polymer blends and copolymers can be found in a wide range of technological domains, from life sciences[162] to photovoltaics[163]. Consequently there is a need for quantitative and sensitive analysis of these materials. SIMS fulfils the sensitivity criterion and has the advantage that well-chosen analytical conditions can preserve molecular information, but quantification is not straightforward due to possible matrix effects.

Several copolymer or polymer blend systems have been studied by TOF-SIMS[57,60,61,63,164-171], often in combination with a quantitative analysis method such as XPS. In most cases, the conclusion was that a linear relationship between SIMS intensities and the actual surface composition was possible, but not for all the considered characteristic ions.

As described in section II.4, matrix effects in SIMS can be classified into sputter-induced and ionization-induced matrix effects[56]. In the case of molecular secondary ions, an additional issue related to the fragmentation mechanisms needs to be considered: they can be formed via different fragmentation pathways from different precursors. Matrix effects in polymer samples can be due to short-range interactions between adjacent functionalities (matrix effect of first type, MEI) or long-range interactions between non-covalently bonded groups (matrix effect of second type, MEII)[58].

The main idea behind the development of the Storing Matter technique was the possibility of quantitative SIMS measurements via an elimination of ionization-induced matrix effects. We chose to apply this technique to a polymer blend system. The application to a copolymer system would be more delicate since short-range interactions between covalently bonded functionalities would most probably persist.

V.1. (b) Sample preparation

The polymer system studied in this chapter is a series of PS/PMMA blends different compositions. Solutions of PS2000 and PMMA2000 in toluene with 5 different mass ratios of both polymers (0/100, 25/75, 50/50, 75/25 and 100/0) were prepared. The corresponding molar concentration ratios are very similar since the monomer units of both polymers have approximately the same mass. The total polymer concentration in each solution was 2 wt%. The solutions were used for spin-coating on cleaned Si wafers with an acceleration of 10 000 rpm/s and a rotation speed of 3000 rpm during one minute. The thickness of the resulting polymer layers is estimated to 50 - 70 nm. The samples were analyzed without annealing.

It is well known that PS and PMMA are immiscible. In most polymer blends, phase separation is observed in the bulk, leading to the formation of microdomains and an enrichment by one component near the polymer/air interface[172-174].

V.1. (c) Determination of the surface composition by XPS

In order to verify if the surface composition is equal to the bulk composition of the spin-coated polymer films, XPS measurements were performed using an Axis Ultra DLD spectrometer (Kratos Analytical). The instrument is equipped with a monochromatized aluminium X-ray source powered at 10 kV and 50 mA that delivers an X-ray beam of 300 · 700 μm^2. Charge compensation was obtained with the built-in charge neutralisation system. The pass energy was set to 160 eV for survey spectra and to 20 eV for high resolution spectra.

On each sample, a survey spectrum was taken, followed by individual spectra of C1s and O1s, and again a spectrum of C1s after 5 minutes in order to check if there was any X-ray induced degradation during the analysis time. This does not seem to be the case since no significant change in the C1s peak's shape or intensity was observed.

In the survey scans, no Si signal was detected, which confirms that the thickness of the polymer layer exceeds the information depth of XPS (~ 10 nm).

In the XPS spectrum of the pure PS sample (a polymer consisting only of C and H atoms), the O1s peak was observed, suggesting that a small amount of oxygen-containing contaminants was present on the sample surface. For the quantification of the blends, only the C1s signal was used. The different contributions in the C1s core-level shift as well as their association with either PS or PMMA are given in Table V-1.

contribution	binding energy (eV)	associated polymer
C-(C,H)	284.7	PS
shake-up	291.4	PS
C-(C,H)	285.0	PMMA
C-C(O)-O	285.8	PMMA
C-O	286.9	PMMA
O=C-O	289.1	PMMA

Table V-1: Binding energies of the different contributions in the C1s core level shift observed in the PS/PMMA blend samples and their association with either PS or PMMA.

Table V-2 shows the composition in the bulk and at the surface of the PS/PMMA blend samples. The bulk compositions are derived from the relative concentrations in the solutions used for spin-coating, and the surface composition was calculated from the XPS results taking into account the C1s contributions of both polymers (except for the shake-up).

bulk composition (PS/PMMA)	surface* composition (PS/PMMA)
25/75	45/55
50/50	66/34
75/25	83/17

Table V-2: Composition in the bulk and at the surface of the PS/PMMA blend samples. *In this context, "surface" refers to the topmost ~ 10 nm of the sample, i.e. the sampling depth of XPS.

According to the XPS measurements, the surface of the PS/PMMA blend samples is enriched with PS, which can be assigned to the difference in surface free energy of PS and PMMA. In the following sections of this chapter, the calculated values for surface composition were used. However it is important to note that the sampling depth of XPS (~ 10 nm) is much larger than that of TOF-SIMS and that the actual composition in the topmost monolayer (which constitutes the main source of information for the latter analysis technique) might be different from the values obtained by XPS.

V.2 Characterization of PS/PMMA blends by TOF-SIMS

V.2. (a) Analysis with monoatomic primary ions

The 5 samples obtained by spin-coating were first analyzed by TOF-SIMS with 25 keV Bi^+ primary ions (0.88 pA, 100 · 100 μm^2, 120 s).

Fig. V-1 and Fig. V-2 display the evolution of the normalized intensities of two positive characteristic PS and PMMA ions: $C_7H_7^+$ (m/z=91), and the protonated monomer $C_8H_9^+$ (m/z=105) for PS, and CH_3O^+ (m/z=31, associated with the methyl ester function), $C_2H_3O_2^+$ (m/z=59, associated with the methyl methacrylate group), and $C_5H_9O_2^+$ (m/z=101, the protonated

monomer unit) for PMMA. The absolute intensities were normalized to that of the pure PMMA sample for a better comparison.

Fig. V-3 displays the evolution of the normalized intensities of some negative characteristic PMMA ions: O^- (m/z=16), CH_3O^- (m/z=31, associated with the methyl ester function), $C_4H_5O_2^-$ (m/z=85, the monomer unit minus a methyl group), and $C_9H_{13}O_4^-$ (m/z=185, the dimer minus a methyl group). The absolute intensities were normalized to those measured on the pure PMMA sample for a better comparison. The peaks in the negative mass spectrum of PS are not very specific (section IV.3. (c) ii)) and will not be considered here.

A linear relationship between peak intensity and PS concentration is only observed for small negative PMMA ions (O^-, OH^-, CHO^-, and CH_3O^-) (Fig. V-3, right). The yields of all the other considered secondary ions are obviously influenced by strong matrix effects in the blend samples:

- The characteristic PS peaks are higher for the blend samples than for the pure PS sample (Fig. V-1).
- The positive (Fig. I-2) and the larger negative (Fig. I-3) peaks of PMMA are all lower in presence of PS than they should be for a linear intensity-concentration relationship.

The intensity evolutions obtained with 10 keV Ar^+ primary ions are very similar (not shown).

The total positive secondary ion intensity strongly decreases with increasing PS concentration (Fig. V-4). In order to check if this is related to a change in sputter yield with sample composition, sputter craters obtained with identical conditions of Bi^+ bombardment were measured by stylus profilometry (Tencor P-10 Surface Profiler, Tencor Instruments). These measurements revealed significant differences in the sputter rates of the 5 studied samples. Fig. V-5 displays the sputter rates normalized to the value measured for the pure PMMA sample. These rates should be considered with care, since they were measured for a relatively high primary ion fluence, and it is not clear if these values can be extrapolated to the low fluence used for the TOF-SIMS analyses. It should also be mentioned that the sputter craters seemed very flat, indicating that there is no significant preferential sputtering of one of the polymers.

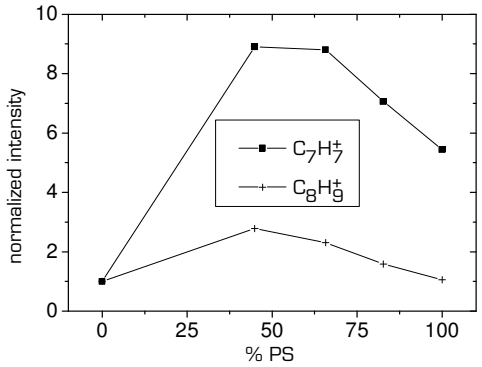

Fig. V-1: Normalized intensities of positive characteristic PS ions as a function of the PS concentration.

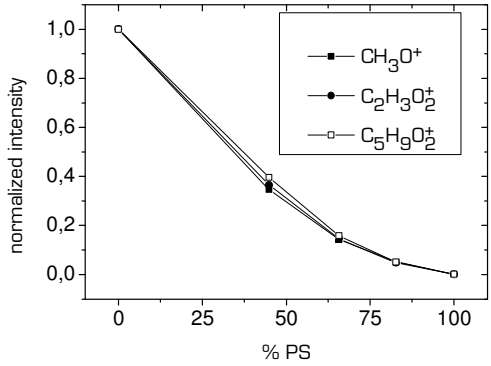

Fig. V-2: Normalized intensities of positive characteristic PMMA ions as a function of the PS concentration.

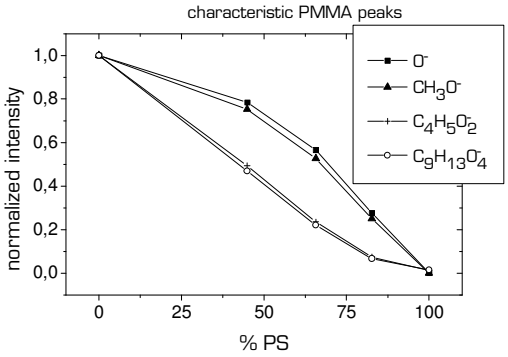

Fig. V-3: Normalized intensities of negative characteristic PMMA secondary ions as a function of the PS concentration.

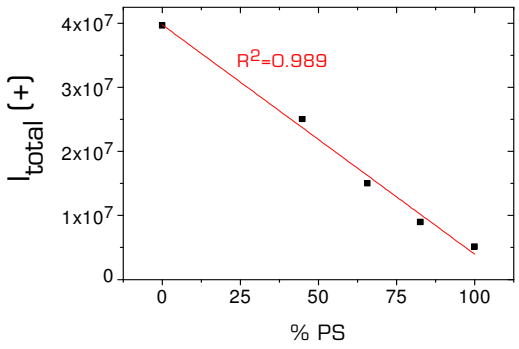

Fig. V-4: Total positive secondary ion intensity measured with Bi^+ primary ions as a function of the PS concentration. R^2 is the coefficient for linear regression.

It is thus likely that the observed matrix effects are a combination of sputtering- and ionization-induced effects. For the ionization contribution, only MEII (long-range interactions) can be considered for this type of samples because the styrene and methyl methacrylate units are not covalently bonded and the end groups are always the same for all the polymer chains (butyl end groups). The origin of this matrix effect is probably hydrogen transfer between spatially close styrene and methyl methacrylate units.

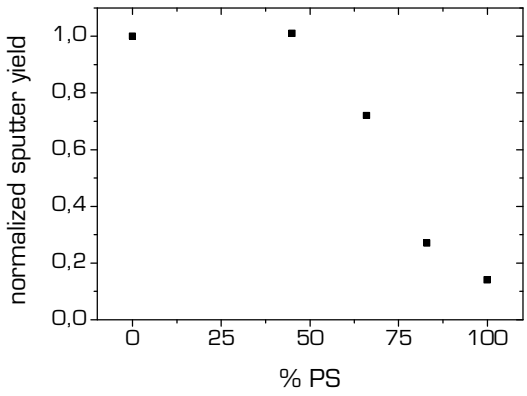

Fig. V-5: Normalized sputter rates for the different blend compositions measured with Bi^+ at high primary ion fluence.

It is interesting to note that the evolution of the absolute secondary ion intensities with the sample composition is qualitatively exactly identical with those obtained by Vanden Eynde et al. for random copolymers with varying

styrene and methyl methacrylate content[166]. This is the case for all the positive and negative secondary ions considered by these authors. They presumed that short-range matrix effects (MEI) between covalently bonded comonomers were the main reason for the non-linear evolution of the peak intensities with styrene content. Based on this assumption, they developed a model that related the statistical distribution of different triads (probability of obtaining a given sequence of 3 comonomers, calculated from the reactivity ratios during the polymerization reaction) to the peak intensity, which allowed them to calculate yield enhancement/suppression factors for different ions[63]. They concluded that hydrogen transfer from MMA units to covalently bonded styrene groups were the main reason for the observed matrix effects. However, the results presented in this section about polymer blends suggest that sputter-induced and ionization-induced MEII effects may also play a significant role in the copolymer system studied by these authors.

V.2. (b) Analysis with polyatomic primary ions

The PS/PMMA blend samples were also analyzed with polyatomic primary ions in the TOF5 instrument. Bi_3^+ ions were used at an impact energy of 25 keV, 0.64 pA ion current, 100 · 100 μm^2 raster size and 100 s acquisition time. C_{60}^+ ions had an impact energy of 10 keV, 0.1 pA, 100 · 100 μm^2 raster size and 180 s acquisition time. Since the trends with both primary ions were the same for all the considered secondary ions, only the results obtained with Bi_3^+ are shown here.

Fig. V-6 shows the evolution of the normalized intensities of some positive characteristic PS and PMMA ions as a function of the sample composition. For a better comparison, the absolute intensities were normalized to those measured on the pure PMMA sample. The evolution of the normalized intensities with Bi_3^+ and C_{60}^+ is different from that obtained with the monoatomic projectiles. The $C_7H_7^+$ curve is much closer to linearity than for Bi^+ bombardment (Fig. V-1), while the $C_8H_9^+$ intensities are still higher in the blend samples than they should be. The intensity-concentration relationship of positive and negative (not shown) PMMA ions is much closer to linearity than with monoatomic ions. It is likely that mono- and polyatomic ions affect the sputter

rates of the blends in different ways. The relative sputtering yields with Bi_3^+ varied with the sample composition in the same way as with Bi^+.

In addition to variations in sputtering yields, most secondary ion intensities seem to be affected by an additional matrix effect related to a dependence of ionization/fragmentation probabilities on the chemical environment (MEII). In the next section, the potential of Storing Matter for reducing this effect will be assessed.

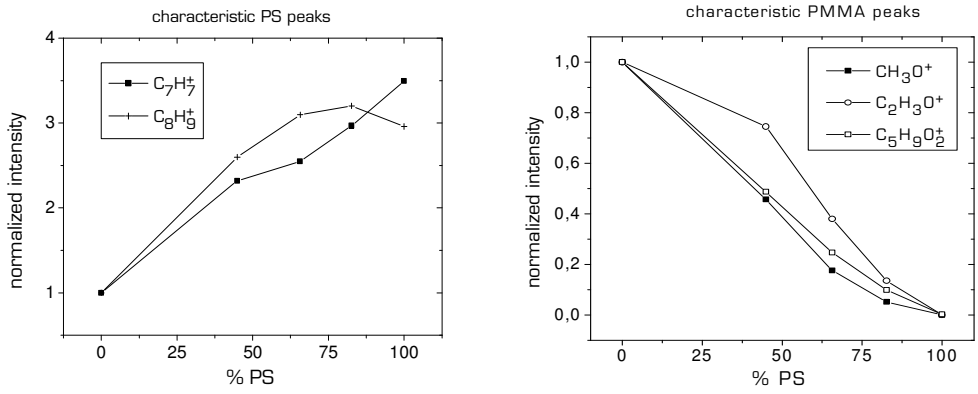

Fig. V-6: Normalized intensities of positive characteristic PS (left) and PMMA (right) ions as a function of the PS concentration.

V.3 Storing Matter deposits of PS/PMMA blends on Ag collectors

The PS/PMMA blends were sputter-deposited onto Ag collectors with a 10 keV Ar^+ beam (experimental conditions given on page 65). After UHV transfer to the TOFIII instrument, the deposits were analyzed with 10 keV Ar^+ primary ions (experimental conditions on page 65).

Fig. V-7 shows the Storing Matter sensitivities of some characteristic positive PS and PMMA ions. The PS peaks clearly increase with PS concentration and the PMMA peaks decrease, but these curves are far from being linear, except for $C_8H_9^+$.

The protonated monomer of PMMA ($C_5H_9O_2^+$) was not observed in the Storing Matter spectra, but its Ag-cationized counterpart was detected. The

Storing Matter sensitivities of the Ag-cationized monomer units of PS and PMMA are shown in Fig. V-8. The sensitivity of $AgC_5H_8O_2^+$ shows an almost linear decrease with PS content, but the sensitivities of the Ag-cationized styrene monomer are low and their evolution is not linear.

The evolution of the Storing Matter sensitivities of the negative PMMA peaks is approximately linear (Fig. V-9).

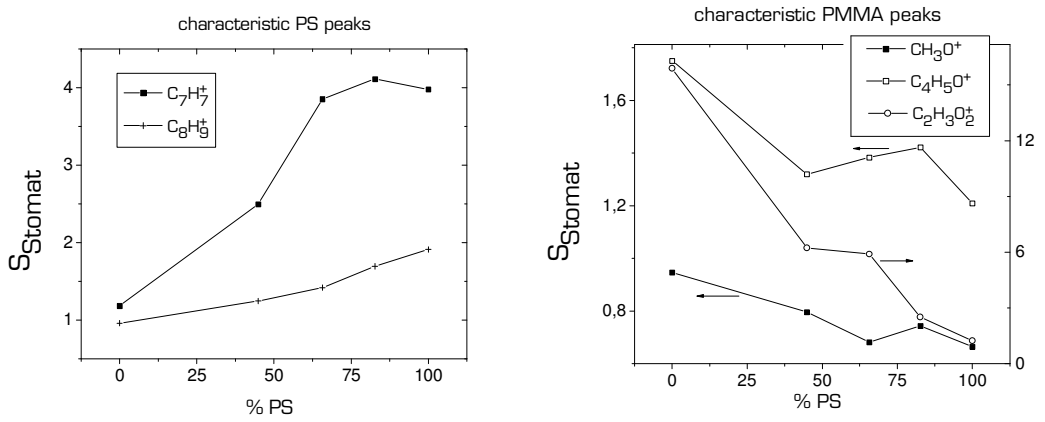

Fig. V-7: Storing Matter sensitivities of characteristic positive PS and PMMA ions as a function of the PS concentration.

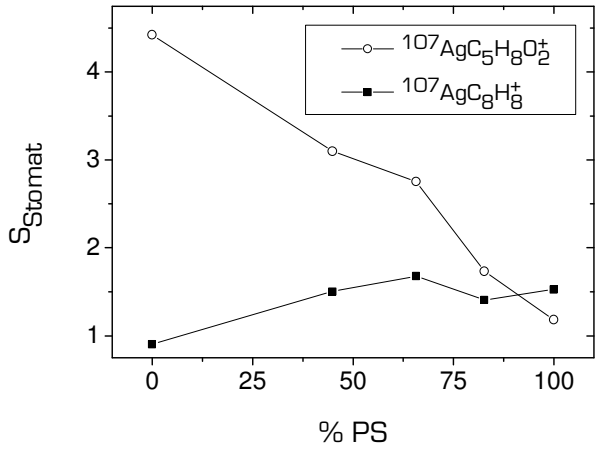

Fig. V-8: Storing Matter sensitivities of the Ag-cationized PS and PMMA monomer units as a function of the PS concentration.

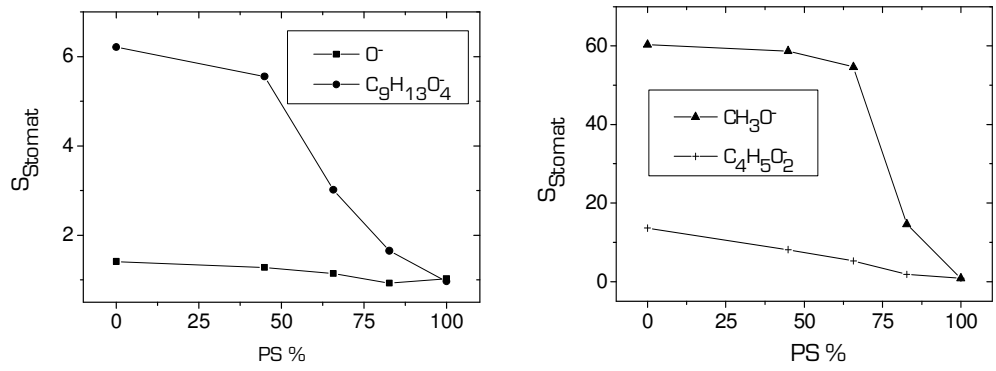

Fig. V-9: Storing Matter sensitivities of characteristic negative PMMA ions as a function of the PS concentration.

It has been shown above that the sputter yields of the PS/PMMA samples decrease strongly with increasing PS content. The amount of matter emitted during the sputter-deposition step is thus not the same for the different blend compositions, but it varies proportionally with the relative sputter rates of the samples. However, correcting the Storing Matter sensitivities by the relative sputter rates does not lead to the expected variations. For example, several negative PMMA peaks increase and some positive PS peaks decrease with increasing PS content (not shown). This indicates that the sputter yield correction by means of the relative sputter rates measured at high fluence is not appropriate to account for the different amounts of matter sputtered during the sputter-deposition of the blend samples. Indeed the difference in sputter yield for the different samples at the low fluence used for sputter-deposition ($5 \cdot 10^{12}$ ions/cm^2) might be significantly lower, because the chemical damage has not accumulated yet. For accurate values, a more sensitive method should be used to measure the sputter rates at low fluence, for example the determination of the sputtered mass with a quartz microbalance[133].

3 series of Storing Matter deposits were prepared with identical sputter-deposition and analysis conditions in order to check the reproducibility. Fig. V-10 shows the average Storing Matter sensitivities and the error bars (corresponding to the standard deviation) calculated for the 3 series. For $C_7H_7^+$

the relative error is quite large, which is probably due to the relatively low values of S_{Stomat} of this fragment. For $C_2H_3O_2^+$ the evaluation is approximately linear and the relative error is smaller.

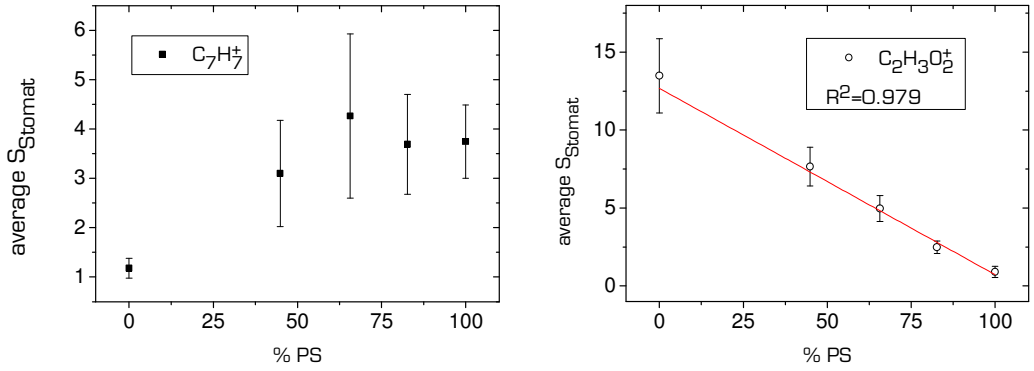

Fig. V-10: Average Storing Matter sensitivities of $C_7H_7^+$ and $C_2H_3O_2^+$ of 3 data series. The red line represents a linear fir of the data points and R^2 is the coefficient for linear regression.

The efficiency of the Storing Matter technique to reduce matrix effects in the PS/PMMA blends is thus hampered by two elements: the lack of knowledge of the relative sputter rates at low fluence and the large error accumulated during the different steps of the technique: sample and collector preparation, sputter-deposition, and analysis of the deposits. Especially the cleanliness of the pristine collectors plays a crucial role since it strongly influences the values of S_{Stomat}.

V.4 MetA-SIMS: a simple way to reduce matrix effects in PS/PMMA blends

Inoue et al. studied the capability of the MetA-SIMS technique to reduce matrix effects observed in TOF-SIMS analyses of Irganox1010 and silicon oil coatings on Si and polypropylene (PP) substrates[175]. After deposition of a small amount of Ag onto these samples, the authors found that the matrix effects observed in a traditional SIMS analysis were strongly reduced.

V.4. (a) Experimental conditions

This approach was tested for the PS/PMMA blends. The samples were covered with 2 nm (nominal thickness) of Ag in the collector coating chamber (page 55), transferred in air to the TOF5 instrument and analyzed with 25 keV Bi^+ primary ions (0.88 pA ion current, 100 · 100 μm^2 raster size, 90 s acquisition time).

V.4. (b) Results and discussion

The intensities of some characteristic PS and PMMA peaks measured on the Ag-coated blend samples are shown in Fig. V-11 and Fig. V-12.

For the characteristic peaks considered in Fig. V-11 and Fig. V-12, the evolution of the intensity with the sample composition is linear (coefficients for linear regression higher than 0.94). This suggests that the ionization- and sputter-induced matrix effects observed in the traditional SIMS analyses on the blend samples are eliminated.

The absolute intensities of the Ag-cationized monomer units, especially for PMMA, also show an approximately linear behaviour (Fig. V-13).

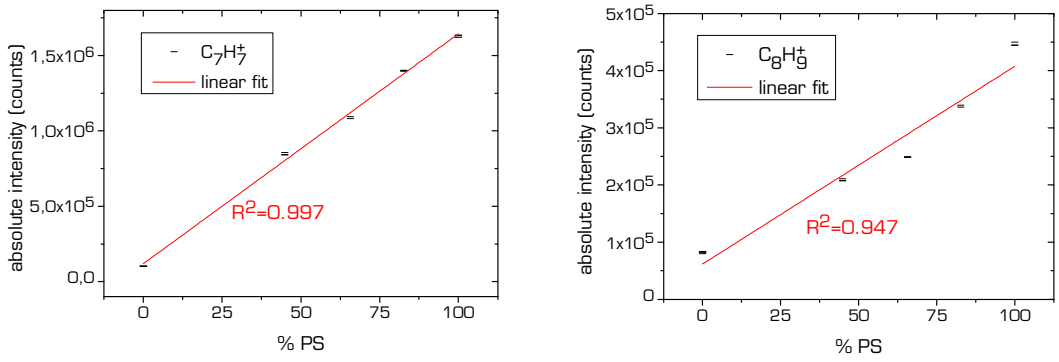

Fig. V-11: Absolute intensities of characteristic PS ions for PS/PMMA blends covered with a small amount of Ag. R^2 is the coefficient for linear regression. Data points resulting from 3 measurements are shown.

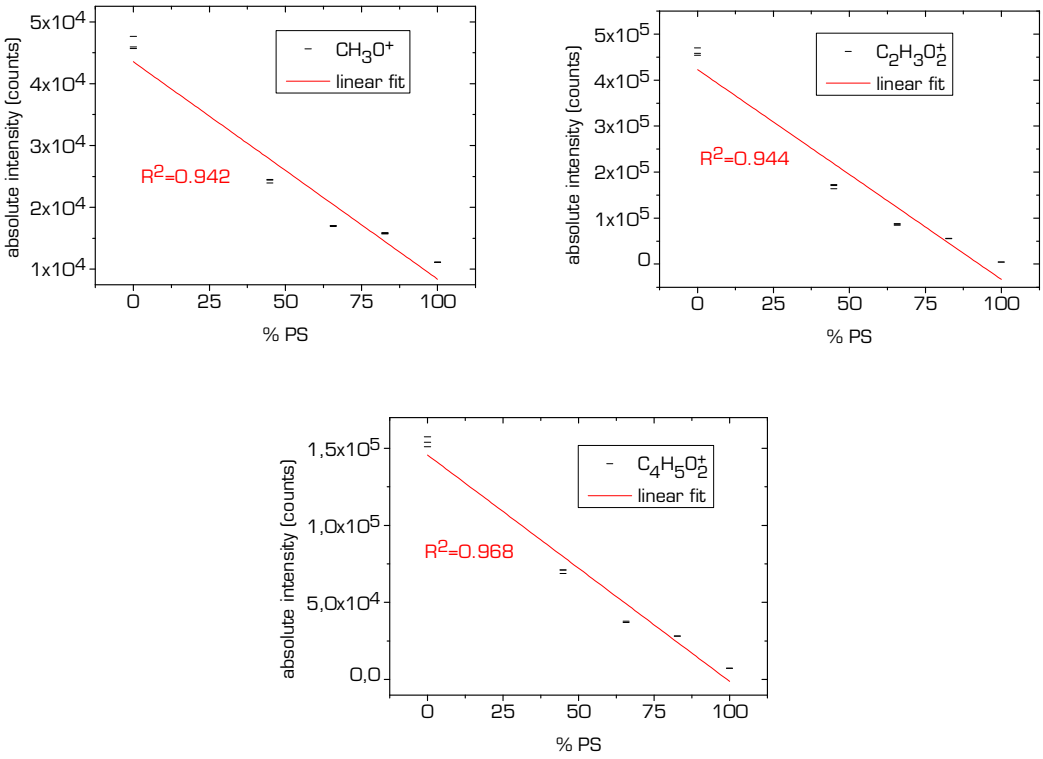

Fig. V-12: Absolute intensities of characteristic PMMA ions for PS/PMMA blends covered with a small amount of Ag. R^2 is the coefficient for linear regression. Data points resulting from 3 measurements are shown.

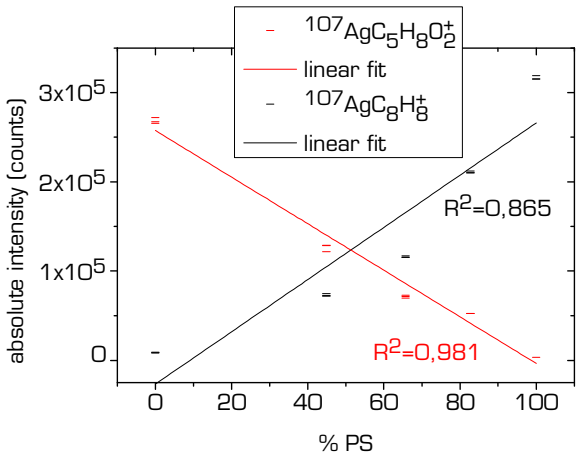

Fig. V-13: Absolute intensities of the Ag-cationized monomer units as a function of PS content. R^2 is the coefficient for linear regression. Data points resulting from 3 measurements are shown.

V.5 Conclusions

The method that gives the best linear evolution of the considered characteristic secondary ions with the blend composition is MetA-SIMS. For the other methods, the trends vary strongly for the different secondary ions.

In the case of MetA-SIMS, the diffusion of polymer chains on Ag clusters (or vice versa) allows to eliminate sputtering- and ionization-induced matrix effects. Short-range matrix effects (MEI, for example due to proton transfers between functionalities that are directly adjacent within a polymer chain) cannot be eliminated by this method. This means that MetA-SIMS could possibly be used to distinguish between MEI and MEII effects in copolymer systems. However, for larger polymer chains the diffusion on the Ag islands is less efficient, and matrix effects might not be fully eliminated in this case.

For the TOF-SIMS analyses of the blends with different primary ions and for the Storing Matter sensitivities, the major difficulty resides in the correction of the sputter rate variations. For a precise correction it would be necessary to measure the relative sputter rates for low primary ion fluences.

Chapter VI. Conclusions and outlook

VI.1 General conclusions

SIMS is a sensitive surface analysis method that has been used for a wide range of applications in various domains. Its major drawback is the so-called matrix effect, which is due to a change of the ionization efficiency as a function of the chemical environment of the considered atom or molecule and which makes quantitative analysis very difficult. The Storing Matter technique was developed in order to circumvent the matrix effect while still keeping an excellent sensitivity: in a first step, the sample surface is sputtered by an ion beam and the emitted matter is deposited at sub-monolayer level onto a dedicated collector. Then the collector is transferred under UHV conditions to a SIMS instrument where the deposit is analyzed. If the deposit coverage is in the sub-monolayer range, all the deposited particles are surrounded by the same matrix, i.e. the collector material.

The main goal of this work was the study and setup of experimental conditions for the application of the Storing Matter technique to organic samples. In this case, it is particularly important that molecular information is preserved. The key parameters of the technique were studied in detail and the optimal conditions with regard to high ionization efficiency and low fragmentation could be defined.

The nature of the collector surface can be considered to be the main parameter of the Storing Matter technique. Indeed, this material constitutes the common matrix for all the deposited particles during the SIMS analysis of the deposit. The collector material should thus be carefully chosen with regard to the desired outcome of the final analysis (i.e. secondary ion polarity, detection of metal-cationized fragments, etc.). It was shown that for a static SIMS analysis with Ar^+ primary ions in positive mode, Ag collectors are a good choice, since the characteristic peaks of the studied organic samples could be easily distinguished from the background signal measured on a pristine Ag surface. This "visibility" of the Storing Matter deposit was quantified by the Storing Matter sensitivity S_{Stomat}, which was defined as the ratio of the absolute

intensity of a given secondary ion in the centre of the deposit by that measured on the pristine collector. For a given characteristic secondary ion of the sample to be analyzed, S_{Stomat} depends on several factors:

- The amount of deposit present on the collector, which can be controlled by the experimental conditions of the sputter-deposition (primary ion energy, fluence, etc.), but which also depends on the sticking coefficient of the emitted particles on the collector;
- the yield enhancing effect of the collector material (resulting from the combination of sputtering, fragmentation, and ionization) for the considered ion during the analysis of the deposit;
- the intensity of this ion measured on the pristine collector (i.e. the "background" signal).

The last point is related to the main drawback associated with the chosen definition of S_{Stomat}: the values obtained for a secondary ions that has a low intensity on the pristine collector can be strongly influenced by a small variation of this intensity. In such a case, a variation of S_{Stomat} cannot be used to draw any conclusions about the Storing Matter deposit.

Another advantage when using Ag collectors is that the proportion of larger fragments in the Storing Matter mass spectra recorded with Ar^+ primary ions is higher, suggesting that there is less fragmentation during the analysis step. Furthermore, it was possible to detect large Ag-cationized fragments in the case of PS, especially if Ag is already present in the initial sample used for sputter-deposition (MetA-SIMS or ME-SIMS samples). This is however only possible for low molecular weight polymers (less than 4000 Da), probably because the diffusion processes are not efficient enough for longer chains. Although Au is widely used in the MetA-SIMS and ME-SIMS domains, Au collectors were found to be inappropriate for the Storing Matter technique because the positive hydrocarbon peak intensities are already very high on a pristine Au collector surface. The reason was found to be a strong matrix effect, and not a higher level of contamination than on the Ag layers prepared with the same experimental conditions. A collector consisting of a Cs coated Si wafer gives useful organic information in the negative polarity as well as in the MCs_x^+ mode.

The design of the Storing Matter prototype and the UHV suitcase make it possible to keep the collectors under UHV conditions during the entire Storing Matter process, from the evaporation of the metallic layer until the final analysis of the deposit. The striking changes in the positive mass spectrum of a pristine Ag collector before and after a brief exposure to air emphasized the importance of the UHV transfer.

The parameters of the Ar^+ beam used for the sputter-deposition step should be chosen carefully. It was shown that the increasing damage by ion irradiation for sputter-deposition fluences above the static limit is well visible in the Storing Matter spectra. Therefore the static limit should not be exceeded for both the sputter-deposition and the analysis steps. The impact energy of the Ar^+ ions during sputter-deposition was varied for different organic samples. It was shown that a lower energy decreases the amount of matter deposited onto the collector because of a decrease in sputtering yield, but also that the proportion of large organic fragments significantly decreased in the case of Alq_3. For PVC and PMMA, the sparseness of Cl- and O-containing fragments in the Storing Matter spectra was not affected by the change in impact energy. However these observations should be relativized since the impact energy used for the analysis step was always 10 keV. Even if sputter-depositions at low energy eject larger fragments, it is possible that the latter are destroyed during the analysis step and cannot be detected in the Storing Matter spectra.

The amount of matter present on the collector should be in the sub-monolayer regime for the Ag collector to be the common matrix for all the deposited particles. This is a prerequisite for the circumvention of the matrix effect in the case of multi-component samples. On the other hand, the deposit density should be high enough to yield reasonable signal intensities in the Storing Matter spectrum. The deposit coverage is influenced by the total number of primary ions used for sputter-deposition, the sputter yield of the organic sample with the given ion beam parameters, and the sticking factor of the emitted matter on the collector surface.

The primary ion type used for the analysis of the Storing Matter deposits also has a significant impact on the Storing Matter mass spectra. With Ag collectors, Ar^+ primary ions yielded the highest Storing Matter sensitivities for most characteristic peaks, while for Si collectors, Bi_3^+ projectiles were more

efficient. The largest proportion of large fragments was found for Ar^+ analysis of Storing Matter deposits on Ag collectors.

Globally it can be concluded that the sputter-deposition step should be optimized with regard to the ejection probability of large organic fragments, while the main objective of the analysis step should be increased ionization efficiencies and a reduction of double fragmentation. The best combination of experimental parameters, at least for the samples studied in this work, is the following:

- samples consisting of a thin organic overlayer on a metal substrate
- sputter-deposition with a low fluence of 10 keV Ar^+ ions
- use of Ag collectors
- UHV transfer of the collectors
- TOF-SIMS analysis with Ar^+ primary ions.

The potential of the Storing Matter technique for the reduction of matrix effects was investigated for PS/PMMA blends with different compositions. It was found that the matrix effects observed in this system are not only ionization-induced, but that they are also due to a change in sputtering yield with the sample composition. This fact also needs to be considered for the Storing Matter technique, since the quantity of deposited particles increases with the sputter yield. For a precise correction of the Storing Matter sensitivities by the sputter rate of each sample, measurements of this rate should be carried out at low fluence. A polymer blend of two components with similar sputter rates would be a good model sample to study the elimination of the ionization-induced matrix effects in more detail.

An alternative method for the reduction of matrix effects in PS/PMMA samples was proposed: MetA-SIMS, which consists in applying a small amount of a noble metal (Ag in this case) onto the organic samples prior to the TOF-SIMS analysis, seems to be a simple and efficient approach to reduce sputter- and ionization-induced matrix effects.

VI.2 Outlook

The Storing Matter spectra obtained for the 4 organic samples with the optimal combination of experimental parameters cited above do not provide any added value compared to a traditional TOF-SIMS, MetA-SIMS or ME-SIMS spectrum. Storing Matter is thus not competitive with these techniques, at least not within the range of experimental conditions explored in this work.

A parameter that could not be tested during this work but that is very likely to have an influence on the amount and size of organic fragments on the collector is the primary ion type used for sputter-deposition. Although TOF-SIMS analyses of Alq_3 reference samples indicate that fragmentation was more important with polyatomic projectiles, many authors have reported a lower degree of fragmentation, less damage accumulation, and much higher sputter yields than with monoatomic primary ions. With polyatomic primary ions it may be possible to increase the fluence for sputter-deposition, which means that a smaller sample area would be required for one deposit.

Furthermore, sputter-deposition of organic samples onto metallic collectors with cluster primary ions would be an innovative way to combine MetA-SIMS and cluster-SIMS. The results reported so far from the combination of these two approaches for TOF-SIMS analyses have been rather disappointing: since the yield enhancement obtained from the two methods separately is based on the same mechanism, i.e. an increased near surface energy deposition, their benefits in terms of yield enhancement do not add up. With the Storing Matter technique, MetA-SIMS and cluster SIMS could be combined in an indirect way: first, sputtering of large intact fragments, and second, analysis (with monoatomic ions) of these fragments embedded in the cationization-enhancing Ag matrix.

The main application of the Storing Matter technique for inorganic samples is quantitative depth profiling. In this case, a small aperture is positioned in front of the collector in order to delimit the solid angle of the deposited matter, and the collector is rotated during sputter-deposition. This experimental setup allows converting depth information from the sample into lateral information on the collector. Since the deposit coverage is in the sub-monolayer range, ionization-induced matrix effects can be eliminated[176]. For

organic materials, Storing Matter depth profiles are in principle possible, but only with carefully chosen ion beam parameters. Cluster primary ions and reactive ions such as Cs^+ would be interesting for this application since they have been successfully used for molecular depth profiling.

Two aspects that also deserve a more thorough investigation are the physical characterization of the organic Storing Matter deposits (island formation, diffusion, etc.) and the sticking factor of organic particles on a given collector surface. This would provide a deeper insight into the fundamental processes involved in the secondary ion emission processes.

The Storing Matter prototype is currently used in the frame of a project dedicated to the preparation and multi-technique characterization of organic submonolayers on different substrates, and the results of the study presented in this work serves as a basis for the choice of experimental conditions.

Reference List

1. P. Philipp, F. Lacour, T. Wirtz, L. Houssiau, J. J. Pireaux, H. N. Migeon, *Appl Surf Sci* 2008; **255**: 1501.
2. C. Mansilla, T. Wirtz, *J. Vac. Sci. Technol. B* 2010; **28**: C1C71.
3. A. Benninghoven, *Z. Physik* 1970; **230**: 403.
4. A. Benninghoven, *Surf Sci* 1971; **28**: 541.
5. J. C. Vickerman, D. Briggs, SurfaceSpectra Limited., *ToF-SIMS : surface analysis by mass spectrometry,* IM, Chichester, **2001**.
6. C. M. Ng, A. T. S. Wee, C. H. A. Huan, A. See, *Nuclear Instruments and Methods in Physics Research Section B: Beam Interactions with Materials and Atoms* 2001; **179**: 557.
7. P. Zalm, *Vacuum* 1994; **45**: 753.
8. Y. Marie, Y. Gao, F. Saldi, H. N. Migeon, *Surf Interface Anal* 1995; **23**: 38.
9. M. L. Yu, N. D. Lang, *Phys. Rev. Lett.* 1983; **50**: 127.
10. M. L. Yu, *Journal of Vacuum Science & Technology A: Vacuum, Surfaces, and Films* 1983; **1**: 500.
11. P. Williams, *Surf Sci* 1979; **90**: 588.
12. P. Williams, *Applications of Surface Science* 1982; **13**: 241.
13. K. Wittmaack, *Surf Sci* 1981; **112**: 168.
14. P. Philipp, T. Wirtz, H. N. Migeon, H. Scherrer, *International Journal of Mass Spectrometry* 2006; **253**: 71.
15. P. Philipp, T. Wirtz, H. N. Migeon, H. Scherrer, *International Journal of Mass Spectrometry* 2007; **264**: 70.
16. G. Stingeder, *ANAL. CHIM. ACTA* 1994; **297**: 231.
17. M. R. Kilburn, R. W. Hinton, *International Journal of Mass Spectrometry* 2001; **207**: 153.
18. H. Oechsner, *Int. J. Mass Spectrom. Ion Proces.* 1995; **143**: 271.
19. Y. Gao, *Journal of Applied Physics* 1988; **64**: 3760.

20. M. A. Ray, J. E. Baker, C. M. Loxton, J. E. Greene, *Journal of Vacuum Science & Technology A: Vacuum, Surfaces, and Films* 1988; **6**: 44.

21. T. Wirtz, H.-N. Migeon, H. Scherrer, *Applied Surface Science* 2003; **203-204**: 189.

22. P. Philipp, T. Wirtz, H.-N. Migeon, H. Scherrer, *Applied Surface Science* 2004; **231-232**: 754.

23. N. Mine, B. Douhard, J. Brison, L. Houssiau, *Rapid Commun. Mass Spectrom.* 2007; **21**: 2680.

24. G. Slodzian, *Enveloppe Soleau No. 13852 deposited by Cameca on 04/05/1998 on behalf of G. Slodzian,* **1998**.

25. T. Wirtz, H. N. Migeon, *Appl Surf Sci* 2008; **255**: 1498.

26. T. Wirtz, C. Mansilla, R. Barrahma, C. Verdeil, *Nucl Instrum Methods Phys Res Sect B* 2009; **267**: 2583.

27. B. Bendler, R. Barrahma, P. Philipp, T. Wirtz, *Surf. Interface Anal.* 2011; **43**: 514.

28. A. Benninghoven, F. G. Rüdenauer, H. W. Werner, *Secondary Ion Mass Spectrometry: Basic Concepts, Instrumental Aspects, Applications and Trends,* John Wiley & Sons, New York, **1987**.

29. B. Hagenhoff, D. van Leyen, E. Niehuis, A. Benninghoven, *Journal of Vacuum Science & Technology A: Vacuum, Surfaces, and Films* 1989; **7**: 3056.

30. P. Sigmund, *Phys. Rev.* 1969; **184**: 383.

31. B. U. R. Sundqvist, in *Sputtering by Particle Bombardment III* (Eds: R. Behrisch,K. Wittmaack)*,* Springer-Verlag, Berlin Heidelberg, **1991***,* pp. 257-

32. P. Sigmund, in *Sputtering by Particle Bombardment I* (Eds: R. Behrisch)*,* Springer Verlag, Berlin, **1981***,* pp. 9-71

33. M. W. Thompson, *Philosophical Magazine* 1968; **18**: 377.

34. R. Behrisch,K. Wittmaack, in *Sputtering by Particle Bombardment III* (Eds: R. Behrisch,K. Wittmaack)*,* Springer, Berlin, **1991***,* pp. 1-

35. K. D. Krantzman, Z. Postawa, B. J. Garrison, N. Winograd, S. J. Stuart, J. A. Harrison, *Nuclear Instruments and Methods in Physics Research Section B: Beam Interactions with Materials and Atoms* 2001; **180**: 159.

36. A. Delcorte, *Phys. Chem. Chem. Phys.* 2005; **7**: 3395.

37. W. Eckstein, in *Sputtering by Particle Bombardment* (Eds: R. Behrisch,W. Eckstein)*,* **2007***,* pp. 33-189

38. A. Oliva-Florio, R. A. Baragiola, M. M. Jakas, E. V. Alonso, J. Ferrón, *Phys. Rev. B* 1987; **35**: 2198.

39. K. Wittmaack, in *Sputtering by Particle Bombardment III* (Eds: R. Behrisch,K. Wittmaack)*,* Springer-Verlag, Berlin Heidelberg, **1991***,* pp. 161-256

40. M. J. Pellin, J. W. Burnett, *Pure and Applied Chemistry* 1993; **65**: 2361.

41. M. H. Shapiro, E. Trovato, T. A. Tombrello, *Nuclear Instruments and Methods in Physics Research Section B: Beam Interactions with Materials and Atoms* 2001; **180**: 58.

42. H. Gnaser, in *Sputtering by Particle Bombardment* (Eds: R. Behrisch,W. Eckstein)*,* Springer-Verlag, Berlin Heidelberg, **2007***,* pp. 231-329

43. G. K. Wehner, D. Rosenberg, *Journal of Applied Physics* 1960; **31**: 177.

44. K. Grais, A. A. Shaltout, S. S. Ali, R. M. Boutros, K. M. El-behery, Z. A. El-Sayed, *Physica B: Condensed Matter* 2010; **405**: 1775.

45. J. F. Hennequin, *J. Phys.* 1968; **29**: 957.

46. G. Slodzian, *Surf Sci* 1975; **48**: 161.

47. G. E. Thomas, *Rad. Eff.* 1977; **31**: 185.

48. C. Plog, W. Gerhard, *Surf Sci* 1985; **152-153**: 127.

49. A. Benninghoven, *International Journal of Mass Spectrometry and Ion Physics* 1983; **53**: 85.

50. R. G. Cooks, K. L. Busch, *International Journal of Mass Spectrometry and Ion Physics* 1983; **53**: 111.

51. S. J. Pachuta, R. G. Cooks, *Chemical Reviews* 1987; **87**: 647.

52. R. A. Zubarev, U. Abeywarna, P. Hakansson, P. Demirev, B. U. R. Sundqvist, *Rapid Commun. Mass Spectrom.* 1996; **10**: 1966.

53. G. Gillen, *Int. J. Mass Spectrom. Ion Proces.* 1991; **105**: 215.

54. A. Delcorte, B. G. Segda, P. Bertrand, *Surf Sci* 1997; **381**: 18.

55. C. W. Diehnelt, M. J. Van Stipdonk, E. A. Schweikert, *Proceedings of the 12th International Conference on Secondary Ion Mass Spectrometry* 2000; 267.

56. A. Schnieders, R. Möllers, A. Benninghoven, *Surf Sci* 2001; **471**: 170.

57. L. T. Weng, P. Bertrand, W. Lauer, R. Zimmer, S. Busetti, *Surf Interface Anal* 1995; **23**: 879.

58. P. M. Thompson, *Analytical Chemistry* 1991; **63**: 2447.

59. L. Li, C. M. Chan, L. T. Weng, M. L. Xiang, M. Jiang, *Macromolecules* 1998; **31**: 7248.

60. S. Liu, C. M. Chan, L. T. Weng, M. Jiang, *Analytical Chemistry* 2004; **76**: 5165.

61. L. T. Weng, C. M. Chan, *Appl Surf Sci* 2003; **203-204**: 532.

62. X. Vanden Eynde, P. Bertrand, *Appl Surf Sci* 1999; **141**: 1.

63. X. Vanden Eynde, K. Reihs, P. Bertrand, *Macromolecules* 2001; **34**: 5073.

64. A. Benninghoven, D. Jaspers, W. Sichtermann, *Applied Physics* 1976; **11**: 35.

65. A. Heile, C. Muhmann, D. Lipinsky, H. F. Arlinghaus, *Surf Interface Anal* 2011; **43**: 20.

66. B. J. Garrison, *Journal of the American Chemical Society* 1982; **104**: 6211.

67. B. J. Garrison, A. Delcorte, K. D. Krantzman, *Acc. Chem. Res.* 2000; **33**: 69.

68. A. Delcorte, X. Vanden Eynde, P. Bertrand, J. C. Vickerman, B. J. Garrison, *J Phys Chem B* 2000; **104**: 2673.

69. A. Delcorte, B. J. Garrison, *J Phys Chem B* 2000; **104**: 6785.

70. A. Delcorte, *Appl Surf Sci* 2006; **252**: 6582.

71. A. Delcorte, N. Médard, P. Bertrand, *Anal. Chem.* 2002; **74**: 4955.

72. A. Delcorte, P. Bertrand, *Appl Surf Sci* 2004; **231-232**: 250.

73. L. Adriaensen, F. Vangaever, R. Gijbels, *Anal. Chem.* 2004; **76**: 6777.

74. A. Delcorte, J. Bour, F. Aubriet, J. F. Muller, P. Bertrand, *Anal. Chem.* 2003; **75**: 6875.

75. A. Marcus, N. Winograd, *Anal. Chem.* 2006; **78**: 141.

76. I. S. Gilmore, M. P. Seah, *Appl Surf Sci* 2002; **187**: 89.

77. I. S. Gilmore, M. P. Seah, *Appl Surf Sci* 2003; **203-204**: 600.

78. A. Delcorte, I. Wojciechowski, X. Gonze, B. J. Garrison, P. Bertrand, *Int. J. Mass Spectrom.* 2002; **214**: 213.

79. A. Delcorte, S. Yunus, N. Wehbe, N. Nieuwjaer, C. Poleunis, A. Felten, L. Houssiau, J. J. Pireaux, P. Bertrand, *Anal. Chem.* 2007; **79**: 3673.

80. A. Heile, D. Lipinsky, N. Wehbe, A. Delcorte, P. Bertrand, A. Felten, L. Houssiau, J. J. Pireaux, R. De Mondt, P. Van Royen, L. Van Vaeck, H. F. Arlinghaus, *Surf Interface Anal* 2008; **40**: 538.

81. A. Heile, D. Lipinsky, N. Wehbe, A. Delcorte, P. Bertrand, A. Felten, L. Houssiau, J. J. Pireaux, R. De Mondt, L. Van Vaeck, H. F. Arlinghaus, *Appl Surf Sci* 2008; **255**: 941.

82. N. Wehbe, A. Delcorte, A. Heile, H. F. Arlinghaus, P. Bertrand, *Appl Surf Sci* 2008; **255**: 824.

83. L. Nittler, A. Delcorte, P. Bertrand, H. N. Migeon, *Surf Interface Anal* 2011; **43**: 103.

84. G. Coullerez, H. J. Mathieu, S. Lundmark, M. Malkoch, H. Magnusson, A. Hult, *Surf Interface Anal* 2003; **35**: 682.

85. H. Grade, R. G. Cooks, *Journal of the American Chemical Society* 1978; **100**: 5615.

86. Y. Travaly, P. Bertrand, *Surf Interface Anal* 1995; **23**: 328.

87. O. Restrepo, A. Prabhakaran, K. Hamraoui, N. Wehbe, S. Yunus, P. Bertrand, A. Delcorte, *Surf Interface Anal* 2010; **42**: 1030.

88. O. A. Restrepo, A. Delcorte, *Surf Interface Anal* 2011; **43**: 70.

89. L. Nittler, *PhD Thesis,* Université Catholique de Louvain, 2011.

90. K. Boussofiane-Baudin, G. Bolbach, A. Brunelle, S. la-Negra, P. Hskansson, Y. Le Beyec, *Nuclear Instruments and Methods in Physics Research Section B: Beam Interactions with Materials and Atoms* 1994; **88**: 160.

91. S. F. Belykh, I. S. Bitensky, D. Mullajanov, U. K. Rasulev, *Nuclear Instruments and Methods in Physics Research Section B: Beam Interactions with Materials and Atoms* 1997; **129**: 451.

92. T. Aoki, J. Matsuo, I. Yamada, *Nucl Instrum Methods Phys Res Sect B* 2001; **180**: 164.

93. S. N. Morozov, U. K. Rasulev, *Nuclear Instruments and Methods in Physics Research Section B: Beam Interactions with Materials and Atoms* 2003; **203**: 192.

94. G. Gillen, S. Roberson, *Rapid Commun. Mass Spectrom.* 1998; **12**: 1303.

95. F. Kollmer, *Appl Surf Sci* 2004; **231-232**: 153.

96. K. Aimoto, S. Aoyagi, N. Kato, N. Iida, A. Yamamoto, M. Kudo, *Appl Surf Sci* 2006; **252**: 6547.

97. D. Weibel, S. Wong, N. Lockyer, P. Blenkinsopp, R. Hill, J. C. Vickerman, *Anal. Chem.* 2003; **75**: 1754.

98. S. V. Verkhoturov, R. D. Rickman, C. Guillermier, G. J. Hager, J. E. Locklear, E. A. Schweikert, *Appl Surf Sci* 2006; **252**: 6490.

99. S. Ninomiya, Y. Nakata, Y. Honda, K. Ichiki, T. Seki, T. Aoki, J. Matsuo, *Appl Surf Sci* 2008; **255**: 1588.

100. J. Matsuo, C. Okubo, T. Seki, T. Aoki, N. Toyoda, I. Yamada, *Nuclear Instruments and Methods in Physics Research Section B: Beam Interactions with Materials and Atoms* 2004; **219-220**: 463.

101. J. Matsuo, S. Ninomiya, Y. Nakata, Y. Honda, K. Ichiki, T. Seki, T. Aoki, *Appl Surf Sci* 2008; **255**: 1235.

102. S. Ninomiya, Y. Nakata, K. Ichiki, T. Seki, T. Aoki, J. Matsuo, *Nuclear Instruments and Methods in Physics Research Section B: Beam Interactions with Materials and Atoms* 2007; **256**: 493.

103. I. Yamada, J. Matsuo, N. Toyoda, A. Kirkpatrick, *Materials Science and Engineering: R: Reports* 30-10-2001; **34**: 231.

104. B. Czerwinski, A. Delcorte, B. J. Garrison, R. Samson, N. Winograd, Z. Postawa, *Appl Surf Sci* 2006; **252**: 6419.

105. Z. Postawa, B. Czerwinski, N. Winograd, B. J. Garrison, *J Phys Chem B* 2005; **109**: 11973.

106. D. W. Ward, T. C. Nguyen, K. D. Krantzman, B. J. Garrison, *Proceedings of the 12th International Conference on Secondary Ion Mass Spectrometry* 2000; 183.

107. M. Kudo, K. Aimoto, Y. Sunagawa, N. Kato, S. Aoyagi, S. Iida, N. Sanada, *Appl Surf Sci* 2008; **255**: 1015.

108. A. Delcorte, C. Poleunis, P. Bertrand, *Appl Surf Sci* 2006; **252**: 6494.

109. R. Kersting, B. Hagenhoff, F. Kollmer, R. Möllers, E. Niehuis, *Appl Surf Sci* 2004; **231-232**: 261.

110. D. D. Wells, H. K. Moon, J. Gardella, *J. Am. Soc. Mass Spectrom.* 2009; **20**: 1562.

111. C. W. Diehnelt, M. J. Van Stipdonk, E. A. Schweikert, *Int. J. Mass Spectrom.* 2001; **207**: 111.

112. B. Boschmans, P. Van Royen, L. Van Vaeck, *Rapid Commun. Mass Spectrom.* 2005; **19**: 2517.

113. C. M. Mahoney, *Mass Spectrom. Rev.* 2010; **29**: 247.

114. N. Sanada, A. Yamamoto, R. Oiwa, Y. Ohashi, *Surf Interface Anal* 2004; **36**: 280.

115. A. G. Shard, P. J. Brewer, F. M. Green, I. S. Gilmore, *Surf Interface Anal* 2007; **39**: 294.

116. S. Ninomiya, K. Ichiki, H. Yamada, Y. Nakata, T. Seki, T. Aoki, J. Matsuo, *Surf Interface Anal* 2011; **43**: 221.

117. L. Houssiau, N. Mine, *Surf. Interface Anal.* 2010; **42**: 1402.

118. K. Norrman, Haugshøj, N. B. Larsen, *J Phys Chem B* 2002; **106**: 13114.

119. D. F. S. Petri, *Journal of the Brazilian Chemical Society* 2002; **13**: 695.

120. C. B. Walsh, E. I. Franses, *Thin Solid Films* 2003; **429**: 71.

121. C. J. Lawrence, *Physics of Fluids* 1988; **31**: 2786.

122. J. F. Ziegler, *SRIM - The Stopping and Range of Ions in Matter; www. srim. org* 2011;

123. C. R. Henry, *Cryst. Res. Technol.* 1998; **33**: 1119.

124. T. Pienkos, A. Proszynski, D. Chocyk, L. Gladyszewski, G. Gladyszewski, *Microelectronic Engineering* 2003; **70**: 442.

125. D. Chocyk, T. Zientarski, A. Proszynski, T. Pienkos, L. Gladyszewski, G. Gladyszewski, *Cryst. Res. Technol.* 2005; **40**: 509.

126. M. C. Barnes, D. Y. Kim, H. S. Ahn, C. O. Lee, N. M. Hwang, *Journal of Crystal Growth* 2000; **213**: 83.

127. J. F. Moulder, W. F. Stickle, P. E. Sobol, B. Boschmans, *Handbook of X-ray Photoelectron Spectroscopy,* Physical Electronics, **1995**.

128. G. Beamson,D. Briggs, *High Resolution XPS of Organic Polymers,* John Wiley & Sons, **1992**.

129. S. Tanuma, C. J. Powell, D. R. Penn, *Surf Interface Anal* 1991; **17**: 911.

130. M. L. Yu, *Journal of Vacuum Science & Technology A: Vacuum, Surfaces, and Films* 1983; **1**: 500.

131. D. R. Lide, *CRC Handbook of Chemistry and Physics,* CRC, Boca Raton, FL, **1995**.

132. A. Seetula, *J. Chem. Soc. , Faraday Trans.* 1998; **94**: 891.

133. J. Zekonyte, V. Zaporojtchenko, F. Faupel, *Nucl Instrum Methods Phys Res Sect B* 2005; **236**: 241.

134. J. G. Newman, B. A. Carlson, R. S. Michael, J. F. Moulder, *Static SIMS Handbook of Polymer Analysis,* Perking-Elmer Corporation, Physical Electronics Division, **1991**.

135. A. M. Leeson, M. R. Alexander, R. D. Short, D. Briggs, M. J. Hearn, *Surf Interface Anal* 1997; **25**: 261.

136. A. Delcorte, P. Bertrand, B. J. Garrison, *Appl Surf Sci* 2003; **203-204**: 166.

137. A. Delcorte, P. Bertrand, *Nuclear Instruments and Methods in Physics Research Section B: Beam Interactions with Materials and Atoms* 1998; **135**: 430.

138. W. Eckstein, C. Garciá-Rosales, J. Roth, J. László, *Nuclear Instruments and Methods in Physics Research Section B: Beam Interactions with Materials and Atoms* 1993; **83**: 95.

139. C. Mansilla, T. Wirtz, *Surf. Interface Anal.* 2010; **42**: 1135.

140. C. Mansilla, T. Wirtz, *J. Vac. Sci. Technol. B* 2010; **28**: C1C71.

141. J. E. Ortega, R. Miranda, *Applied Surface Science* 1992; **56-58**: 211.

142. D. Heskett, T. M. Wong, A. J. Smith, W. R. Graham, N. J. DiNardo, E. W. Plummer, *PROCEEDINGS OF THE 16th ANNUAL CONFERENCE ON THE PHYSICS AND CHEMISTRY OF SEMICONDUCTOR INTERFACES* 1989; **7**: 915.

143. B. Kierren, D. Paget, *J Vac Sci Technol A* 1997; **15**: 2074.

144. J. Gordon, H. Shechter, M. Folman, *Phys. Rev. B* 1994; **49**: 4898.

145. W. B. Sherman, R. Banerjee, N. J. DiNardo, W. R. Graham, *Phys. Rev. B* 2000; **62**: 4545.

146. H. Y. Xiao, X. T. Zu, Y. F. Zhang, L. Yang, *The Journal of Chemical Physics* 2005; **122**: 174704.

147. M. L. Yu, *Journal of Vacuum Science & Technology A: Vacuum, Surfaces, and Films* 1983; **1**: 500.

148. J. Brison, T. Conard, W. Vandervorst, L. Houssiau, *Appl Surf Sci* 2004; **231-232**: 749.

149. N. Mine, B. Douhard, L. Houssiau, *Appl Surf Sci* 2008; **255**: 973.

150. A. Delcorte, P. Bertrand, *Anal. Chem.* 2005; **77**: 2107.

151. D. C. Muddiman, A. H. Brockman, A. Proctor, M. Houalla, D. M. Hercules, *J Phys Chem* 1994; **98**: 11570.

152. N. Wehbe, T. Mouhib, A. Prabhakaran, P. Bertrand, A. Delcorte, *J. Am. Soc. Mass Spectrom.* 2009; **20**: 2294.

153. A. Schnieders, M. Schröder, D. Stapel, H. F. Arlinghaus, A. Benninghoven, *Proceedings of the 12th International Conference on Secondary Ion Mass Spectrometry* 2000; 263.

154. G. J. Leggett, J. C. Vickerman, *Int. J. Mass Spectrom. Ion Proces.* 1992; **122**: 281.

155. G. J. Leggett, J. C. Vickerman, *Appl Surf Sci* 1992; **55**: 105.

156. I. S. Gilmore, M. P. Seah, *Surf Interface Anal* 1996; **24**: 746.

157. A. Delcorte, L. T. Weng, P. Bertrand, *Nuclear Instruments and Methods in Physics Research Section B: Beam Interactions with Materials and Atoms* 1995; **100**: 213.

158. I. S. Gilmore, M. P. Seah, *Appl Surf Sci* 2000; **161**: 465.

159. D. Briggs, M. J. Hearn, *Int. J. Mass Spectrom. Ion Proces.* 1985; **67**: 47.

160. A. Delcorte, X. Vanden Eynde, P. Bertrand, D. F. Reich, *Int. J. Mass Spectrom.* 11-8-1999; **189**: 133.

161. M. H. Shapiro, E. Trovato, T. A. Tombrello, *Nuclear Instruments and Methods in Physics Research Section B: Beam Interactions with Materials and Atoms* 2001; **180**: 58.

162. B. Jeong, Y. H. Bae, D. S. Lee, S. W. Kim, *Nature* 1997; **388**: 860.

163. J. N. Audinot, P. Lévêque, R. Bechara, N. Leclerc, J. Guillot, H. N. Migeon, G. Hadziioannou, T. Heiser, *Surf Interface Anal* 2010; **42**: 1010.

164. L. T. Weng, K. M. Ng, Z. L. Cheung, Y. Lei, C. M. Chan, *Surf Interface Anal* 2006; **38**: 32.

165. X. Vanden Eynde, P. Bertrand, *Appl Surf Sci* 1999; **141**: 1.

166. X. Vanden Eynde, P. Bertrand, J. Penelle, *Macromolecules* 2000; **33**: 5624.

167. A. G. Shard, S. Clarke, M. C. Davies, *Surf Interface Anal* 2002; **33**: 528.

168. S. Liu, L. T. Weng, C. M. Chan, L. Li, N. K. Ho, M. Jiang, *Surf Interface Anal* 2001; **31**: 745.

169. S. Liu, C. M. Chan, L. T. Weng, M. Jiang, *Polymer* 2004; **45**: 4945.

170. A. A. Galuska, *Surf Interface Anal* 1997; **25**: 1.

171. J. Feng, C. M. Chan, L. T. Weng, *Polymer* 2000; **41**: 2695.

172. L. Kailas, J.-N. Audinot, H.-N. Migeon, P. Bertrand, *Appl Surf Sci* 2004; **231-232**: 289.

173. L. Kailas, B. Nysten, J. N. Audinot, H. N. Migeon, P. Bertrand, *Surf Interface Anal* 2005; **37**: 435.

174. L. Kailas, J.-N. Audinot, H.-N. Migeon, P. Bertrand, *Composite Interfaces* 2006; **13**: 423.

175. M. Inoue, A. Murase, *Surf Interface Anal* 2005; **37**: 1111.

176. C. Mansilla, T. Wirtz, *Applied Surface Science*, submitted.